UNIVERSITÀ DEGLI STUDI DI PADOVA

DIPARTIMENTO DI BIOLOGIA

Corso di Laurea in Biologia Molecolare

ELABORATO DI LAUREA

ALTERAZIONI COMPORTAMENTALI E FUNZIONALI ASSOCIATE A MUTAZIONI DI *syngap1* IN *Danio rerio*

Tutor: Prof. Marco Dal Maschio
Dipartimento di Scienze Biomediche

Laureando: Lorenzo Tirelli

ANNO ACCADEMICO 2023/2024

Sommario

Abstract 2

Indice abbreviazioni 3

Capitolo 1. Stato delle conoscenze 4

1.1 *SYNGAP1*, mutazioni osservate e aploinsufficienza 4

1.2 Modelli animali mutanti di *SYNGAP1* 5

1.3 Caratterizzazione di mutanti zebrafish 6

Capitolo 2. Materiali e metodi 8

2.1 Confronto tra morfolino oligo e CRISPR/Cas9 8

2.2 Kozol et al. (2015) bersagliano l'mRNA di *syngap1b* con MO 13

2.3 Sumathipala et al. (2024) generano mutanti *syngap1a* e *1b* mediante la tecnica CRISPR/Cas9 16

Capitolo 3. Discussione dei risultati 18

3.1 Kozol et al. correlano morfogenesi alterata e iperattività in modelli di zebrafish ottenuti con MO 18

3.2 Sumathipala et al. approfondiscono le alterazioni funzionali dei modelli mutati ottenuti con CRISPR/Cas9 20

Capitolo 4. Confronto conclusivo 23

Capitolo 5. Bibliografia 25

Appendice 27

Abstract

SYNGAP1 è un gene associato allo spettro autistico e a disabilità intellettive. In questo elaborato ho analizzato due articoli scientifici che studiano l'impatto della mutazione di Syngap1 in zebrafish utilizzando due approcci alternativi di interferenza genica, ovvero morfolino oligonucleotidi e CRISPR/Cas9. Le modifiche ottenute hanno confermato che il gene è fondamentale nelle prime fasi di sviluppo embrionale del cervello, ma anche nei comportamenti spontanei e associati a stimoli sensoriali degli esemplari nelle fasi successive dello sviluppo. Entrambi i lavori confermano che aploinsufficienze di Syngap1 causano comportamenti stereotipati, risposte di fuga improduttive, iperattività contesto-dipendente. Questo lavoro si propone di confrontare i metodi di ottenimento dei mutanti e dei morfanti, e i risultati a essi associati.

Indice abbreviazioni

AChR: Acetyl-Choline Receptor
ADHD: Attention Deficit Hyperactivity Disorder
AMPAR: α-Amino-(3-hydroxy-5-Methyl-4-isoxazol)-Propionic Acid Receptor
ASD: Autism Spectrum Disorder
ASR: Acoustic Startle Response
Cas: CRISPR-Associated
CoMO: Control Morpholino Oligonucleotides
CRISPR: Clustered Regularly Interspaced Short Palindromic Repeats
crRNA: CRISPR RNA
DSB: Double Strand Break
dpf: Days Post Fertilization
EI: Eccitazione-Inibizione
ESE: Exonic Splicing Enhancer
GABA: Gamma-AminoButyric Acid
HDR: Homology Directed Repair
hpf: Hours Post Fertilization
ID: Intellectual Disorder
ISI: Inter-Stimulus Interval
ISS: Intronic Splicing Silencer
LTP: Long-Term Potentiation
MO: Morpholino Oligonucleotides
NHEJ: Non-Homologous End Joining
NMDAR: *N*-Methyl-D-Aspartate Receptor
PAM: Protospacer Adjacent Motif
PM: Peso Molecolare
PSD: Post-Synaptic Density
RT-(q)PCR: Reverse Transcriptase-(quantitative) PCR
SIGNOR: SIGnalling Network Open Resource
sgRNA: single-guide RNA
SNC: Sistema Nervoso Centrale
snRNA: Small-Nuclear RNA
snRNP: snRNA Particle
tracrRNA: trans-activating crRNA
VMR: Visual Motor Response
WT: Wild Type

Capitolo 1. Stato delle conoscenze

Lo spettro autistico (ASD) è una malattia multifattoriale, il cui manifestarsi dipende sia da fattori genetici sia da fattori ambientali. Tra i sintomi più comuni ci sono problemi sociali, deficit linguistici, comportamenti stereotipati e ripetitivi, ADHD, ansia e altro. Tuttavia, la variabilità dei sintomi è così alta da permettere di parlare di differenti manifestazioni per ogni paziente. L'alta ereditabilità della malattia (~ 90%) suggerisce che la componente genetica abbia un grande impatto nella sua manifestazione [10].

Negli ultimi anni diversi studi si sono concentrati nell'individuazione di diversi geni correlati con la ASD. Nel 2024 Iannuccelli e collaboratori hanno cercato in letteratura tutti i geni causalmente correlati alla ASD e li hanno riordinati su SIGNOR[1], un database in cui vengono prima annotate manualmente le relazioni causali tra proteine, composti chimici di rilevanza biologica, stimoli e fenotipi. Quindi, le informazioni sono riordinate in reti statiche [5]. I risultati di questo studio mostrano che i geni implicati nella ASD sono clusterizzati e i vari raggruppamenti hanno diverse interconnessioni che confermano la natura poligenica della malattia. Sulla base di questi dati, il gruppo ha sviluppato un algoritmo per stimare l'impatto fenotipico e regolativo sulla malattia a carico dei *pathway* annotati su SIGNOR, permettendo di individuare mutazioni di *SYNGAP1* come responsabili di diversi fenotipi disfunzionali e correlandolo ad altri geni ad alto rischio. Anche *SHANK3* (analizzato da Kozol et al., 2015) è risultato avere numerose connessioni causali con fenotipi disfunzionali.

Numerose problematiche legate alla ASD sembrano nascere da disfunzioni legate a sinapsi GABAergiche, glutamatergiche e dopaminergiche, suggerendo l'importanza dell'equilibrio eccitazione-inibizione nel normale funzionamento cerebrale, in particolare dei circuiti legati alla locomozione, alle interazioni sociali e al comportamento in generale [1, 2, 5, 10].

1.1 *SYNGAP1*, mutazioni osservate e aploinsufficienza

Il gene *SYNGAP1* è stato da tempo associato a disturbi riguardanti il SNC, in particolare ha un ruolo fondamentale nello sviluppo cerebrale e, più tardi, nel funzionamento sinaptico [1, 2, 4, 7]. Il suo ruolo è altamente rilevante nelle sinapsi glutamatergiche, più nello specifico è localizzato nella densità postsinaptica (PSD). Nella PSD, il prodotto proteico di *SYNGAP1* è coinvolto nella plasticità sinaptica tramite la modulazione di proteine Ras (delle GTPasi), che a loro volta hanno effetti diversi (a volte opposti) a seconda dello stimolo [4].

Le mutazioni del gene umano possono essere ereditarie, ma la maggior parte avviene *de novo* [1]. Diversi studi hanno dimostrato che le mutazioni sulla sequenza di *SYNGAP1* sono associate a disturbi cognitivi e a malattie neurodegenerative: tutti i pazienti con mutazioni *loss of function* presentano disturbi intellettuali (ID),

[1] https://signor.uniroma2.it/

mentre circa il 50% dei casi è affetto anche da ASD [4], spesso causata da patofisiologie sinaptiche e mutazioni di proteine alle sinapsi.

SYNGAP1 (*Synaptic GTPase Activating Protein*) è una proteina che interagisce con Ras o Rap, due GTPasi con ruoli opposti nelle sinapsi glutamaterigiche. Ras è attivata tramite CaMKII (una chinasi Ca^{2+}-dipendente) in seguito ad attivazione di recettori NMDA ed è responsabile dell'inserimento di recettori AMPA nella membrana postsinaptica. Gli AMPAR sono recettori con un ruolo fondamentale nel potenziamento sinaptico e nell'aumento dell'eccitabilità del neurone stesso. Rap, invece, è attivata in risposta a bassi livelli di Ca^{2+} e contribuisce alla rimozione dei soli AMPAR contenenti la subunità GluA2, con risultato finale opposto sul livello di eccitabilità neuronale [4].
Poiché CaMKII può fosforilare anche determinati domini di SYNGAP1, si pensa che la mutazione comporti un aumento di interazione con Rap1 e, dunque, limiti l'inserzione di AMPAR in membrana. D'altro canto, aploinsufficienza di SYNGAP1 porta all'eccessiva attivazione di Ras, che induce un eccessivo inserimento di AMPAR sulla membrana postsinaptica e, di conseguenza, un livello elevato di eccitabilità neuronale basale. Questa alterazione compromette la plasticità sinaptica, perché la membrana è già satura di AMPAR, e causa difetti nella LTP, coinvolta in memoria e apprendimento, ma anche nel normale funzionamento dei neuroni glutamatergici, la cui disfunzione è correlata a ID [4].

SYNGAP1 è fondamentale anche nella morfogenesi cerebrale di molti vertebrati (tra cui uomo, topo, zebrafish e *Xenopus* [2]): una sua disfunzione, infatti, sembra essere strettamente correlata a successive comparse di ID, tra cui ASD, in particolare dovute all'alterato sviluppo del cervello e delle architetture circuitali. Ad esempio, in zebrafish mutanti sono state osservate significative riduzioni dei neuroni GABAergici nel mesencefalo e nel rombencefalo, ma anche di quelli glutamatergici nel rombencefalo [2].
Inoltre, è stato osservato che mutazioni in omozigosi di *Syngap1* in modelli murini sono letali in periodo perinatale, un dato che dimostra il suo ruolo nello sviluppo dell'embrione [4].

1.2 Modelli animali mutanti di *SYNGAP1*

Il gene *SYNGAP1* è ortologo in diverse specie di vertebrati. Questo ha permesso l'utilizzo di diversi modelli, tra cui zebrafish, che presenta diversi vantaggi rispetto a topo, come la facile manipolazione genetica, l'accessibilità dell'embrione, il veloce sviluppo embrionale e i costi ridotti rispetto al mammifero [2].

Una delle linee di topo usate per lo studio di mutazioni su *Syngap1* in eterozigosi presenta gravi disfunzioni nella LTP e, dunque, nell'apprendimento e nella memoria. I soggetti mutati presentano un'elevata attività di Ras, che porta a

un eccessivo inserimento di AMPAR e che impedisce ulteriori attivazioni di Ras stessa. Questo causa una diminuzione delle connessioni neuronali e una ridotta plasticità sinaptica, interferendo con la normale adattabilità e struttura dei circuiti neuronali.
In generale sembra esserci uno sbilanciamento tra l'eccitazione e l'inibizione dei neuroni di importanti circuiti cerebrali, che causa anche, in alcuni soggetti, epilessia e comportamenti convulsivi (*seizure-like*) [7].
È stata riscontrata anche maggiore inclinazione ad assumere comportamenti rischiosi. Tutte queste anomalie sono riconducibili a vari aspetti della ASD, fornendo così i dati necessari per una correlazione tra *SYNGAP1* e spettro autistico [7].

Negli ultimi anni, zebrafish ha riscosso un grande successo come modello di malattie neurodegenerative. Per quanto riguarda la ASD e *SYNGAP1*, *Danio rerio* mostra diversi aspetti studiabili e quantificabili. In particolare, sono stati condotti diversi studi adattati da esperimenti su modelli murini, come il test di sociabilità, di aggressione, di locomozione in circolo (anche indotta da alcuni farmaci come la ketamina), che hanno tutti confermato la manifestazione di sintomi tipici della ASD e, di conseguenza, la possibilità di studiare la malattia su zebrafish [10].
Oltre a questi tratti, *D. rerio* presenta mutazioni *loss of function* con fenotipi sovrapponibili a quelli murini, nello specifico in comportamenti stereotipati e in deficit di memoria.

È necessario, infine, tenere presente che su zebrafish il gene è duplicato: sono presenti *syngap1a* e *syngap1b*, che rendono più complicato l'ottenimento di mutanti con un fenotipo *loss of function*. La localizzazione nel cervello è leggermente differente: *syngap1a* è più espresso nel proencefalo anteriore e nel rombencefalo dorsale, mentre *syngap1b* nel rombencefalo dorsale [2]. Mutazioni su uno solo dei due geni causano disfunzioni di intensità diverse nei due studi oggetto di questo elaborato, ad esempio sbilanciamenti troppo forti in favore di *syngap1b* impattano la sopravvivenza e il comportamento delle larve [1].

1.3 Caratterizzazione di mutanti zebrafish

Kozol e collaboratori (2015) hanno confrontato nel loro studio sequenze amminoacidiche e nucleotidiche di *syngap1* e del rispettivo prodotto proteico, al fine di costruire un albero filogenetico e capire l'origine del gene. Essi scoprirono che *syngap1* è un'innovazione dei vertebrati, derivata però da evoluzioni di una proteina antica, presente anche nei Choanoflagellati [2]. L'allineamento proteico ha dimostrato che tra pesci teleostei e mammiferi, i quattro domini principali di interazione proteica sono conservati, validando gli studi su zebrafish. Nello specifico, si tratta dei domini *pleckstrin homology* (PH), C2, RasGAP e *coiled-coiled* (CC), tutti presi in considerazione negli studi dei due articoli in analisi.

Il gruppo di Sumathipala (2024), in particolare, ha studiato tutte le isoforme pubblicate e predette ed è riuscito a individuare cinque isoforme di *syngap1a* e undici di *syngap1b*, constatando che i quattro domini di interazioni sono sempre presenti [1]. Le isoforme di mammifero che è possibile confrontare con quelle di zebrafish sono quattro (individuate già nel 1998) e originano tutte da *splicing alternativo* del C-terminale (α1, α2, β, γ) [7].

A causa dell'alta variabilità del C-terminale nelle isoforme di zebrafish, è stato possibile individuare solo il corrispondente dell'isoforma α1 di mammifero. Si tratta di X5, una delle isoforme di *syngap1b*, trovata grazie a un suo dominio putativo omologo a quello *PDZ-interacting* mammifero, con undici su dodici amminoacidi terminali identici [1] (*Fig. 1*).

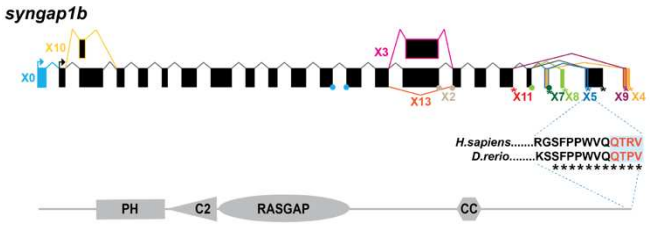

Figura 1. Isoforme di Syngap1b su zebrafish, con evidenziato l'ortologo di uomo (da Sumathipala et al., 2024).

L'isoforma umana α1, in ogni caso, è la più studiata proprio a causa del suo dominio *PDZ-interacting*, capace di regolare il legame di proteine della PSD e, dunque, con un ruolo fondamentale nell'organizzazione della PSD stessa e nella determinazione dei potenziali soglia per l'inserimento di AMPAR, necessario per la LTP [7].

Al fine di non escludere isoforme che potrebbero comunque avere un ruolo importante nei processi neuronali, Sumathipala e collaboratori hanno optato per un *editing* genetico che coinvolgesse i primi esoni di entrambi i geni, condivisi da tutte le isoforme. In questo modo, tutti gli individui modificati presentavano solo proteine troncate, a prescindere dall'isoforma finale [1].

Capitolo 2. Materiali e metodi

I due gruppi di ricerca hanno utilizzato metodi sostanzialmente diversi per ottenere aploinsufficienza di *syngap1*: il primo i morfolino oligo, un metodo che consiste nell'inattivazione transiente dei trascritti dei geni bersaglio, mentre il secondo CRISPR/Cas9, una tecnica di modifica diretta del DNA genomico.

2.1 Confronto tra morfolino oligo e CRISPR/Cas9

I morfolino oligonucleotidi (MO) sono simili a degli mRNA antisenso, che però presentano dei legami sintetici molto diversi da quelli zucchero-fosfato, tipici degli acidi nucleici. Infatti, i nucleotidi in questo caso sono tenuti insieme da una catena di metilene-morfolino, polimerizzata tramite gruppi fosforodiammidato; questa sostanziale differenza dalla struttura tipica di un mRNA rende i MO inattaccabili dagli enzimi cellulari, non causa una risposta immunitaria (che invece gli mRNA estranei possono attivare) e rende il loro funzionamento indipendente da eventuali enzimi. Vengono utilizzati per il *knock-down* genico in embrioni, *in primis* perché iniettando MO a stadi precoci è più semplice far sì che essi diffondano a più cellule durante lo sviluppo, secondariamente perché nelle cellule adulte è più facile l'interazione con off-target.
I MO si appaiano al trascritto del gene bersaglio e possono agire in diversi modi: (a) impedire la generazione di variazioni (*splicing*) del pre-mRNA, ad esempio sintetizzandoli in modo da farli accoppiare a una giunzione introne-esone prima che il trascritto venga processato o (b) impedire l'attacco del ribosoma, ad esempio facendo appaiare il MO al 5'-UTR dell'mRNA (vicino al codone di *start*) e prevenendo così la traduzione proteica.
Nel caso specifico dell'interferenza di *splicing*, i metodi sono svariati: (1) impedire che il complesso snRNA leghi il sito di *splicing* (il complesso è necessario per indirizzare tutte le componenti dello spliceosoma), (2) bloccare l'adenina del sito di ramificazione e prevenire la formazione della struttura a lariat (non avviene l'attacco nucleofilo sul 2'-OH di questa adenina), (3) interferire coi siti di *binding* di *silencer* e/o *enhancer* (ISS, ESE, su introni ed esoni rispettivamente) o (4) bloccare i siti catalitici di ribozimi. Nel caso (1), i MO possono essere progettati per il legame sia al sito accettore per U2 snRNP (introne-esone), includendo l'introne precedente, sia al sito donatore per U1 snRNP (esone-introne), includendo l'introne successivo (vedi *Fig. 2*) [8]. Targettare contemporaneamente una giunzione di *splicing* e un intero sito di legame per U2 snRNP porta invece alla delezione dell'esone successivo.

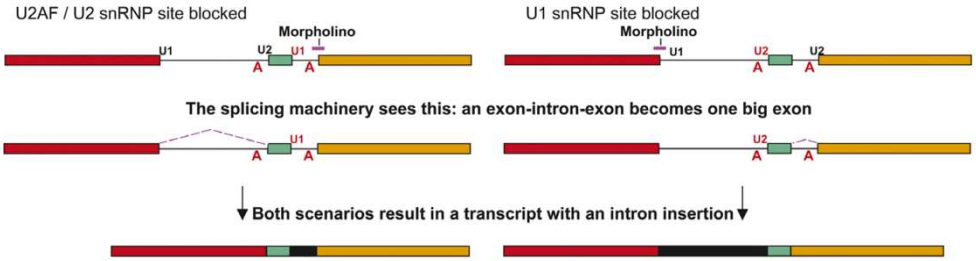

Figura 2. Appaiamento dei morfolino oligo al sito accettore (sinistra) o donatore (destra), con diversa inclusione di introni (in nero) (da Morcos, 2007).

Un'accortezza necessaria è quella di sintetizzare più MO che si appaiano in più punti del trascritto, in modo tale da avere maggiore certezza che il fenotipo mutante sia dato da un *knock-down* del gene target e non da un appaiamento casuale; infatti, si è anche osservato che co-iniettare MO complementari a più siti (ad esempio uno per la giunzione introne-esone, l'altro per il *branchsite*) è più efficiente rispetto all'iniezione di una singola molecola [8]. Si è notato anche che non ci sono grandi differenze nell'efficienza di interferenza tra MO complementari alla giunzione introne-esone, rispetto a quella esone-introne. Tuttavia, puntare la giunzione esone-introne può in potenza attivare siti di *splicing* criptici, generando trascritti imprevisti: se questi sono da evitare (a seconda delle condizioni dell'esperimento), è meglio optare per MO complementari alle giunzioni introne-esone. È da tenere presente, però, che scegliere di bersagliare il sito accettore potrebbe generare appaiamenti meno specifici rispetto al sito donatore, a causa della sua natura intrinseca (sito ridotto a due basi) [8].

Per la sintesi dei morfolino è necessario conoscere la sequenza del gene o del trascritto target. Nel caso specifico di interferenza nello *splicing*, è necessario essere in possesso della sequenza completa del pre-mRNA, ottenibile tramite *reverse transcriptase* qPCR (RT-qPCR). Una delle limitazioni più critiche è quella della selezione di primer adatti, ma anche quella della scelta di un esone o di un introne di dimensioni adeguate all'amplificazione in PCR (necessario al confronto tra mRNA con e senza esone, o con e senza introne, di norma condotto eseguendo una corsa elettroforetica post-amplificazione). Si deve anche considerare, come già accennato, che alterare lo *splicing* di un trascritto può portare all'attivazione di un sito di *splicing* criptico: si deve perciò prestare attenzione a questo possibile risultato ed essere in grado di identificarlo e, se necessario, di cambiare strategia. Questi siti criptici, infatti, potrebbero condurre all'espressione normale della proteina (o poco alterata), in quanto spesso presenti nei pre-mRNA, ma non utilizzati perché disponibili siti di taglio più favorevoli.

L'efficacia e l'effetto dei MO sono dose-dipendenti: alcuni, ad alte concentrazioni, possono anche risultare tossici per l'embrione (come nel caso del MO contro *syngap1a* nel nostro articolo [2]). Questo passaggio può essere semplificato tramite la co-iniezione di più MO, in modo da ridurre gli off-target dose-dipendenti.

Per verificare che i MO abbiano agito nel modo giusto, si può procedere con un Western Blot, in modo da quantificare una proteina di un estratto cellulare. Un altro metodo di verifica è la RT-qPCR, più accurata e attendibile rispetto al Western

Blot, ma più costosa. Il metodo più validato per escludere off-target è quello di iniettare MO in un mutante con doppio allele nullo (ad esempio ottenuto con una delezione accurata di entrambi gli alleli del gene target): se il mutante non mostra nessun fenotipo aggiuntivo in seguito a iniezione di MO, allora questi non dovrebbero interferire con nessun altro processo cellulare [8].
Per verificare con ancora più robustezza la specificità del *knock-down*, si può procedere con la tecnica di *RNA rescue*, ovvero nell'iniezione di mRNA (senza le sequenze target dei MO) e nella verifica di ritorno al fenotipo selvatico. A volte, però, non è possibile tornare al fenotipo *wild-type* (WT) a causa dell'espressione ectopica dell'mRNA target.
I controlli sui MO, dunque, devono essere molto accurati, a causa della natura dei trascritti e della variabilità di effetti che si possono ottenere con questa tecnica.

La tecnica di mutagenesi CRISPR/Cas9 è una versione semplificata del sistema di difesa di alcuni batteri e Archaea contro attacchi virali (e plasmidiali) [6]. Le sequenze CRISPR sono brevi segmenti di DNA ripetitivo e palindromico, separati da sequenze spaziatrici derivate da frammenti di materiale genetico virale. L'integrazione di questi segmenti avviene in seguito a un'infezione da parte di un batteriofago e costituisce un sistema di difesa contro successivi attacchi da parte dello stesso patogeno. Le proteine Cas (CRISPR-Associated) sono nucleasi che riconoscono e tagliano acidi nucleici estranei, proprio grazie a queste sequenze spaziatrici; infatti, il sito specifico (*locus*) CRISPR viene trascritto per intero (pre-CRISPR RNA, o pre-crRNA), l'RNA viene poi tagliato e ogni proteina Cas si associa a un segmento (crRNA), necessario per l'appaiamento all'acido nucleico target estraneo [3, 9]. La natura palindromica delle sequenze spaziatrici rende possibili appaiamenti intrasequenza, generando così diverse forcine, riconosciute e degradate da RNAsi specifiche. Le sequenze spaziatrici non vengono scelte a caso, ma tramite brevi sequenze di 3-5 basi, chiamate *Protospacer Adjacent Motifs* (PAM) [3, 6]; le PAM sono anche fondamentali per il taglio sito-specifico da parte di Cas9 nel sistema di tipo II (esistono tre sistemi, ma verrà discusso solo il secondo).

Entrando nel dettaglio del sistema II, l'enzima che taglia il dsDNA è Cas9 – i più utilizzati sono quelli derivati da *Streptococcus pyogenes*, ma ormai ne esistono numerose varianti, anche ingegnerizzate [6]. Cas9 necessita di due RNA complementari: il primo è il crRNA, trascritto dal *locus* CRISPR, il secondo è un *trans-activating* crRNA (tracrRNA). Il tracrRNA si appaia al pre-crRNA nelle sequenze ripetute e, in presenza di Cas9, recluta la RNAsi III, responsabile del taglio del dsRNA (*Fig. 3*). Dopo il processamento del crRNA, Cas9 lo utilizza insieme al tracrRNA per l'appaiamento sito-specifico al DNA bersaglio, assieme alle sequenze PAM (RNA guida e siti PAM sono entrambi necessari per il funzionamento del sistema) (*Fig. 3*). Due diversi domini di Cas9 tagliano il dsDNA target, ovvero HNH, che taglia il filamento complementare alla guida crRNA, e RuvC, che taglia il filamento non complementare [3, 6].

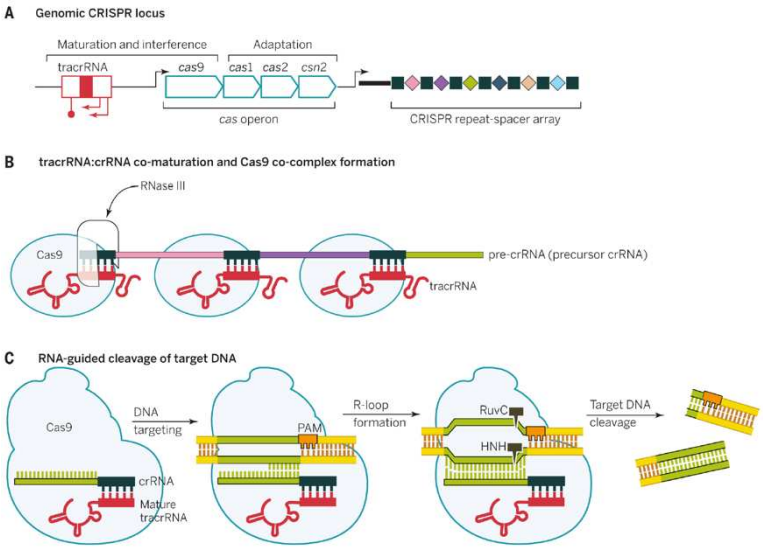

Figura 3. Biologia del sistema II CRISPR/Cas9 *in vivo*. **(A)** Operone del gene *cas*, con tracrRNA e array CRISPR. **(B)** Assemblaggio del macchinario CRISPR durante un'infezione virale in *S. pyogenes*. **(C)** Dettagli del taglio naturale del DNA associato al duplex tracrRNA:crRNA. (da Doudna e Charpentier, 2014).

Questo sistema può essere manipolato in modo da tagliare e modificare il DNA genomico anche degli eucarioti superiori, grazie alla fusione di crRNA e tracrRNA in una singola molecola guida di RNA (sgRNA) lunga circa 20 nt [3, 9]. Quando lo sgRNA è unito a Cas9, il complesso può tagliare con alta specificità un dsDNA nucleare.

Il sistema di editing può essere utilizzato in diversi modi: i più semplici sono il *gene knock-out* e le inserzioni-delezioni (indels) senza ricombinazione omologa, in cui Cas9 taglia il dsDNA in modo sito-specifico, ma non viene fornita nessuna sequenza da inserire nel DSB (*Double Strand Break*). Questo porta a una riparazione di tipo NHEJ, ovvero all'unione delle due estremità dei filamenti rotti per mezzo di sistemi di emergenza cellulari [9]. Si può effettuare anche un *knock-in*, ma in questo caso la strategia cellulare di riparazione del DNA sfruttata è la HDR, che necessita di un DNA template esogeno. La rottura del DNA, in questo secondo caso, può essere sia doppio filamento (*double strand*) che singolo filamento (*single strand*) [9]: la principale differenza risiede nel tipo di inserzione che si vuole fare, ovvero per piccole modifiche al genoma (ad esempio di singola base), può bastare una rottura a singolo filamento, mentre per inserzioni più estese è consigliata la DSB. È importante tenere in considerazione che, contrariamente alla NHEJ, la HDR è attiva solo in cellule in divisione e la sua efficienza varia molto a seconda di diversi parametri.

Esiste una nickase Cas9 (Cas9n), che può formare nick anziché tagli, sia a singola che a doppia elica: questo può essere un modo per ridurre gli off-target, in particolare per la HDR [9].

Come per i MO, anche per CRISPR/Cas9 è necessario essere a conoscenza della sequenza genica bersaglio. Se si lavora su un organismo modello sequenziato, è più facile trovare il sito bersaglio (grazie alla conoscenza dell'intero genoma) e disegnare lo sgRNA (vedi sotto). Un aspetto limitante di questa tecnologia è che le sequenze PAM sul genoma dell'ospite sono riconosciute direttamente da Cas9 (al contrario del sito bersaglio, che viene riconosciuto grazie allo sgRNA, personalizzabile) e devono essere direttamente al 3' della sequenza target [3, 9].

Questo restringe la scelta dei siti bersaglio, ma non è estremamente limitante, poiché si tratta spesso di corte sequenze, frequenti nel genoma. Esistono, inoltre, diversi ortologhi di Cas9, ognuno con una sequenza PAM specifica, aumentando così le possibilità di lavoro.
Per disegnare lo sgRNA esistono strumenti bioinformatici, come il CRISPR Design Tool, che permette contemporaneamente di (a) disegnare il costrutto sgRNA, (b) saggiare l'efficienza della modifica della sequenza target e (c) prevedere potenziali tagli off-target [9]. Gli off-target, in particolare, possono essere dati da mismatch in posizioni critiche, dalla quantità di mismatch, dalla sensibilità della guida stessa o dalle concentrazioni di Cas9 e sgRNA (il rapporto è importante per la buona riuscita dell'esperimento). Alcune piattaforme online forniscono sgRNA già progettati, rendendo la procedura ancora più semplice e veloce. Alcuni studi consigliano di disegnare due sgRNA per ogni *locus* e di testarne le efficienze *in vivo* perché, per ragioni ancora sconosciute, alcuni sgRNA non funzionano.
La possibilità di disegnare la guida, di scegliere l'ortologo più adatto della proteina Cas9 e anche la possibilità di co-iniettare più sgRNA, modificando più *loci* contemporaneamente rendono la tecnologia CRISPR/Cas9 molto flessibile, facile da usare e altamente efficiente.

Le verifiche che possono essere condotte in questo tipo di esperimenti sono varie. Il metodo più veloce e diretto di controllare che il sistema abbia agito sui giusti target è quello di eseguire una PCR con primer specifici per le sequenze modificate: se l'*editing* consiste in indels, basterà confrontare i PM dei frammenti mutanti con quelli WT, se invece è importante verificare che sia stata inserita una specifica sequenza, è necessario sequenziare i *loci*. Nel caso di NHEJ, si suggerisce di disegnare i primer ad almeno 50 bp dal sito target di Cas9, in modo da rilevare indels più lunghe [9]. Per le delezioni maggiori, i primer dovrebbero essere disegnati al di fuori della regione deleta.
È raccomandabile sequenziare anche i *loci* non-indirizzati (off-target), spesso suggeriti dai tools di progettazione degli sgRNA. Tuttavia, l'unico modo per verificare se Cas9 ha eseguito tagli al di fuori dei siti previsti (anche off-target) è quello di sequenziare l'intero genoma. Quest'ultima operazione dà la maggiore sicurezza in termini di specificità, ma è anche la più lunga e costosa. Le indels off-target (se ci sono) vengono analizzate con programmi di allineamento (es. ClustalW).
È anche possibile eseguire una qPCR per verificare il livello di espressione dei geni mutati. Infine, si può procedere con un Western Blot (se il gene codifica una proteina), così da stimare il livello di prodotto proteico finale.

Tra le differenze più evidenti tra le due tecniche, vi è senz'altro il modo di interferire con l'espressione genica: i morfolino vanno ad agire sui trascritti e costituiscono un silenziamento transiente del gene, mentre con CRISPR/Cas9 si possono creare mutanti stabili, cioè con modifiche direttamente sul DNA genomico, irreversibili ed ereditabili.

CRISPR/Cas9 richiede la maggior parte delle accortezze nella fase di design dello sgRNA, ma è altamente personalizzabile e le modifiche possono essere di altissima precisione (es. mutazioni di singola base). Il ritorno al genoma WT non è però scontato, per la natura stessa della mutazione.
I MO agiscono in diversi modi sui trascritti, a seconda di come vengono progettati, lasciando però il genoma inalterato e rendendo le modifiche non ereditabili. È bene evidenziare però che spesso si consiglia di avere organismi con alleli nulli (per la verifica degli off-target) [8]: se non sono disponibili, è necessario ottenerli con metodi di *editing* genetico, rendendo CRISPR/Cas9 la scelta più pratica. I MO, in generale, hanno più possibili effetti secondari (come la già citata attivazione di siti di *splicing* criptici), rendendo il loro effetto leggermente meno prevedibile.

In generale, non si può affermare che esista un metodo assolutamente migliore di un altro: la valutazione e la scelta finale dipendono dal contesto, dall'esperimento, dalle necessità degli operatori e da numerose altre variabili. In questo caso, entrambi i metodi si sono rivelati validi, ma un grande vantaggio di CRISPR/Cas9 è la possibilità di mantenere linee transgeniche, grazie all'ereditarietà della modifica. Se si vuole condurre l'esperimento su più generazioni, senz'altro CRISPR è da preferire ai MO. Oltre a permettere di studiare gli effetti delle modifiche genetiche per tempi prolungati, se e in che modo queste vengono ereditate, l'*editing* genetico rende necessarie operazioni dirette sugli embrioni della sola generazione F0. Al contrario, lavorando esclusivamente con MO, sarebbe indispensabile iniettarli in ogni embrione su cui si vogliono vedere gli effetti del *knock-down*.

La possibilità di ereditare le modifiche genetiche permette implicitamente di incrociare individui con diversi alleli, ottenendo eterozigoti, omozigoti e WT in diverse combinazioni (se sono coinvolti più geni, come nel nostro caso [1]): ciò consente di osservare gli effetti di differenti genotipi ottenuti da incroci adeguati. Col mantenimento delle linee transgeniche per più generazioni è anche possibile studiare gli effetti delle mutazioni nel tempo e il loro tipo di ereditarietà.

Infine, con CRISPR/Cas9 ci sono più modi di intervenire sul genoma e sull'espressione genica, mentre coi MO è possibile solo l'interferenza. CRISPR è anche una tecnica più precisa e con meno off-target, oltre a offrire più possibilità di gestire e prevedere questi ultimi, che restano invece più problematici per i MO.

2.2 Kozol et al. (2015) bersagliano l'mRNA di *syngap1b* con MO

Kozol e collaboratori hanno fatto studi di *behavior* approfonditi su zebrafish morfanti, portando a termine un lavoro preciso e accurato sotto diversi aspetti. Per completezza, specifichiamo che il gruppo ha studiato fenotipi comportamentali e morfogenetici interferendo sia con *syngap1* che con *shank3* (su un gruppo di individui è stato anche eseguito *knock-down* su *syngap1b* e *shank3a* contemporaneamente, per confermare l'esistenza di interazioni tra i due geni e la possibilità di iniettare minor quantità di ciascuno dei due MO [2]).

Innanzitutto, il gruppo ha studiato variazioni fenotipiche iniettando alternativamente per i 4 geni target (e per loro diverse combinazioni) diverse concentrazioni di MO corrispondenti[2] – in questo elaborato ci concentreremo però solo su *syngap1*. Questo passaggio ha permesso di constatare che i MO per *syngap1a* hanno bassa efficienza e che le concentrazioni a cui potrebbero causare fenotipi interessanti sono tossiche. Di conseguenza, il gruppo ha lavorato esclusivamente su *syngap1b*. Inoltre, i MO per *syngap1a* bersagliano una giunzione esone-introne, mentre quelli per *syngap1b* una giunzione introne-esone: la seconda modalità di *targeting* è più vantaggiosa anche secondo quanto sostiene Morcos (2007), poiché evita l'attivazione di siti criptici di *splicing* alternativo [8].

Studi sull'alterazione dei livelli di espressione dei geni sono stati condotti con RT-qPCR: l'RNA totale su cui eseguire le analisi è stato estratto a 2, 5, 8, 12, 15, 24, 36, 48, 72, 96 hpf, in modo da avere il livello di espressione dei geni nel corso del tempo e da poter confrontare i morfanti coi WT [2]. Il gene *housekeeping* di riferimento era il fattore di allungamento *eef1a1/1*. Oltre all'andamento temporale dell'espressione (ottenuto grazie al confronto di livelli di mRNA a vari stadi di sviluppo), è stato verificato il corretto funzionamento dei MO tramite elettroforesi su cDNA dei geni target. Grazie al confronto col controllo, si è potuto osservare che i morfanti avevano mRNA più leggero rispetto ai controlli (a causa di codoni di stop prematuri), validando dunque la tecnica (*Fig. 4A* e *4C*).

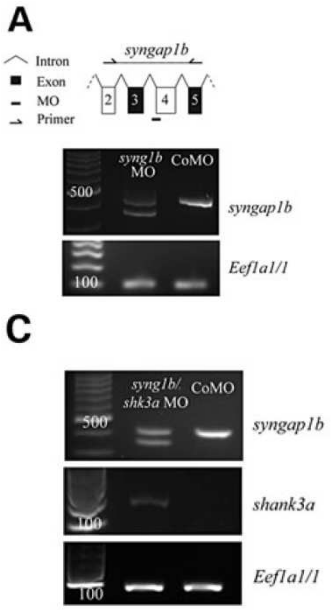

Figura 4. MO inibitori di *splicing*, che puntano alla giunzione introne-esone. RT-PCR di campioni da individui 48 hpf per verificare l'efficacia dei MO contro **(A)** *syngap1b* e **(C)** *syngap1b*/*shank3a*. CoMO: *Control MO*. Iniezioni **(A)** di MO *syngap1b* (10 ng, *n* = 131) e **(C)** di MO *syngap1b*/*shank3* (5/4 ng, *n* = 121) (da Kozol et al., 2015).

L'iniezione di MO è stata eseguita allo stadio di singola cellula, in modo tale da ottenere una migliore distribuzione della molecola nell'individuo adulto. I MO sono anche stati diluiti con colorante fast green all'1%, in modo da poterli seguire più facilmente e per selezionare più velocemente gli individui in cui l'iniezione è andata a buon fine.

Infine, lo studio ha valutato il fenotipo "*cell-death*", perché la morte cellulare spesso si presenta come effetto di tossicità indotta da MO [2]. Per capire se si trattasse di un processo apoptotico gene-specifico oppure p53-dipendente, sono stati iniettati su individui diversi (assieme ai MO) (a) mRNA di *SYNGAP1* umano (in modo da non essere complementare ai MO) e (b) MO contro p53: l'mRNA umano ristabiliva il fenotipo WT, mentre i MO per p53 no. Gli stessi test sono stati condotti per *shank3*, con risultati opposti; ciò significa che alterazioni su questi geni portano a fenotipi strutturali simili, ma tramite vie di segnale differenti.

[2] I MO sono stati disegnati sulla base delle sequenze d'interesse annotate su Ensembl.

In questo studio non sono stati iniettati MO complementari a più punti degli mRNA target e non sono stati fatti Western Blot per verificare la concentrazione proteica finale. Tuttavia, sono stati estratti gli mRNA, è stata fatta una RT-PCR e il cDNA è stato poi sequenziato, per verificare se i morfolino avessero agito nel modo giusto. Questo passaggio rende trascurabile l'analisi tramite Western Blot, ma è da sottolineare che i test di interferenza sono stati condotti solo sui siti bersaglio (previsti).

Per verificare che tutte le altre sinapsi dei motoneuroni fossero funzionanti, è stato iniettato tetrametilrodammina-αBungarotissina negli zebrafish per visualizzare i recettori per l'acetilcolina (AChR), confermando così che i motoneuroni spinali non erano intaccati dall'interferenza genica da MO.

Come sostiene Morcos nel suo studio sui MO, sarebbe anche buona norma fare controlli su individui con doppi alleli nulli, per verificare se fenotipi interessanti osservati nei morfanti siano dovuti effettivamente a interferenza con gli mRNA target o ad altri meccanismi non previsti [8].

La mancata verifica di ulteriori off-target può lasciare aperta la domanda sulla causalità del fenotipo osservato, ma la varietà e la robustezza dei test condotti validano ugualmente lo studio. Inoltre, studi precedenti avevano già osservato fenotipi simili correlati a mutazioni su *syngap1*, a ulteriore supporto delle indagini di Kozol e collaboratori.

Oltre agli off-target, il gruppo ha controllato se l'interferenza con uno dei geni bersaglio variasse l'espressione degli altri: riduzioni di espressione di *syngap1* diminuiva i livelli di tutti gli altri geni in analisi (si ricordi che questo studio è stato condotto anche su *shank3*).

Per quanto riguarda i controlli sui WT nei test motori, in alcuni individui sono stati iniettati CoMO (*Control MO*), con effetto nullo: questi sono stati presi come punto di riferimento per alterazioni comportamentali e strutturali (che avvengono perlopiù durante lo sviluppo embrionale). A livello comportamentale, si sono studiate variazioni nella fuga in risposta a stimolo tattile: le reazioni sono state scomposte in velocità di fuga e durata dei *bout* (colpi di coda).

Infine, per approfondire il ruolo del bilanciamento tra eccitazione e inibizione neuronale, sono state quantificate le sinapsi eccitatorie e inibitorie in proencefalo, mesencefalo e rombencefalo, eseguendo crio-sezioni trasversali di queste aree. Le sinapsi eccitatorie sono state misurate utilizzando la linea transgenica stabile vglut (*vescicular glutamate transporter*), caratterizzata dall'espressione di un marcatore fenotipico sotto il controllo del promotore del gene *vglut*. Le sinapsi inibitorie sono state invece quantificate tramite *immunostaining*, con anticorpi complementari ai trasportatori GABA.

Come già accennato, inoltre, sono state visualizzati gli AChR, per escludere che le risposte motorie modificate fossero dovute a problemi nella giunzione neuromuscolare.

2.3 Sumathipala et al. (2024) generano mutanti *syngap1a* e *1b* mediante la tecnica CRISPR/Cas9

L'approccio di Sumathipala e collaboratori è radicalmente diverso da quello del gruppo di Kozol: essi, infatti, hanno modificato il DNA di zebrafish con la tecnica CRISPR/Cas9, già descritta al paragrafo 2.1.

L'iniezione dello *small guide-RNA* (sgRNA, complementare alternativamente a *syngap1a* o *syngap1b*) e di Cas9 è stata eseguita su zigoti in un rapporto 1:5 (l'individuazione del giusto rapporto tra sgRNA e Cas9 è molto importante per la buona riuscita dell'esperimento [9]).

Per disegnare al meglio lo sgRNA e per determinare al meglio le isoforme su cui agire, sono state studiate le sequenze di mRNA di *syngap1* registrate sul database NCBI. I risultati ottenuti sono stati ricercati sui database *Expressed Sequence Tags* (EST) e *Transcriptome Shotgun Assembly* (TSA), in modo da individuare varianti di *splicing*; queste ultime sono state poi allineate con BLAST al genoma di zebrafish, in modo da identificare regioni uniche, comuni e varianti di *splicing* su cui agire [1].

Questo passaggio ha permesso di escludere a priori molteplici off-target, poiché maggiore è l'unicità della sequenza, minore è la probabilità di appaiamento dello sgRNA a siti diversi dal target.

Per genotipizzare gli individui, i primer per PCR sono stati selezionati sulla base delle regioni target di Cas9, mentre quelli per la qPCR (per quantificare l'espressione genica di *syngap1a* e *1b*) sono stati presi dal lavoro di Kozol et al. (2015). Questa analisi è anche servita a quantificare il *nonsense-mediated mRNA decay* nei mutanti (in confronto ai WT) e, anche in questo caso, il gene *house-keeping* era *eef1a1/1* [1] (*Fig. 5*).

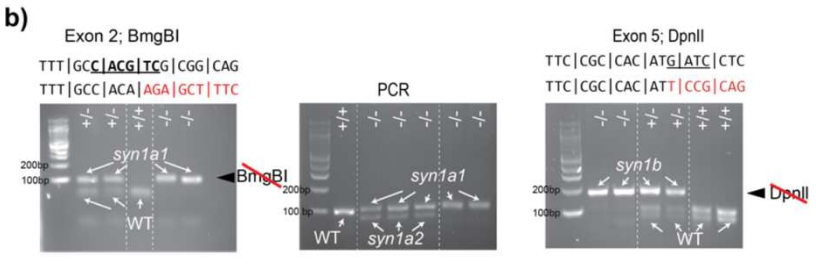

Figura 5. Genotipizzazione di tutti gli alleli di zebrafish mutanti *syngap1a* e *syngap1b*. In *syngap1a1*, il sito di restrizione per BmgBI è distrutto. *syngap1a2* ha uno *shift* di 22 bp (delezione). In *syngap1b* il sito di restrizione per DpnII è perso (da Sumathipala et al., 2024).

Per il sequenziamento del DNA ottenuto dalla genotipizzazione degli zebrafish, il gruppo si è affidato a un ente esterno.

Siccome le isoforme di *syngap1a* e *1b* sono molteplici, per fare in modo di colpirle tutte, Sumathipala e collaboratori hanno progettato uno sgRNA complementare ai primi esoni. Procedendo così, sono state ottenute proteine troncate molto precocemente, prevenendo la sintesi di varianti che avrebbero interferito coi risultati.

A ogni individuo veniva iniettato alternativamente sgRNA complementare a *syngap1a* o *syngap1b* per minimizzare la competizione tra RNA guida. In seguito, individui delle generazioni successive sono stati incrociati per ottenere i mutanti desiderati (doppi eterozigoti e doppi omozigoti, d'ora in poi denominati

rispettivamente *syngap1ab*$^{+/-}$ e *syngap1ab*$^{-/-}$). Ciò ha permesso di sequenziare la F1 e capire esattamente come e in che punto il gene veniva alterato: *syngap1a* ha subito un'inserzione di 7 bp (*syngap1a1*) o una delezione di 22 bp (*syngap1a2*), mentre *syngap1b* una delezione di 14 bp [1] (*Fig. 5*). Tutte le proteine sono risultate precocemente troncate a causa di codoni di stop prematuri indotti dalle mutazioni.

Infine, per i fenotipi *loss of function* sono stati testati mRNA e proteine (RT-PCR e Western Blot): in entrambi i casi i livelli erano molto ridotti, validando i modelli per studi di aploinsufficienza di questo gene.

Un difetto di questo studio è il mancato sequenziamento di *loci* off-target, che non vengono nominati. Probabilmente l'individuazione di corte regioni uniche nelle isoforme di *syngap1a* e *1b* rende poco probabile l'azione off-target del sistema CRISPR/Cas9; tuttavia, è buona norma escludere questa possibilità.
Si noti però che uno dei passaggi iniziali per l'individuazione dei giusti target per gli sgRNA è stato l'allineamento delle isoforme con l'intero genoma di zebrafish (UCSC Genome Browser), che ha permesso di escludere gran parte degli off-target a priori.

In ogni caso, le verifiche sono state numerose e accurate (RT-qPCR, Western Blot, sequenziamento di DNA e cDNA). Questo, assieme alle informazioni precedenti di studi su mutanti *syngap1*, conferisce consistenza ai dati ottenuti. Inoltre, questo tipo di modifica genetica è generalmente molto affidabile e preciso.

Non sono state nominate sequenze PAM, molto importanti per il corretto funzionamento di Cas9, ma visti i risultati ottenuti, devono essere state prese in considerazione durante la fase di design degli sgRNA o, almeno, durante la scelta dell'isoforma della proteina Cas9 più adatta (come suggeriscono Ran et al., 2014).

I WT (*syngap1ab*$^{+/+}$) sono stati presi come riferimento per il confronto di mutazioni nella sequenza genica, ma anche per gli esperimenti comportamentali.

Anche il gruppo di Sumathipala ha studiato risposte motorie, ma stavolta gli stimoli sono stati uditivi e visivi.

Individui con diverse combinazioni alleliche sono stati studiati per quanto riguarda la sopravvivenza larvale e la distanza percorsa in contesto luci accese/spente (VMR, *Visual Motor Response*) [1] – questo, ricordiamo, è stato possibile proprio grazie alla natura della modifica tramite CRISPR/Cas9 e ai successivi incroci tra portatori di determinati alleli *syngap1ab*. I risultati ottenuti sembrano suggerire che i diversi tassi di sopravvivenza di mutanti *syngap1b* siano correlati a sbilanciamenti funzionali tra *syngap1a* e *1b*. Tuttavia, il gruppo ha approfondito solo «mutazioni bilanciate in eterozigosi sia su *syngap1a* sia su *syngap1b*, per rappresentare al meglio la condizione di aploinsufficienza nei mammiferi» [1].

Capitolo 3. Discussione dei risultati

I lavori qui in analisi hanno entrambi analizzato risposte motorie (di nuoto) a stimoli di diversa natura. Questa scelta è stata condotta dalla possibilità (a) di standardizzare gli stimoli e le registrazioni e (b) di studiare funzioni precoci del sistema nervoso di zebrafish, grazie al repertorio sempre più preciso di comportamenti locomotori stereotipati [4, 10]. Nel repertorio, inoltre, sono presenti associazioni a circuiti neuronali ben caratterizzati, il che rende ancora più facile studiare alterazioni dei circuiti stessi e collegarle a comportamenti inusuali.
I comportamenti motori di zebrafish, inoltre, sono altamente stereotipati: deviazioni dagli standard, dunque, sono facili da riconoscere e da studiare. Come suggerisce Stewart, zebrafish agisce in seguito al processamento di informazioni sensoriali, caratteristica che consente di riprodurre più volte lo stesso comportamento e migliorare la qualità dei dati [10].

Entrambi gli studi sono giunti alla conclusione che alterazioni della proteina Syngap1 sono correlate a iperattività contesto-dipendente, ma gli approfondimenti successivi sono diversi. In breve, l'approccio di Kozol e collaboratori è più strutturale e morfogenetico, mentre quello di Sumathipala et al. è più funzionale. È stato soprattutto questo diverso focus che ha spinto i ricercatori a muoversi in direzioni differenti.

3.1 Kozol et al. correlano morfogenesi alterata e iperattività in modelli di zebrafish ottenuti con MO

Kozol et al. (2015) hanno indotto la fuga di zebrafish (mutati e non) tramite stimolo tattile. I risultati sono stati subito evidenti: i CoMO avevano risposte produttive (sia in termini di velocità, sia in termini di *bout*), mentre i morfanti mostravano comportamenti convulsivi spontanei e *bout* improduttivi (*Fig. 6*) [2].

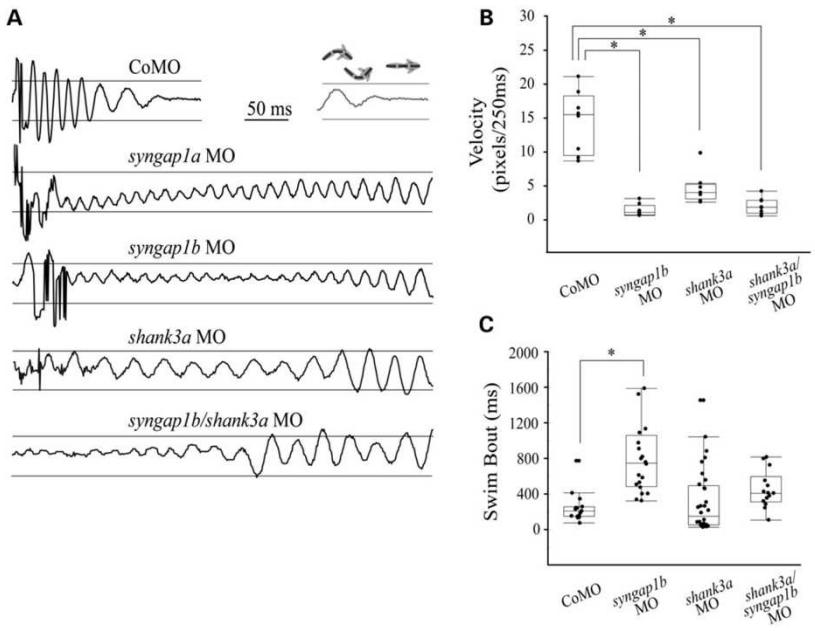

Figura 6. Risposte di fuga (72 hpf) dal lavoro di Kozol et al. (2015). Per completezza, sono inseriti anche i risultati di morfanti *shank3a* e doppi morfanti *syngap1b* e *shank3a*. **(A)** Schematizzazione delle risposte di fuga dei vari individui (registrati tramite una videocamera ad alta velocità). **(B)** Velocità di fuga; per ogni gruppo di morfanti $n = 8$. **(C)** durata *bout* motori: *syngap1b* ($n = 20$), CoMO ($n = 15$). Asterisco *P < 0.01.

Minore durata dei *bout* e maggiore velocità indicano una risposta di fuga efficace e veloce.

I risultati suggeriscono una iperattività dei pesci morfanti, causata probabilmente da ipereccitabilità del sistema nervoso. In particolare, il comportamento natatorio in zebrafish è innescato da neuroni glutamatergici discendenti dal rombencefalo, fatto che ha indotto il gruppo ad approfondire questi particolari circuiti neuronali [2].

Come anticipato, lo studio si è concentrato maggiormente su modifiche nella morfogenesi e nella struttura del cervello: per analizzare più nel dettaglio l'ipereccitabilità dei neuroni nei circuiti motori d'interesse, il gruppo ha quantificato le sinapsi eccitatorie e inibitorie. Dall'analisi di sezioni di cervello, si è evinto che c'era una significativa riduzione di sinapsi GABAergiche nei neuroni del mesencefalo e del rombencefalo e di sinapsi glutamatergiche nei neuroni del rombencefalo [2]. Questi risultati possono potenzialmente spiegare l'ipereccitabilità dei morfanti e i comportamenti di nuoto atipici (in questo caso, dovuti a stimoli tattili).

Per escludere che le osservazioni sui morfanti fossero dovute a modifiche degli AChR, i ricercatori hanno visualizzato le sinapsi alla giunzione neuromuscolare con tetrametilrodammina-αBungarotissina. In effetti, si è osservato che i motoneuroni formavano sinapsi inalterate con le cellule postsinaptiche, a dimostrazione del fatto che i motoneuroni spinali non presentavano anomalie nei morfanti [2].

Lo sbilanciamento tra eccitazione e inibizione (EI), secondo Kozol et al., poteva essere tra le cause dell'ipereccitabilità contesto-dipendente degli zebrafish morfanti, dovuta a un'eccitabilità aumentata o da una incapacità di inibire correttamente i neuroni secernenti neurotrasmettitori eccitatori e inibitori di proencefalo, mesencefalo e rombencefalo. In effetti, su *H. sapiens*, analisi *post mortem* di individui con ASD hanno riscontrato alterati processi glutamatergici e GABAergici in mini-colonne corticali (probabilmente coinvolte nei processi fondamentali di calcolo della corteccia cerebrale) e una ridotta produzione di GABA [2].

Lo sbilanciamento EI non è però l'unica possibile causa dell'iperattività. Infatti, il gruppo di ricerca suggerisce che l'ipereccitabilità neuronale sia dovuta ad alterazioni nello sviluppo di particolari aree del cervello, controllato da *syngap1*. In particolare, come anticipato nel Capitolo 1, aploinsufficienze del gene causano una significativa riduzione delle sinapsi GABAergiche nel mesencefalo e nel rombencefalo, mentre di quelle glutamatergiche solo nel rombencefalo. Questi dati giustificano l'ipotesi di ipereccitabilità del mesencefalo nei morfanti, suggerendo anche che, nei soggetti affetti da ASD, i comportamenti iperattivi siano dovuti ad alterazioni o ritardi nello sviluppo di regioni specifiche del cervello.

In conclusione, oltre ad avere un grande impatto sulla funzione sinaptica, mutazioni di *SYNGAP1* (e *SHANK3*) determinerebbero modifiche strutturali, a loro volta correlate alla malattia. I periodi embrionale e neonatale sono dunque cruciali nel contesto della ASD.

3.2 Sumathipala et al. approfondiscono le alterazioni funzionali dei modelli mutati ottenuti con CRISPR/Cas9

Per questa ricerca, Sumathipala et al. (2024) hanno approcciato il problema da un punto di vista diverso da quello di Kozol et al., portandoli ad approfondire altri aspetti rispetto al primo gruppo.

Sfruttando la tecnica di *editing* CRISPR/Cas9, sono stati ottenuti mutanti con diverse combinazioni alleliche nel corso di diverse generazioni e sono stati mantenuti principalmente i portatori di mutazioni più interessanti. Come già specificato, le ricerche più approfondite sono state condotte su eterozigoti bilanciati (si ricordi che *syngap1* è duplicato in zebrafish, dunque con bilanciati si intendono mutanti doppi eterozigoti e doppi omozigoti). Nel corso della ricerca sono comunque stati osservati i tassi di sopravvivenza di tutti i genotipi (*Fig. 7*), portando alla luce che *syngap1b* sembra essere più importante per la sopravvivenza larvale rispetto a *1a* [1]. Oltre a questo aspetto, per i diversi genotipi è stata studiata la distanza percorsa in contesti ad alto (buio) e basso (luce) *arousal*, facendo particolare attenzione al comportamento dei WT, dei doppi eterozigoti e dei doppi omozigoti recessivi. Kozol e collaboratori non sarebbero mai riusciti a raccogliere questo tipo di dati, poiché essi non hanno lavorato direttamente sul genoma, ma hanno ottenuto interferenze sugli mRNA.

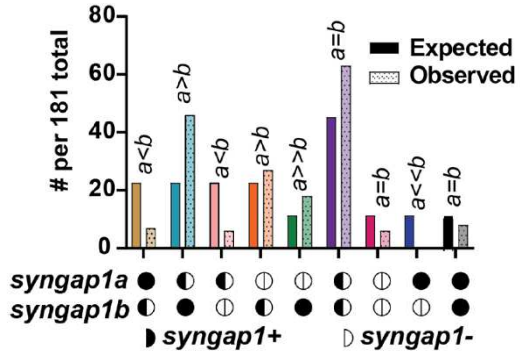

Figura 7. Tassi di sopravvivenza attesi e osservati per tutte le possibili combinazioni alleliche *syngap1a* e *1b*, risultati da *in-cross* di *syngap1ab*$^{+/-}$ (n = 181) (da Sumathipala et al., 2024).

È chiaro ora come i differenti approcci permettono di approfondire aspetti diversi di una medesima problematica. Sumathiapala et al., concentrandosi sul gene in sé e sulla sua funzionalità alterata, hanno studiato l'ereditarietà, le isoforme e come quelle individuate potessero essere paragonate alle mutazioni umane, le loro anomalie strutturali e funzionali, nonché le già nominate diverse combinazioni alleliche per quanto riguarda vitalità e locomozione alla luce e al buio [1].

Anche per questa ricerca è stata valutata l'iperattività dei mutanti tramite saggi di locomozione; gli stimoli sono stati acustici (ASR, *Acoustic Startle Response*) e visivi (VMR, *Visual Motor Response*). Durante i test acustici, è stata studiata anche la capacità dei pesci di abituarsi a stimoli ripetuti ad alta intensità e frequenza, evidenziando una *habituation* normale nei mutanti.

Il test ASR è stato suddiviso in 5 fasi, con stimoli a diversa intensità e frequenza: (1, 2) 10 colpi a media e alta intensità rispettivamente, 20 s ISI (*Inter-Stimulus Interval*), (3) *habituation*, 30 colpi ad alta intensità e frequenza (1 s ISI), (4) riposo 3 min, (5) ripetizione della fase 2 (vedi *Fig. 8* per la schematizzazione del test e dei risultati).

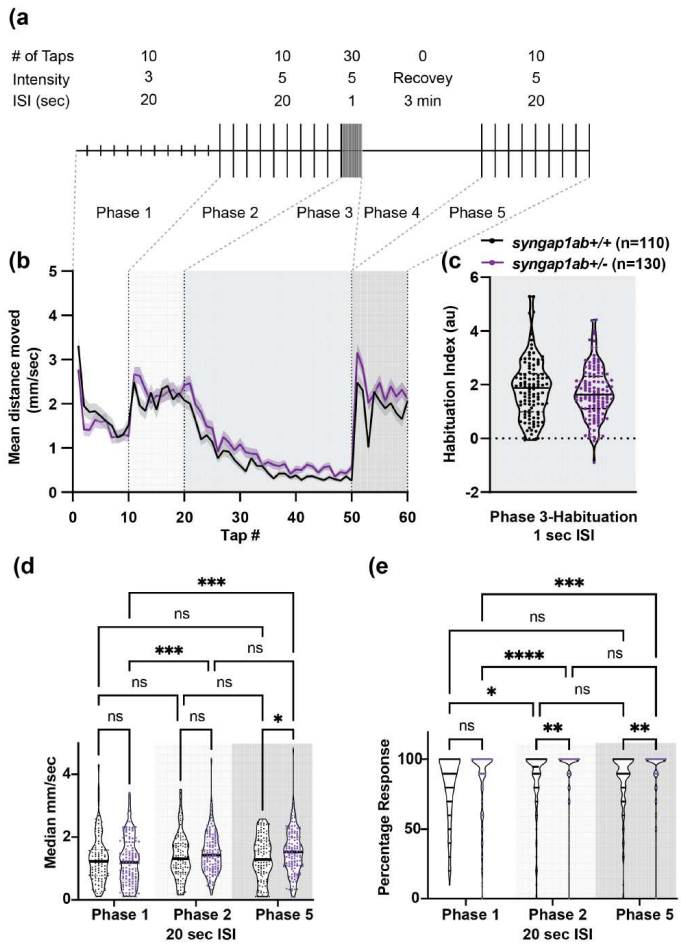

Figura 8. **(a)** Schematizzazione degli stimoli durante il test ASR. **(b, c)** Distanze medie di *syngap1ab*$^{+/-}$ (*n* = 130) e WT (*n* = 110) e indice di *habituation*. L'indice è calcolato sottraendo la distanza media mossa post-*habituation* (taps 41-50) da quella pre-*habituation* (taps 11-20). **(d, e)** Distanza media mossa e probabilità di risposta agli stimoli. Asterischi *P < 0.05; **P < 0.01; ***P < 0.001; ****P < 0.0001 (da Sumathipala et al., 2024).

I mutanti *syngap1ab*$^{+/-}$ mostrano una risposta consistentemente elevata a stimoli ad alta intensità (fasi 2, 5) rispetto ai WT. Inoltre, in queste condizioni, i mutanti si muovono per maggiori distanze mentre i WT non esibiscono sostanziali differenze tra le fasi 1, 2 e 5 (media e alta intensità degli stimoli) (*Fig. 8*) [1]. Anche la probabilità di muoversi con stimoli più intensi aumenta per le larve *syngap1ab*$^{+/-}$ (*Fig. 8*). Insomma, i mutanti doppi eterozigoti, con stimoli più forti, sono più inclini a muoversi più velocemente e per distanze maggiori: questo risultato è in linea con quello che anche Kozol et al. avevano sospettato, ovvero che i *syngap1ab*$^{+/-}$ hanno stati di *arousal* basali più alti rispetto ai WT.

La VMR ha invece evidenziato che i mutanti mostrano una pronunciata iperattività in contesti a basso *arousal* (luce) [1]. Il test consisteva nell'alternanza improvvisa di luce e buio per 4 cicli e nella misurazione della distanza totale mossa ogni 30 s (*Fig. 9*). Sia per *syngap1ab*$^{+/-}$ che per *syngap1ab*$^{-/-}$ si sono riscontrati aumenti nell'attività locomotoria durante il passaggio improvviso da luce a buio, ma durante il periodo di luce spenta, *syngap1ab*$^{+/-}$ ha mostrato la maggiore attività (anche se, tra i 5 batch indipendenti su cui sono stati condotti questi esperimenti, si è evidenziata una certa variabilità) [1].

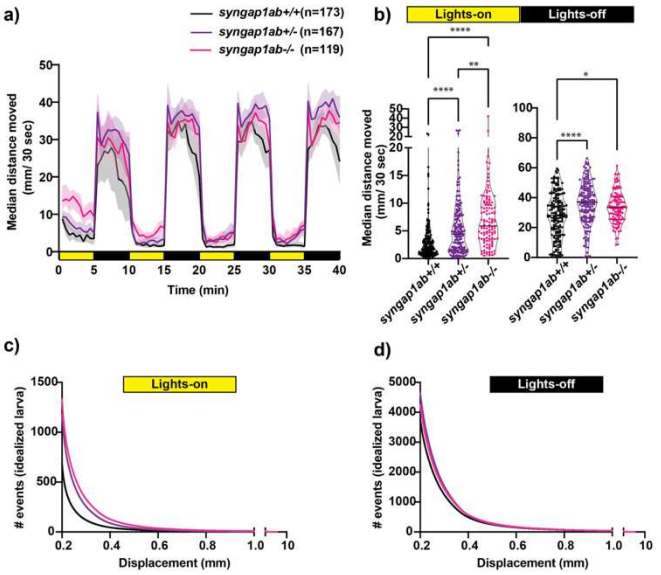

Figura 9. L'iperattività dei mutanti è più pronunciata rispetto ai WT durante i cicli *lights-on* (risultati medi dei 5 batch su cui sono stati condotti gli esperimenti), con WT: n = 173; *syngap1ab*$^{+/-}$: n = 167; *syngap1ab*$^{-/-}$: n = 119. **(a)** Distanza media mossa da larve 6 dpf (mm/30 s), con alternanza luce-buio ogni 5 min. **(b)** Distanza media riassuntiva nei cicli di luce e buio. **(c, d)** Distribuzione degli spostamenti di una larva ideale; grafici generati riunendo tutti gli eventi di spostamento (WT: n = 119135; *syngap1ab*$^{+/-}$: n = 196594; *syngap1ab*$^{-/-}$: n = 158443). Asterischi *P < 0.05; **P < 0.01; ***P < 0.001; ****P < 0.0001 (da Sumathipala et al., 2024).

Durante la fase di luci accese, l'iperattività era consistente tra tutti i batch di larve ed era proporzionale al numero di alleli mutati di *syngap1a* e *1b* (*syngap1ab*$^{-/-}$ si è mosso di più). Le differenze tra i vari genotipi, in questo contesto, erano molto più pronunciate rispetto al contesto ad alto *arousal* (buio). Alla luce, cioè, i mutanti omozigoti ed eterozigoti hanno mostrato *dwell times* più brevi (tempo tra un *bout* e l'altro) e maggiori movimenti rispetto ai WT.

In conclusione, sembra che i mutanti si comportino alla luce (*low arousal setting*) come i WT al buio (*high arousal setting*), dimostrando ancora una volta che mutazioni sul gene siano causa di uno stato eccitatorio innalzato [1, 2] – in questo senso i mutanti sono ipereccitabili in modo contesto-dipendente.

Capitolo 4. Confronto conclusivo

Come si è potuto vedere da questo elaborato, i due studi hanno approfondito aspetti diversi di una stessa problematica. Inoltre, Kozol et al. hanno studiato anche le interazioni e le causalità legate a *shank3ab*, un gene correlato alla ASD.
Entrambi gli studi sono concordi nell'affermare che un disequilibrio EI sia probabilmente legato (se non addirittura tra le cause principali) all'iperattività contesto-dipendente. Gli individui portatori di mutazioni su *SYNGAP1* (anche umani) mostrano uno stato di *arousal* innalzato rispetto alla norma e questo potrebbe essere causa dell'ipereccitabilità neuronale in circuiti che controllano determinati comportamenti. Si ricordi, infatti, che un'aploinsufficienza di SYNGAP1 porta all'eccessiva attivazione di Ras nei neuroni postsinaptici glutamatergici e all'aumentato inserimento di AMPAR nella membrana cellulare, che a sua volta è causa di un'eccitabilità basale più elevata [4].
L'aploinsufficienza di SYNGAP1 causa, anche in topi e umani, alterazioni nelle risposte sensoriali in modo contesto-dipendente, con impatti su *habituation* e su comportamenti inclini al rischio [1, 7].

Sumathipala et al. hanno approfondito gli aspetti legati ai geni *syngap1a* e *1b* e alle isoforme da esse derivanti; hanno condotto così una prima caratterizzazione su zebrafish, riuscendo a individuare il corrispondente dell'isoforma α1 di mammifero e le anomalie nella sequenza amminoacidica.

Kozol et al. hanno preferito un approccio più ampio, considerando anche un altro gene correlato alla ASD (*SHANK3*), cercando le cause delle alterazioni comportamentali nella malformazione cerebrale in periodo embrionale e perinatale. Con questo approccio, i ricercatori hanno proposto una nuova interpretazione riguardo l'ipereccitabilità dovuta a mutazioni su *SYNGAP1* (e *SHANK3*): oltre allo sbilanciamento EI (spesso sottovalutato a causa degli attacchi epilettici, presenti nel 25-30% di individui con ASD [2]), essi hanno avanzato l'ipotesi di un ruolo rilevante nella struttura cerebrale in sé. La morfogenesi cerebrale, cioè, sarebbe fondamentale per la costruzione di circuiti cruciali che, quando interrotti, contribuirebbero al manifestarsi della ASD.

Il gruppo di Sumathipala, insomma, si è focalizzato più sulla funzione di SYNGAP1 nei neuroni postsinaptici glutamatergici, mentre quello di Kozol nel suo ruolo durante la morfogenesi.
Probabilmente, anche se Sumathipala e collaboratori si sono concentrati quasi esclusivamente su *SYNGAP1*, verificare lo stato delle sinapsi GABAergiche, glutamatergiche e quelle della giunzione neuromuscolare (come invece hanno fatto Kozol et al.) sarebbe stato un esperimento interessante.

I risultati degli studi, in ogni caso, conducono nella stessa direzione: correlazione tra ASD e iperattività contesto-dipendente, correlazioni tra mutazioni su *SYNGAP1* e iperattività, morfogenesi alterata e alto rischio di presentare la patologia [4], nonché comportamenti simili (improduttivi) in seguito a particolari stimoli sensoriali.

Un singolo studio non può analizzare tutte le sfaccettature di una malattia come la ASD, vista la sua natura multifattoriale, poligenica e la sua singolarità su ogni paziente. Forse consapevoli di alcune limitazioni del loro studio, Kozol et al., in chiusura all'articolo, suggerivano infatti ai futuri ricercatori di ottenere mutanti stabili di *SYNGAP1* (e *SHANK3*), per approfondire le conseguenze a lungo termine di disfunzioni dello sviluppo cerebrale. Sumathipala et al., supportati dall'avanzamento tecnologico di una tecnica efficace e semplice di *editing* genetico come CRISPR/Cas9, hanno colto la sfida, proseguendo le ricerche su *SYNGAP1* in particolare e sulle disfunzioni a esso collegate.

In futuro, la ricerca potrà sicuramente concentrarsi su altri aspetti e altri sintomi correlati a disfunzioni di *SYNGAP1*, perché queste non sono causa di sintomi esclusivamente tipici della ASD, ma di diverse problematiche in differenti distretti corporei. Ad esempio, possono manifestarsi epilessie resistenti ai trattamenti, disturbi del sonno e problemi gastrointestinali [1, 2, 4, 7], che suggeriscono un coinvolgimento di SYNGAP1 in svariate funzioni e, probabilmente, altrettanti processi biologici. Un altro esempio può essere il coinvolgimento di SYNGAP1 nel processamento sensoriale: alcuni gruppi di ricerca stanno già lavorando su questo aspetto, come quello di Carreño-Muñoz, dell'università di Montréal.

Visto il numero e la diversità degli effetti di aploinsufficienze di *SYNGAP1*, risulta evidente che gli autori dei due articoli non avrebbero potuto approfondire tutte le problematiche connesse al gene. Entrambi si sono concentrati su aspetti relativi alla ASD, analizzando più in profondità i lati che ritenevano inerenti alle domande che si erano posti.

Per concludere, Sumathipala et collaboratori hanno fatto grandi passi in avanti per quanto riguarda la caratterizzazione di *syngap1a* e *1b* su zebrafish e per la determinazione di linee mutanti stabili, validando definitivamente la ricerca su zebrafish in questo campo.

Capitolo 5. Bibliografia

(1) Sumathipala, S. H., Khan, S., Kozol, R. A., Araki, Y., Syed, S., Huganir, R. L., & Dallman, J. E. (2024). Context-dependent hyperactivity in *syngap1a* and *syngap1b* zebrafish models of SYNGAP1-related disorder. *Frontiers in molecular neuroscience*, *17*, 1401746. https://doi.org/10.3389/fnmol.2024.1401746.

(2) Kozol, R. A., Cukier, H. N., Zou, B., Mayo, V., De Rubeis, S., Cai, G., Griswold, A. J., Whitehead, P. L., Haines, J. L., Gilbert, J. R., Cuccaro, M. L., Martin, E. R., Baker, J. D., Buxbaum, J. D., Pericak-Vance, M. A., & Dallman, J. E. (2015). Two knockdown models of the autism genes SYNGAP1 and SHANK3 in zebrafish produce similar behavioral phenotypes associated with embryonic disruptions of brain morphogenesis. *Human molecular genetics*, *24*(14), 4006–4023. https://doi.org/10.1093/hmg/ddv138.

(3) Doudna, J. A., & Charpentier, E. (2014). Genome editing. The new frontier of genome engineering with CRISPR-Cas9. *Science (New York, N.Y.)*, *346*(6213), 1258096. https://doi.org/10.1126/science.1258096.

(4) Gamache, T. R., Araki, Y., & Huganir, R. L. (2020). Twenty Years of SynGAP Research: From Synapses to Cognition. *The Journal of neuroscience: the official journal of the Society for Neuroscience*, *40*(8), 1596–1605. https://doi.org/10.1523/JNEUROSCI.0420-19.2020.

(5) Iannuccelli, M., Vitriolo, A., Licata, L., Lo Surdo, P., Contino, S., Cheroni, C., Capocefalo, D., Castagnoli, L., Testa, G., Cesareni, G., & Perfetto, L. (2024). Curation of causal interactions mediated by genes associated with autism accelerates the understanding of gene-phenotype relationships underlying neurodevelopmental disorders. *Molecular psychiatry*, *29*(1), 186–196. https://doi.org/10.1038/s41380-023-02317-3.

(6) Jinek, M., Chylinski, K., Fonfara, I., Hauer, M., Doudna, J. A., & Charpentier, E. (2012). A programmable dual-RNA-guided DNA endonuclease in adaptive bacterial immunity. *Science (New York, N.Y.)*, *337*(6096), 816–821. https://doi.org/10.1126/science.1225829.

(7) Kilinc, M., Creson, T., Rojas, C., Aceti, M., Ellegood, J., Vaissiere, T., Lerch, J. P., & Rumbaugh, G. (2018). Species-conserved SYNGAP1 phenotypes associated with neurodevelopmental disorders. *Molecular and cellular neurosciences*, *91*, 140–150. https://doi.org/10.1016/j.mcn.2018.03.008.

(8) Morcos P. A. (2007). Achieving targeted and quantifiable alteration of mRNA splicing with Morpholino oligos. *Biochemical and biophysical research communications*, *358*(2), 521–527. https://doi.org/10.1016/j.bbrc.2007.04.172.

(9) Ran, F. A., Hsu, P. D., Wright, J., Agarwala, V., Scott, D. A., & Zhang, F. (2013). Genome engineering using the CRISPR-Cas9 system. *Nature protocols*, *8*(11), 2281–2308. https://doi.org/10.1038/nprot.2013.143.

(10) Stewart, A. M., Nguyen, M., Wong, K., Poudel, M. K., & Kalueff, A. V. (2014). Developing zebrafish models of autism spectrum disorder (ASD). *Progress in neuro-psychopharmacology & biological psychiatry*, *50*, 27–36. https://doi.org/10.1016/j.pnpbp.2013.11.014.

Appendice

Human Molecular Genetics, 2015, Vol. 24, No. 14 4006–4023

doi: 10.1093/hmg/ddv138
Advance Access Publication Date: 16 April 2015
Original Article

ORIGINAL ARTICLE

Two knockdown models of the autism genes *SYNGAP1* and *SHANK3* in zebrafish produce similar behavioral phenotypes associated with embryonic disruptions of brain morphogenesis

Robert A. Kozol[1,*], Holly N. Cukier[2], Bing Zou[1], Vera Mayo[2], Silvia De Rubeis[3], Guiqing Cai[3,†], Anthony J. Griswold[2], Patrice L. Whitehead[2], Jonathan L. Haines[4], John R. Gilbert[2], Michael L. Cuccaro[2], Eden R. Martin[2], James D. Baker[1], Joseph D. Buxbaum[3], Margaret A. Pericak-Vance[2] and Julia E. Dallman[1,*]

[1]Department of Biology, University of Miami, Coral Gables, FL, USA, [2]John P. Hussman Institute for Human Genomics, University of Miami Miller School of Medicine, Miami, FL, USA, [3]Seaver Autism Center for Research and Treatment, Department of Psychiatry, Friedman Brain Institute and Mindich Child Health and Development Institute, Icahn School of Medicine at Mount Sinai, New York, NY, USA and [4]Department of Epidemiology and Biostatistics, Institute for Computational Biology, Case Western Reserve University School of Medicine, Cleveland, OH, USA

*To whom correspondence should be addressed at: Department of Biology, 03 Cox Science Center, 1301 Memorial Dr., Coral Gables, FL 33146, USA. Tel: +1 8604028415; Fax: +1 3052843039; Email: robkozol@bio.miami.edu (R.A.K.); Department of Biology, 03 Cox Science Center, 1301 Memorial Dr., Coral Gables, FL 33146, USA. Tel: +1 3052843954; Fax: +1 3052843039; Email: jdallman@bio.miami.edu (J.E.D.)

Abstract

Despite significant progress in the genetics of autism spectrum disorder (ASD), how genetic mutations translate to the behavioral changes characteristic of ASD remains largely unknown. ASD affects 1–2% of children and adults, and is characterized by deficits in verbal and non-verbal communication, and social interactions, as well as the presence of repetitive behaviors and/or stereotyped interests. ASD is clinically and etiologically heterogeneous, with a strong genetic component. Here, we present functional data from *syngap1* and *shank3* zebrafish loss-of-function models of ASD. *SYNGAP1*, a synaptic Ras GTPase activating protein, and *SHANK3*, a synaptic scaffolding protein, were chosen because of mounting evidence that haploinsufficiency in these genes is highly penetrant for ASD and intellectual disability (ID). Orthologs of both *SYNGAP1* and *SHANK3* are duplicated in the zebrafish genome and we find that all four transcripts (*syngap1a*, *syngap1b*, *shank3a* and *shank3b*) are expressed at the earliest stages of nervous system development with pronounced expression in the larval brain. Consistent with early expression of these genes, knockdown of *syngap1b* or *shank3a* cause common embryonic phenotypes including delayed mid- and hindbrain development, disruptions in motor behaviors that manifest as unproductive swim attempts, and spontaneous, seizure-like behaviors. Our findings indicate that both *syngap1b* and *shank3a* play novel roles in morphogenesis resulting in common brain and behavioral phenotypes.

† Present address: Department of Genetics and Genomic Sciences, Icahn School of Medicine at Mount Sinai, New York, NY 10029, USA.
Received: December 7, 2014. **Revised:** March 16, 2015. **Accepted:** April 13, 2015

Introduction

Autism spectrum disorder (ASD) is a heritable neurodevelopmental disorder diagnosed in 1–2% of children and adults worldwide (1). ASD core phenotypic features include social deficits and stereotyped behavioral patterns (2). While many contributing genetic loci have been identified, hundreds of other rare genetic disruptions are likely to contribute to ASD, making this disorder genetically heterogeneous (3–11). Moreover many ASD-associated genes have been linked to multiple, often comorbid, neurological disorders including epilepsy and intellectual disability (12–15), indicating that specific combinations of genetic mutations (16,17), polygenic background (18), genetic-environmental interactions (19–21) or other factors determine how DNA alterations manifest clinically.

To explore how diverse genetic disruptions linked to ASD in humans may converge on common neuropathology, we sought to compare animal models of two genes linked to ASD: *SYNGAP1* (*synaptic Ras GTPase activating protein 1*) and *SHANK3* (*SH3 and multiple ankyrin repeat domains 3*). In humans, heterozygous mutations in either *SYNGAP1* or *SHANK3* produce partially overlapping clinical pathologies that include epilepsy, intellectual disability and ASD (22–35). Similarly, both *Syngap1* and *Shank3* loss-of-function mouse models have overlapping phenotypes that include seizures, increased stereotyped behavior and spatial memory deficits (36–41). Consistent with convergent phenotypes, Syngap1 and Shank3 proteins are both enriched at glutamatergic post-synaptic densities (PSDs) and interact directly in yeast two-hybrid assays (42). Despite these commonalities, *Syngap1* and *Shank3* loss-of-function mutations cause divergent functional synaptic deficits: decreasing murine Syngap1 causes precocious maturation of synapses and increased synaptic transmission (37,43) while decreasing murine Shank3 reduces the density and size of PSDs and decreases synaptic transmission (36,39,40,44). Given similar ASD-related behavioral phenotypes, we wanted to test the hypothesis that Syngap1 and Shank3 have other non-synaptic roles that might provide convergent disease mechanisms.

Zebrafish (*Danio rerio*) models complement extant mouse models by providing insight into how genes linked to ASD impact early neural circuit development (45,46). In contrast to mammals, optically transparent zebrafish develop externally and gene knockdown technologies are inexpensive and rapid (47). Previous zebrafish models of ASD genes, such as *zdisc1*, *met* and *chd8* demonstrate convergent roles for these genes in mid- and hindbrain morphogenesis (46,48,49). Coincident with morphogenesis, zebrafish develop reflexive, stereotyped escape behaviors that can be used to assess how developmental phenotypes affect functional neuronal output (50). Together the ability to identify convergent morphogenetic phenotypes and their impact on emerging neural circuits make zebrafish a well-suited model to study ASD gene function early in development.

Here we report that knockdown of *SYNGAP1* and *SHANK3* zebrafish orthologs produce common phenotypes associated with embryonic disruptions of brain morphogenesis. Consistent with functional roles that extend beyond synapses, a phylogenetic analysis of these proteins indicates that both *SYNGAP1* and *SHANK3* are vertebrate-specific versions of more ancient protein families that are found in animals lacking nervous systems. At the level of gene expression, zebrafish *syngap1a, syngap1b*, *shank3a* and *shank3b* are all expressed in the brain during embryogenesis. Knockdown of either *syngap1b* or *shank3a* results in similar disruptions in the nervous system characterized by extensive neuronal cell death, pronounced developmental delay in mid- and hindbrain regions, and seizure-like behaviors. Moreover, co-injecting sub-phenotypic doses of *syngap1b* and *shank3a* morpholino (MO) recapitulates phenotypes seen in embryos injected with higher doses of either *syngap1b* or *shank3a* MOs, demonstrating a synergistic loss-of-function between *syngap1b* and *shank3a*. In summary, our data suggest that in addition to their roles at synapses, both shank3a and syngap1b are also required more broadly for brain morphogenesis.

Results

SYNGAP1 and SHANK3 are duplicated in zebrafish

Zebrafish gene orthologs of human *SYNGAP1* and *SHANK3* were identified using Ensembl databases. While *SYNGAP1* and *SHANK3* each appear once in the human genome, both genes are duplicated in zebrafish (Fig. 1A and B). Using the Blast-Like Alignment Tool (BLAT; Kent informatics, Inc.), protein alignments of *Homo sapiens* and *Danio rerio* orthologs reveal a high level of amino acid identity: syngap1a (chromosome 19; 82.4%), syngap1b (chromosome 16; 84.9%), shank3a (chromosome 18; 84.5%) and shank3b (chromosome 4; 83.3%). A closer evaluation shows that all major functional domains in human SYNGAP1 are equally conserved in the two-zebrafish syngap1 ohnologs (Fig. 1A and B). In contrast, several important protein–protein interaction motifs contained in the proline rich and SAM C-terminal region, of human *SHANK3* are more highly conserved in *shank3a* than *shank3b*. Therefore, *shank3a* is more suitable as a model for human *SHANK3*.

SYNGAP1 and SHANK3 are innovations of the vertebrate lineage

SYNGAP1 and *SHANK3* are evolutionarily derived members of larger gene families that expanded by gene and whole genome duplication events in the vertebrate lineage (51). SYNGAP1, RASAL3, RASAL2 and DAB2IP belong to a sub-group of the Ras GTPase activating proteins (RasGAPs), distinguished from the larger RasGAP family by a typical domain structure: pleckstrin homology (PH), calcium-dependent membrane localization (C2), Ras GTPase activating protein (RasGAP) and coil-coiled domains (CC; Fig. 1C). The *SHANK1*, *SHANK2* and *SHANK3* gene family is also distinguished by a typical domain structure: Ankyrin repeats (Ank), Src Homology 3 (SH3), Post-synaptic density protein 95/Disc large/Zona occludens 1 (PDZ), and Sterile Alpha Motif domains (SAM; Fig. 1D). Additional short Abp-, Homer- and Cortactin-interacting domains (52,53) were previously identified in vertebrate Shanks 1–3 using functional assays and are not as clearly reflected by conserved sequence (Supplementary Material, Fig. S1). To identity unique signatures of vertebrate Shank3, multiple alignments of zebrafish, *Xenopus*, rat, mouse and human Shank3 reveal 12 regions (each over 16 amino acids in length) of 80% or greater amino acid identity (Supplementary Material, Fig. S1), with only four of these 12 found in the single Shank protein encoded in the amphioxus genome. Like amphioxus, other metazoans have single versions of both a DAB2IP-like protein and a SHANK-like protein. Ancestral forms of both SYNGAP1 and SHANK can even be found in single-celled choanoflagellates. These proteins have the same collection of domains in a different order along the protein (Fig. 1C and D), indicating that SYNGAP1 and SHANK protein families originated before the divergence of single-celled animals and metazoans. In summary, both *SYNGAP1* and *SHANK3* are vertebrate innovations of ancient

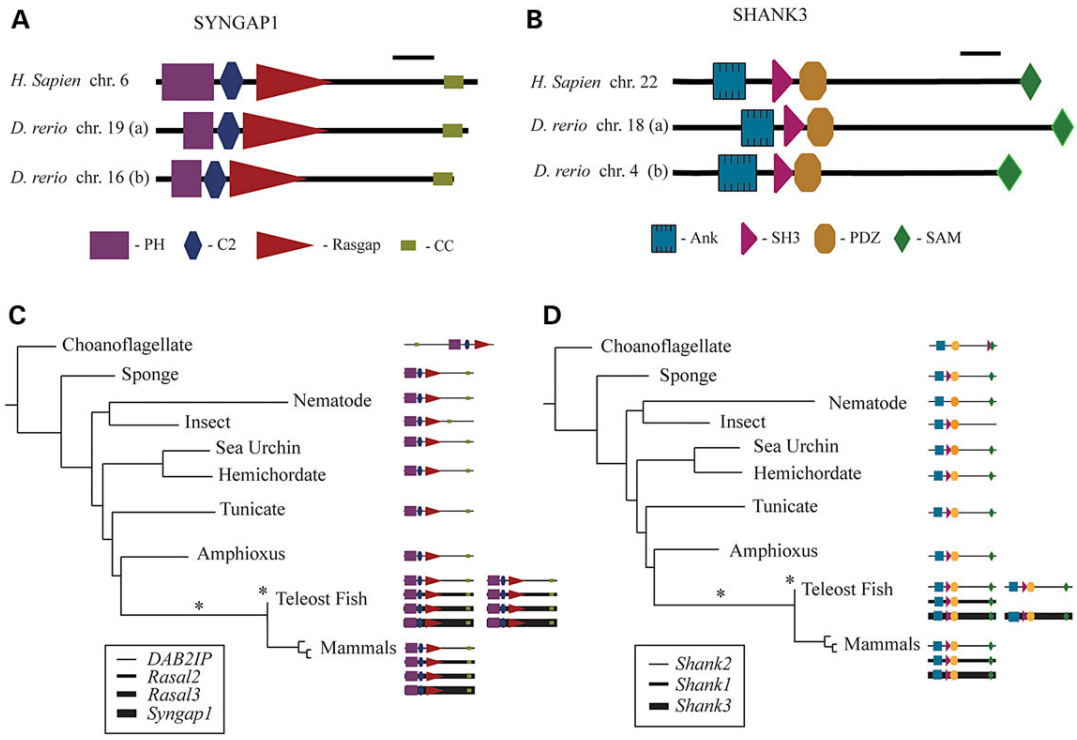

Figure 1. Protein diagrams and phylogenetic trees depict domain order and gene expansion through evolutionary time. (**A** and **B**) Protein diagrams of SYNGAP1 and SHANK3 orthologs for *H. sapiens* and *D. rerio* were generated using SMART (http://smart.embl-heidelberg.de/) from published Ensembl protein sequences. Diagrams represent the longest isoform available for each ortholog, denoted by species name and chromosome number (chr.). All major functional domains are conserved between the *H. sapien* and *D. rerio* gene duplicates with the exception that *shank3b* has a sixth ankyrin repeat. Scale bar = 200 amino acids (aa). SYNGAP1 protein domains: PH, pleckstrin homology; C2, calcium-dependent membrane localization; RasGAP, Ras GTPase activator protein; and CC, coiled coil. SHANK3 protein domains: ANK, ankyrin repeat; SH3, SRC homology 3; PDZ, post-synaptic density-drosophila disc large suppressor-Zonula occludens-1; SAM, sterile alpha motif. RasGAP sub-family (**C**) and Shank family (**D**) proteins from diverse animal phyla were identified by best reciprocal blast with Human SYNGAP1 and SHANK3 and are mapped onto a phylogenetic tree adapted from a recent genomic study (97). This analysis highlights deep evolutionary roots of both SYNGAP1 and SHANK3 protein families with expansion by genome duplication events (asterisk) in vertebrates and again in teleost fish. Within expanded vertebrate gene families, *syngap1* and *shank3* are derived from ancestral family members most similar to *DAB2IP* and *Shank2*.

proteins, suggesting a derived set of functional roles for these proteins in vertebrates.

Zebrafish *syngap1a/b* and *shank3a/b* are expressed in the central nervous system during embryogenesis

To determine the developmental expression patterns of *syngap1a*, *syngap1b*, *shank3a* and *shank3b*, we harvested RNA from 11 developmental stages ranging in age from 2 to 120 hours post-fertilization (hpf) and used gene-specific primers for reverse transcription and quantitative polymerase chain reaction (RT–qPCR; Fig. 2A and B). *Syngap1b*, *shank3a* and *shank3b* transcripts are expressed from fertilization and gradually increase after 12–15 hpf, a developmental stage when the body-axis forms and the earliest neurons exit the cell cycle and start to differentiate (54). In contrast, *syngap1a* transcripts show constant expression until 36–48 hpf, when larval expression gradually increases. Together, these results show all four transcripts to be expressed in the early embryo.

To determine where *syngap1a*, *syngap1b*, *shank3a* and *shank3b* transcripts are expressed in zebrafish, we performed whole mount *in situ* hybridization at 48 hpf. All four transcripts are expressed in the brain with each showing unique patterns of concentrated expression (Fig. 2C and D). *Syngap1a* expression is most pronounced in the anterior forebrain and dorsal hindbrain. Like *syngap1a*, *syngap1b* is expressed in the dorsal hindbrain; however, *syngap1b* is also expressed at high levels in the optic tectum of the midbrain. *shank3a* expression is most pronounced in the ventral regions of the fore-, mid- and hindbrain, while *shank3b* is expressed throughout fore- and midbrain with the highest levels of expression in the anterior-ventral forebrain. In addition to their expression in the brain, *syngap1b* and *shank3a* also exhibit low levels of expression throughout the body consistent with their higher level of expression at early developmental stages by RT–qPCR (Fig. 2A and B).

Splice-inhibiting morpholinos knockdown zebrafish *syngap1* and *shank3* ohnologs

To functionally characterize the *syngap1a*, *syngap1b*, *shank3a* and *shank3b* genes, we designed splice-inhibiting morpholinos (MOs) against intron/exon junctions corresponding to conserved domains. To test gene knockdown efficacy, we amplified MO-targeted genes and a loading control *elongation factor 1α* (55)

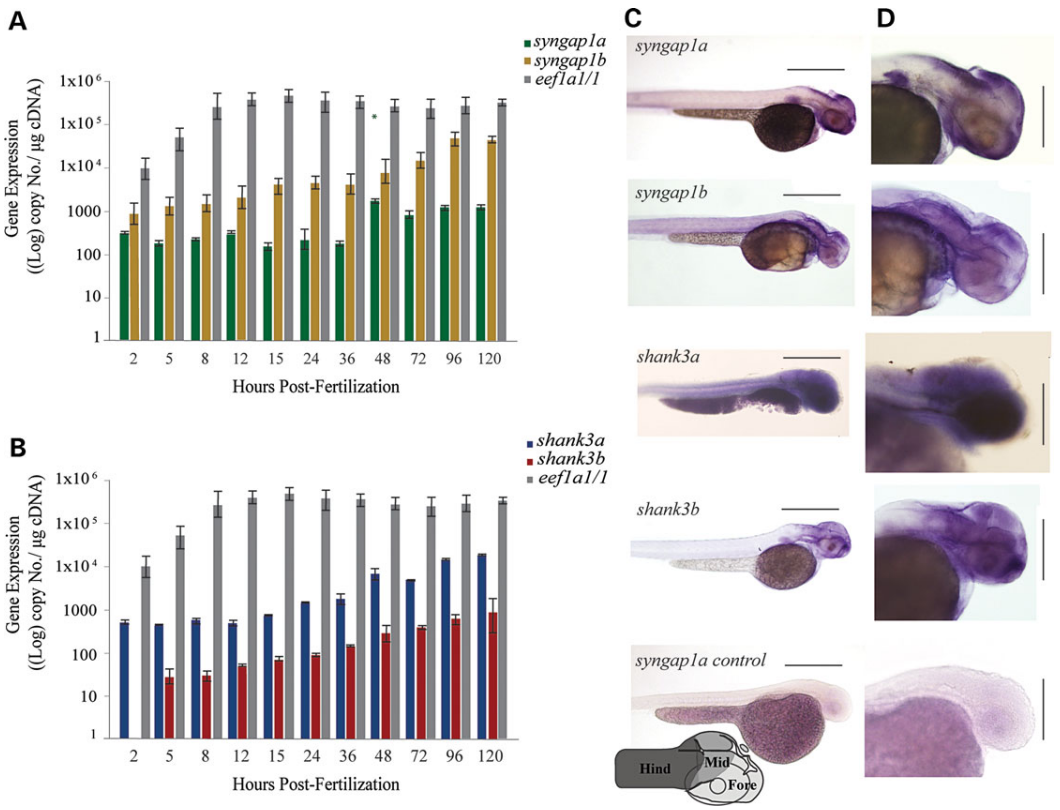

Figure 2. Zebrafish *shank3* and *syngap1* ohnologs are expressed during embryogenesis and enriched in the brain. Developmental gene expression of (**A**) *syngap1a* and *syngap1b* and (**B**) *shank3a* and *shank3b* from 2 to 120 h post fertilization was determined using RT–qPCR. Absolute copy numbers were derived for each gene and plotted as a log function, adjusted for no template control, with error bars denoting standard deviation for three RNA sample replicates per developmental time-point. The asterisk for *syngap1a*-48 hpf represents an outlier by three orders of magnitude. 48 hpf whole mount *in situ* hybridization gene expression patterns for (**C**) whole body and (**D**) brain and rostral spinal cord. *Syngap1a* is enriched in the dorsal hindbrain and anterior forebrain, while *syngap1b* is enriched throughout the midbrain and hindbrain. *Shank3a* is enriched throughout the entire brain, while *shank3b* is enriched in the anterior forebrain. Scale bars = 500 µm (C) and 250 µm (D). The line drawing of the brain was adapted from Mueller *et al.* (103) with fore-, mid-, and hindbrain regions denoted by shades of grey.

from cDNA generated from MO-injected larvae (Fig. 3A–C; Supplementary Material, Fig. S2). *Syngap1a/b* and *shank3a/b* MOs disrupted the expression of the targeted genes either by causing intron retention (*syngap1a* and *shank3a/b*) or by causing exon skipping (*syngap1b*). Based on sequencing of morphant-specific rtPCR products, all MOs would be predicted to result in N-terminal protein truncations (data not shown).

The *syngap1a* MO targets the exon 5/intron 5 splice-junction. Injection of *syngap1a* MO reduced *syngap1a* expression and produced three larger MO-specific bands due to intron retention (Supplementary Material, Fig. S2). The *syngap1b* MO targets the intron 3/exon 4 splice-junction and produced one smaller MO-specific band due to exon skipping (Fig. 3A). Both *syngap1a* and *syngap1b* MOs would be predicted to truncate the corresponding syngap1 protein in the pleckstrin homology domain.

The *shank3a* MO targets the exon 8/intron 8 splice-junction, produces intron retention and would be predicted to truncate the protein within the fourth ankyrin repeat (Fig. 3B). The *shank3b* MO targets the exon 10/intron 10 splice-junction, produces intron retention (Supplementary Material, Fig. S2) and would be predicted to truncate the protein within the sixth ankyrin repeat.

To test whether disrupting single *shank3* and *syngap1* ohnologs would impact expression of the others, we compared the levels of all four ohnologs in all morphant samples (Supplementary Material, Fig. S2). Consistent with its milder effect on phenotype, the *shank3b* MO specifically and completely disrupted expression of *shank3b* without impacting the expression of the other genes. In contrast, *syngap1a*, *syngap1b* and *shank3a* MOs each reduced expression of all ohnologs compared with constant *eef1a1/1* levels. We attribute reduced *syngap1a*, *syngap1b*, *shank3a* and *shank3b* expression to a dramatic developmental delay in the nervous system produced by *syngap1a*, *syngap1b* and *shank3a* MOs (see sections on morphology and cell death).

Dose/response curves identify doses and ohnologs for subsequent analyses

By generating dose/response curves for *syngap1a/b* and *shank3a/b* MOs, we identified single doses that optimized the penetrance of gene-specific phenotypes without inducing general toxicity (Fig. 3D and E). These doses were then used for all subsequent phenotypic analyses. Dose/response analyses also identified

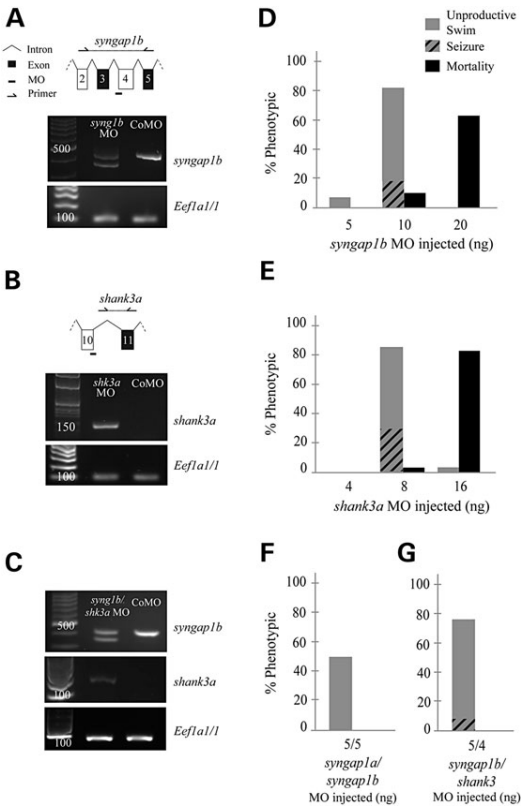

Figure 3. Splice-inhibiting morpholinos target intron/exon junctions resulting in dosage sensitive phenotypes at 48 hpf. Morpholino design strategy and RT–PCR detection of splice-inhibiting events for *syngap1b* (**A**), *shank3a* (**B**) and *syngap1b/shank3a* (**C**) morphants. Arrows and dashed lines represent PCR primers and amplicons, respectively. Exons (boxes) and introns (bent lines) are not drawn to scale. Morphant cDNA used as template for PCR are noted above each gel while genes targeted by primer sets are indicated to the right. Morphant templates are abbreviated as *syng1b* and *shk3a* for *syngap1b* and *shank3a*, respectively. (**D–F**) Stacked histograms show percentages of larvae exhibiting mortality and unproductive swim bouts (proportion with seizure-like behavior shown by hatching) with different amounts of morpholino injected. Morphants that displayed severe morphological phenotypes such as curved and bent tails were not assayed for swimming ability. Injection amounts producing the highest behavioral penetrance of 10 and 8 ng were used for (D) *syngap1b* MO ($n = 131$) and (E) *shank3a* MO ($n = 125$), respectively. Co-injection of either (F) *syngap1a/syngap1b* (5/5 ng, $n = 16$) or (**G**) *syngap1b/shank3a* MO (5/4 ng, $n = 121$) recapitulated phenotypes observed in higher doses of singly injected morpholinos. CoMO injected fish showed no defects in swimming behavior on days assayed ($n = 87$).

syngap1b and *shank3a* MOs as the most penetrant at 48–72 hpf (Table 1; Fig. 3D and E) consistent with the dominant expression of these two ohnologs at early embryonic stages. *Syngap1a* and *syngap1b* were also co-injected to test for interplay between *syngap1* ohnologs. Co-injection of 5 ng each of *syngap1a/b* MOs had an additive effect, suggesting *syngap1a/b* impact similar developmental processes (Fig. 3F). Despite this interplay between *syngap1* ohnologs, singly injected *syngap1a* MO produced phenotypes of low penetrance and with increasing doses became toxic. While not toxic at any dose, *shank3b* MO failed to produce a phenotype despite a molecularly efficient knockdown (Supplementary Material, Fig. S2). Due to a low phenotypic penetrance in *syngap1a* morphants and a lack of phenotypes in *shank3b* morphants, all subsequent analyses focus on knockdown phenotypes of *syngap1b* and *shank3a* ohnologs and the roles these genes play in the early embryo.

Table 1. Quantification of behavioral phenotypes and mortality for *syngap1* and *shank3* morphants

Target gene	Amount MO injected (ng)	Behavioral phenotype (%)		
		Swim	Seizure	Mortality
syngap1a	5 ($n = 57$)	5	0	0
	10 ($n = 120$)	32	0	7
	20 ($n = 33$)	—	—	58
syngap1b	5 ($n = 74$)	7	0	0
	10 ($n = 131$)	82	18	10
	20 ($n = 45$)	—	—	63
shank3a	4 ($n = 50$)	14	0	0
	8 ($n = 125$)	86	30	2
	16 ($n = 66$)	—	—	82
shank3b	30 ($n = 49$)	0	0	20
syngap1a/syngap1b	5/5 ($n = 16$)	48	0	0
shank3a/shank3b	4/10 ($n = 30$)	0	0	30
syngap1a/shank3a	10/04 ($n = 28$)	0	0	50
syngap1a/shank3b	10/10 ($n = 33$)	0	0	0
syngap1b/shank3a	5/4 ($n = 121$)	75	8	0
syngap1b/shank3b	5/10 ($n = 30$)	0	0	0
CoMO	30 ($n = 87$)	0	0	0

Due to a previously identified interaction between SYNGAP1 and SHANK3 in a yeast-2-hybrid screen (42), we tested whether *syngap1b* and *shank3a* function synergistically by co-injecting these MOs at doses [*syngap1b* MO (5 ng) or *shank3a* MO (4 ng)] that show low penetrance when injected singly. *Syngap1b/shank3a* double morphant phenotypes were comparable to single MO injections at higher doses and included altered mid/hindbrain boundaries, cardiac edema, developmental delay and unproductive swim bouts (Fig. 3G). To test whether this synergy between *sygap1b* and *shank3a* extended to other combinations of *syngap1/shank3* ohnologs, *syngap1a/shank3a and syngap1b/shank3b* were also co-injected (Table 1). These other co-injections did not produce morphological and behavioral phenotypes with the same penetrance, further supporting the specificity of synergy between *syngap1b* and *shank3a*.

Seizure-like behaviors and unproductive escape responses characterize both *syngap1b* and *shank3a* morphants

To quantify morphant behaviors, we conducted kinematic analyses of zebrafish escape responses at 72 hpf (56). Escape responses in larvae injected with control MO (CoMO) were highly stereotyped (Supplementary Material, Movie S1), characterized by a strong C-bend away from the stimulus followed by sinusoidal undulations that decreased in frequency and amplitude as larvae swam away from the stimulus (Fig. 4A, CoMO). In contrast *syngap1b* (Supplementary Material, Movie S2), *shank3a* (Supplementary Material, Movie S3) and double *syngap1b/shank3a* (Supplementary Material, Movie S4) morphant swim attempts were unproductive, characterized by undulations with constant rather than graded frequencies and sustained amplitudes (Fig. 4A, *syngap1b*: 82%; *shank3a*: 86%; double *syngap1b/shank3a*: 75%). Indeed, rather than a transition from high to low amplitude bends as seen in CoMO larvae, *syngap1b*, *shank3a* and double *syngap1b/shank3a* morphants produced an inverted transition from low to high

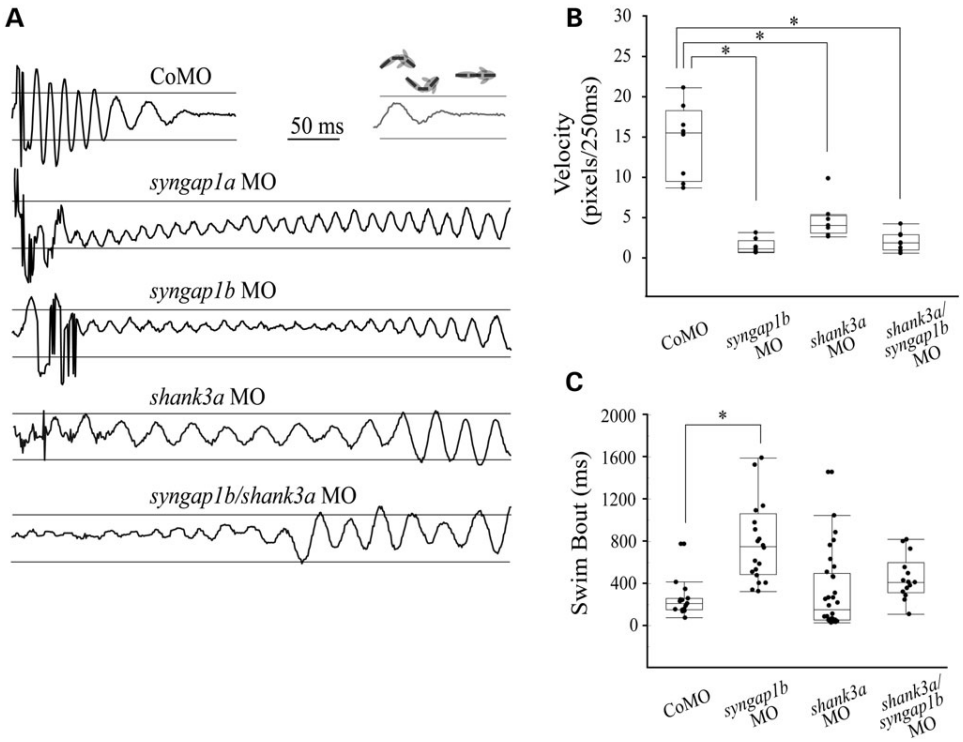

Figure 4. Escape responses in 72 hpf *syngap1b*, *shank3a* and *syngap1b/shank3a* morphants are unproductive. (**A**) Touch-evoked escape responses were recorded using a high-speed camera and analyzed using FLOTE analysis software. FLOTE software divides the larvae into three segments and swimming traces depict body curvature as the sum of the angles between segments, where positive values denote a bend in one direction and negative values bends in the opposite direction. *Syngap1b*, *shank3a* and *syngap1b/shank3a* double morphants show a steady swimming frequency, reduced flexion and increased swimming durations in comparison to controls. (**B**) Swimming velocities (pixels/ms) were determined using the kinematic analysis function in FLOTE. (**C**) Bout lengths were calculated in milliseconds as the first to last frame of a continuous swimming bout. Both swimming velocity and bout lengths were analyzed by Student's *t*-test between *syngap1b*, *shank3a* and *syngap1b/shank3a* morphants and CoMO. Box plot lines represent the first quartile (bottom), median (middle) and third quartile (top). Asterisks indicate significance, $^*P < 0.01$.

amplitude bends. These unproductive swim attempts were also characterized by significantly reduced swimming velocities for *syngap1b* (1.15 ± 0.9 pixels/ms; $n = 8$), *shank3a* (4.45 ± 2.32 pixels/ms, $n = 8$) and *syngap1b/shank3a* double morphants (1.8 ± 1.23 pixels/ms, $n = 8$), compared with control morphants (14.4 ± 4.65 pixels/ms, $n = 8$; Fig. 4B). In addition to reduced swimming velocities, *syngap1b* morphants also displayed significantly increased swimming-bout durations (858 ± 552 ms; $n = 20$) compared with control morphants (247 ± 169 ms; $n = 15$; Fig. 4C). In addition to increased swimming bout duration similar to *syngap1b* morphants, *shank3a* morphants also exhibited a single-coiled response, recapitulating the main phenotype reported in a previous study (57). In contrast to the previous study, we did not observe single-coiled responses in *shank3b* morphants. In our experiments, both *syngap1b* and *shank3a* morphant behavioral phenotypes were most pronounced between 48 and 72 hpf.

A subset of behaviorally phenotypic *syngap1b* (18%; Supplementary Material, Movie S5), *shank3a* (30%; Supplementary Material, Movie S6) and double *syngap1b/shank3a* (8%; Supplementary Material, Movie S7) morphants also exhibited spontaneous (occurring in the absence of a touch stimulus) seizure-like behaviors characterized by prolonged (lasting seconds to minutes rather than the typical <500 ms) unproductive swim bouts (Fig. 3D, E and G), suggesting that knockdown of either *syngap1b*, *shank3a* or the combination produces hyper-excitability in the nervous system.

Reducing *syngap1b* or *shank3a* and double *syngap1b/shank3a* alters brain morphology and increases cell death in embryonic nervous system

In addition to behavioral deficits, *syngap1b*, *shank3a* and double *syngap1b/shank3a* morphants exhibited altered brain morphologies suggestive of developmental delay (Fig. 5). At 28–30 hpf, *syngap1b*, *shank3a* and double *syngap1b/shank3a* morphants had malformed mid/hindbrains (Fig. 5A and B). At 48–52 hpf, *syngap1b*, *shank3a* and double *syngap1b/shank3a* morphant heads were still curved around the yolk as would be stage-appropriate for 24–28 hpf (Fig. 5A and C) and some larvae had edema around their hearts (Fig. 5C and D). At 72 hpf, *syngap1b*, *shank3a* and double *syngap1b/shank3a* morphant developmental delay was still apparent with head morphologies resembling CoMO injected larvae at 48 hpf. In addition to developmental delay, *shank3a* morphants had shorter tails. These qualitative changes in gross morphology indicate *syngap1b*, *shank3a* and double *syngap1b/shank3a* morphants have delayed brain development.

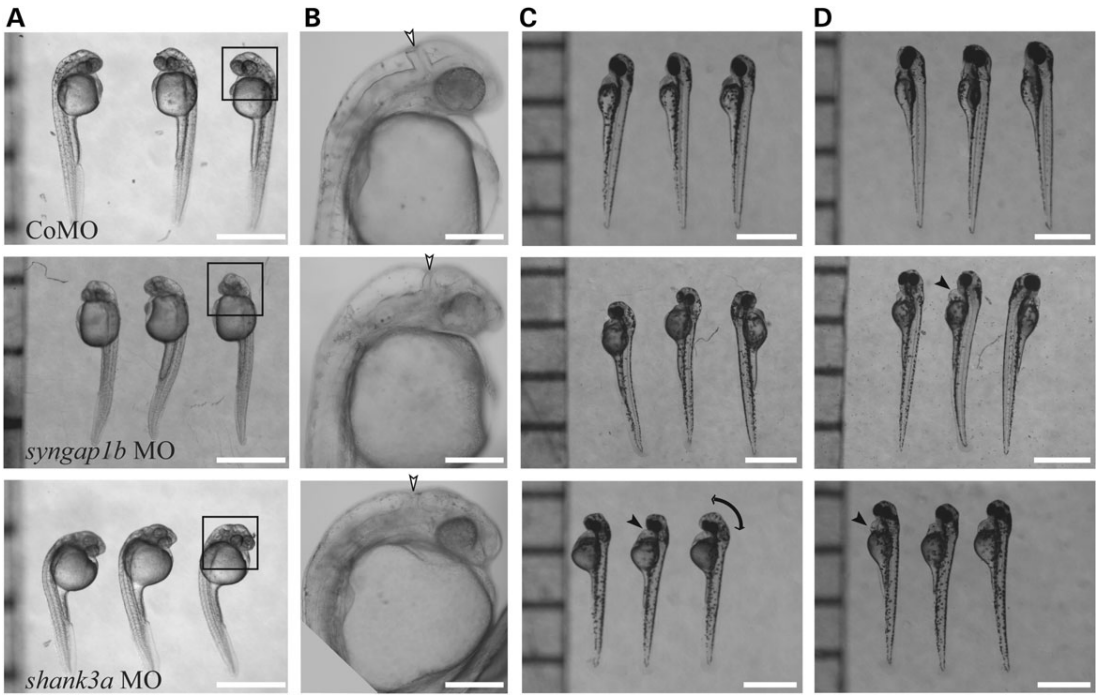

Figure 5. Brains of *syngap1b* and *shank3a* morphants at 28–30, 48 and 72 hpf show developmental delay compared with control morphants. (**A** and **B**) At 28–30 hpf, both *syngap1b* and *shank3a* morphants have changes in ventricle size and disruptions of the mid-hindbrain boundary (white arrowheads). (**C** and **D**) At 48 and 72 hpf, both *syngap1b* and *shank3a* morphants exhibit microencephaly and developmental delay with curved head to trunk angles (curved arrow) that resemble earlier control stages. Both *syngap1b* and *shank3a* morphants also sometimes have cardiac edema (black arrowheads) and *shank3a* morphants have a shorter body axis. Scale bars = 1 mm (**A**, **C** and **D**; 28–30, 48, 72 hpf) and 250 μm (**B**; 28–30 hpf).

To better understand hyper-excitable phenotypes in 48 hpf *syngap1b*, *shank3a* and double *syngap1b/shank3a* morphants, we quantified excitatory (glutamate-using stable vglut transgenic) and inhibitory (GABA-using antibody staining) neurotransmitter expression in transverse frozen brain sections. This approach also enabled us to compare cross-sectional head areas for 48 hpf fore-, mid- and hindbrain sections of *syngap1b*, *shank3a* and CoMO larvae (Supplementary Material, Table S7). Overall, *syngap1b* and *shank3a* morphant brains were microencephalic as reflected in significantly decreased cross-sectional areas in all brain regions measured. Moreover, reductions in the mid- and hindbrain areas could largely be accounted for by the absence of dorsal structures in both *syngap1b* and *shank3a* morphants (Fig. 6A). Both *syngap1b* and *shank3a* morphants were characterized by a significant reduction of GABAergic neurons in the mid- and hindbrain, while vglut expression was only significantly reduced in the hindbrain (Fig. 6B and C, Tables 2 and 3). These results demonstrate the potential for hyper-excitability in the midbrain of *syngap1b* and *shank3a* morphants. Developmental delay was improved but still apparent in 96 hpf *syngap1b*, *shank3a* and double *syngap1b/shank3a* morphant larvae, wherein dorsal structures had formed but overall morphology remained delayed in mid/hindbrain regions with 96 hpf *syngap1b* and *shank3a* morphant brains resembling those of controls at 48 hpf (Supplementary Material, Fig. S3).

In contrast to delays in the mid/hindbrain regions, *syngap1b* and *shank3a* morphant spinal motor neurons were stage-appropriate (Fig. 7). Spinal motor neurons were visualized using SaigFF213A that drives GFP in Caudal Primary motor neurons, a subset of interneurons and Rohon Beard sensory neurons (58). These transgenic morphant embryos were then injected with tetramethylrhodamine-αBungarotoxin, to visualize post-synaptic clusters of acetylcholine receptors (59). Co-localization of motor axons with receptors reflects that morphant motor neurons have formed synapses on their post-synaptic muscle targets (Fig. 7). In addition to demonstrating that spinal motor neurons were not delayed in *syngap1b* and *shank3a* morphants, this analysis strickingly revealed that Rohon Beard neurons were reduced/absent in *shank3a* but not *syngap1b* morphants (Fig. 7B and C).

To determine whether developmental delays in brain development might be explained by earlier developmental disruptions, we quantified cell death by staining 1-day-old morphant embryos with acridine orange (60). *Syngap1b*, *shank3a* and double *syngap1b/shank3a* morphants all exhibited increased cell death in the central nervous system (CNS) that was most pronounced at 24–28 hpf. In both *syngap1b* and *shank3a* and double *syngap1b/shank3a* morphants, cell death was pronounced in the midbrain, hindbrain and spinal cord (Fig. 8A and B). Because cell death is a common off-target result of siRNA and morpholino knockdown technologies (61), morphants were coinjected with either orthologous human mRNA or *p53* MO to distinguish between gene-specific and off-targeting effects, respectively. In *syngap1b* morphants, co-injection of the *p53* morpholino did not rescue cell death (Fig. 8A, $n = 3$). In contrast, in *shank3a* morphants, co-injection of the *p53* MO almost entirely rescued cell death

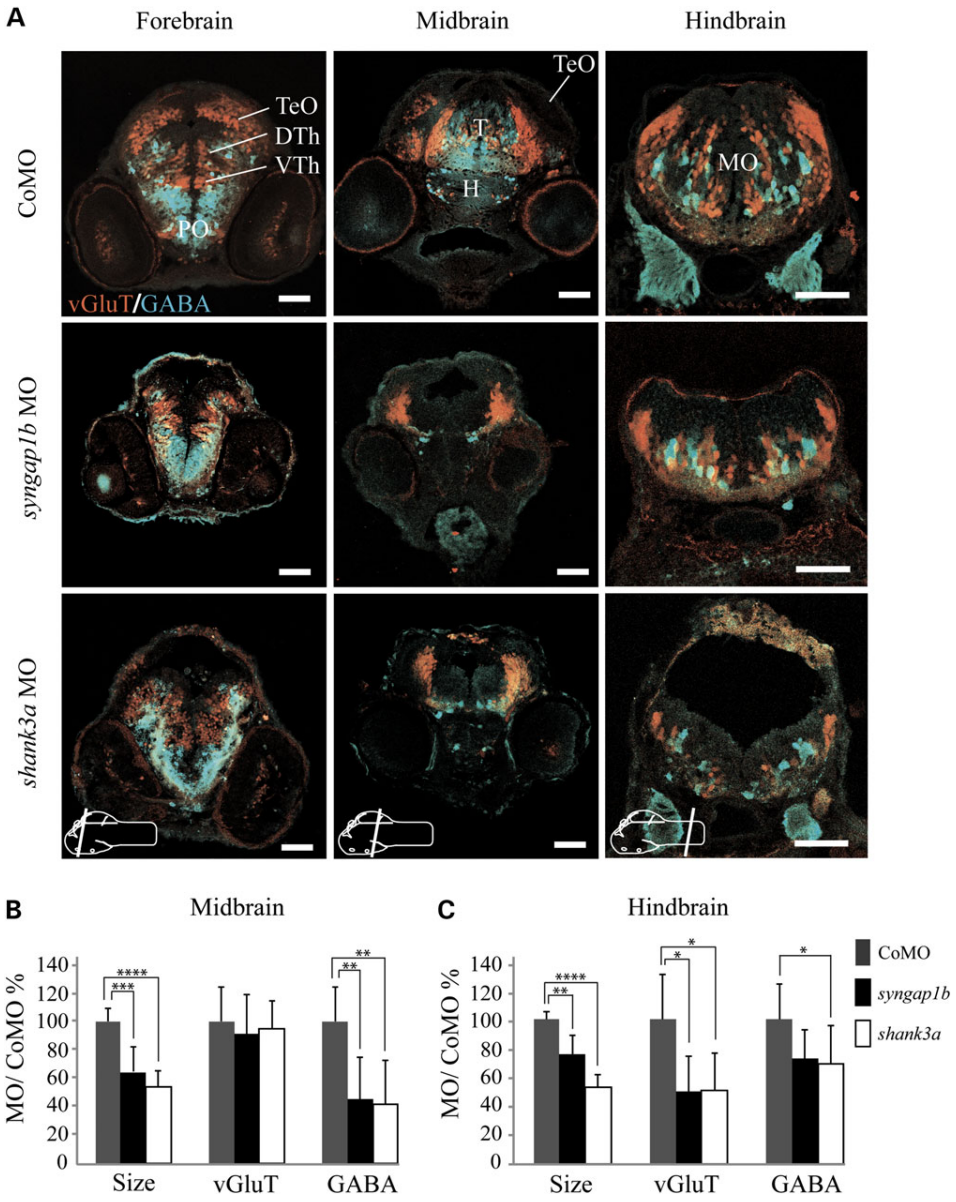

Figure 6. Excitatory (vGluT) and inhibitory (GABA) neurons are reduced in 48 hpf *syngap1b* and *shank3a* morphants. Three transverse sections represent the three major brain divisions; forebrain, midbrain and hindbrain. Scale bars = 50 μm. The line drawn brain atlas was adapted from Mueller *et al.* (103). Brain regions are indicated in wild-type sections: DTh, dorsal thalamus; H, hypothalamus; MO, medulla oblongata; T, tegmentum; TeO, Optic Tectum; VTh, ventral thalamus. Expression of vGlut and GABA in *syngap1b*, *shank3a* and control morphant (**D**) midbrain and (**E**) hindbrain regions were quantified in Fiji as a percentage of brain area. Size on the x-axis is defined as the percentage of total brain area (μm^2). All values were normalized to CoMO and analyzed using Student's *t*-test. Asterisks indicate significance values, $^{*}P < 0.05$, $^{**}P < 0.01$, $^{***}P < 0.001$, $^{****}P < 0.0001$ (Tables 3 and 4).

(Fig. 8B, $n = 3$). Although cell death rescue with *p53* MO can suggest off-targeting effects, *SHANK3* mRNA co-injection also rescued cell death indicating that cell death is gene-specific and that decreasing *shank3a* expression may trigger one of several *p53*-dependent cell death pathways (62).

Indeed, cell death could be partially rescued for both *syngap1b* and *shank3a* morphants by injecting the longest isoform of human *SYNGAP1* and *SHANK3* mRNAs, respectively, suggesting that morphant cell death was gene-specific (Fig. 8C and D). One-way ANOVAs with *post hoc* means comparisons (Tables 4

Table 2. Measurements of anti-GABA and vglut:DsRed for morphant midbrain sections

	GABA (# cells)	vGluT (% μm^2)	Cortical area (μm^2)
CoMO	22.2 ± 5.42	14.5 ± 3.51	$5.41 \times 10^4 \pm 4.81 \times 10^3$
syngap1b MO	8.6 ± 5.56**	12.7 ± 3.22	$2.71 \times 10^4 \pm 9.42 \times 10^{3***}$
shank3a MO	10.0 ± 6.36**	13.32 ± 2.02	$3.45 \times 10^4 \pm 3.19 \times 10^{3****}$

Sample sizes; CoMO $n = 6$, for *syngap1b* MO $n = 6$ and *shank3a* MO $n = 6$.
Student's *t*-test significance:
*$P < 0.05$.
**$P < 0.01$.
***$P < 0.001$.
****$P < 0.0001$.

Table 3. Measurements of anti-GABA and vglut:DsRed for morphant hindbrain sections

	GABA (# cells)	vGluT (% μm^2)	Cortical area (μm^2)
CoMO	20.7 ± 5.0	16.6 ± 5.16	$2.15 \times 10^4 \pm 1.22 \times 10^3$
syngap1b MO	15 ± 4.0	8.26 ± 3.4*	$1.63 \times 10^4 \pm 2.36 \times 10^{3**}$
shank3a MO	14.2 ± 2.8*	8.44 ± 4.05*	$1.14 \times 10^4 \pm 1.68 \times 10^{3****}$

Sample sizes; CoMO $n = 6$, for *syngap1b* $n = 5$ and *shank3a* $n = 6$.
Student's *t*-test significance:
*$P < 0.05$.
**$P < 0.01$.
***$P < 0.001$.
****$P < 0.0001$.

Table 4. Statistical results for *SYNGAP1* cell death ANOVA

Neuronal region	df	Sum of squares	Mean square	*F*	Sig. (*P*<)
Midbrain					
Between Subjects	2	151	65.8	11.5	0.0003
Within Subjects	27	155	5.72		
Total	29	286			
Hindbrain					
Between Subjects	2	221	110	25.3	0.0001
Within Subjects	27	118	4.36		
Total	59	338			
Spinal chord					
Between Subjects	2	4254	2127	26	0.0001
Within Subjects	27	2208	81.8		
Total	30	6462			

See Supplementary Material, Tables S10–S12 for means comparison analysis.

and 5, Supplementary Material, Tables S8–15) revealed that cell death was significantly increased in all brain regions for both *syngap1b* and *shank3a* knockdown experiments. Co-injection of *syngap1b* MO and human *SYNGAP1* mRNA produced a nearly complete rescue, significantly reducing cell death in the hindbrain and spinal cord compared with embryos injected with *syngap1b* MO alone (Supplementary Material, Tables S11 and S12). Likewise, co-injection of *shank3a* MO and human *SHANK3* mRNA produced a partial rescue, significantly reducing cell death in the midbrain, hindbrain and spinal cord, compared with embryos injected with *shank3a* MO alone (Supplementary Material, Table S13–S15). Overall, these results indicate that

Table 5. Statistical results for *SHANK3* cell death ANOVA

Neuronal Region	df	Sum of squares	Mean square	*F*	Sig. (*P*<)
Midbrain					
Between Subjects	2	979	490	10.7	0.0004
Within Subjects	27	1230	45.6		
Total	29	2209			
Hindbrain					
Between Subjects	2	1108	554	32	0.0001
Within Subjects	27	467	17		
Total	29	1575			
Spinal chord					
Between Subjects	2	1711	855	49.2	0.0001
Within Subjects	27	469	17.4		
Total	29	2180			

See Supplementary Material, Tables S13–S15 for means comparison analysis

decreasing expression of either *syngap1b* or *shank3a* causes increased CNS cell death.

Similar to singly injected morphants, *syngap1b/shank3a* double morphants exhibited increased cell death in the mid- and hindbrain compared with controls (Supplementary material, Table S10–S15). However, in comparison to singly injected morphants, *syngap1b/shank3a* double morphants did not show significantly increased cell death of the spinal cord. This brain-specific increase of cell death in *syngap1b/shank3a* double morphants suggests that disruptions in the mid- and hindbrain are sufficient to cause morphant behavioral phenotypes.

Discussion

Our results demonstrate that prior to their established roles in synaptogenesis, *SYNGAP1* and *SHANK3* play critical roles in embryonic development. A major research focus in models of human *SYNGAP1* and *SHANK3* haploinsufficiency has been synapse function (24,28,32,36–39,44,63,64–67). While reductions in *SYNGAP1* or *SHANK3* gene expression induce overlapping behavioral phenotypes in both animal models and individuals with ASD (36–38,41,68), these proteins have divergent roles at glutamatergic synapses: reductions in SYNGAP1 precociously strengthen synaptic transmission (37,43) while reductions in SHANK3 weaken synaptic transmission (38,63). Therefore, to look beyond their defined synaptic role and to complement previous mammalian models, we chose zebrafish to provide an embryonic window into the unknown developmental roles of *SYNGAP1* and *SHANK3*.

By assessing developmental phenotypes in zebrafish morphant models of *SYNGAP1* and *SHANK3*, we build upon studies modeling ASD-linked genes *DISC1*, *CHD8*, *MET*, *AUTS2*, *FMR1* and *SHANK3* in zebrafish (46,48,57,69–71). In addition to embryonic phenotypes that are consistent with previous zebrafish ASD models, we describe a digenic model wherein a combined sub-phenotypic reduction in gene expression of both *syngap1b* and *shank3a* recapitulate phenotypes seen in more severe single gene loss-of-function mutations. Therefore, our study is unique in directly comparing two 'single gene' ASD models, demonstrating their genetic synergy, and bringing to light both commonalities and differences in underlying embryonic processes that explain phenotypes. We find that reducing either single gene or a mild reduction of both genes resulted in embryonic cell death, developmental delays, unproductive locomotion and seizure-like behaviors. We suggest that this early pathology

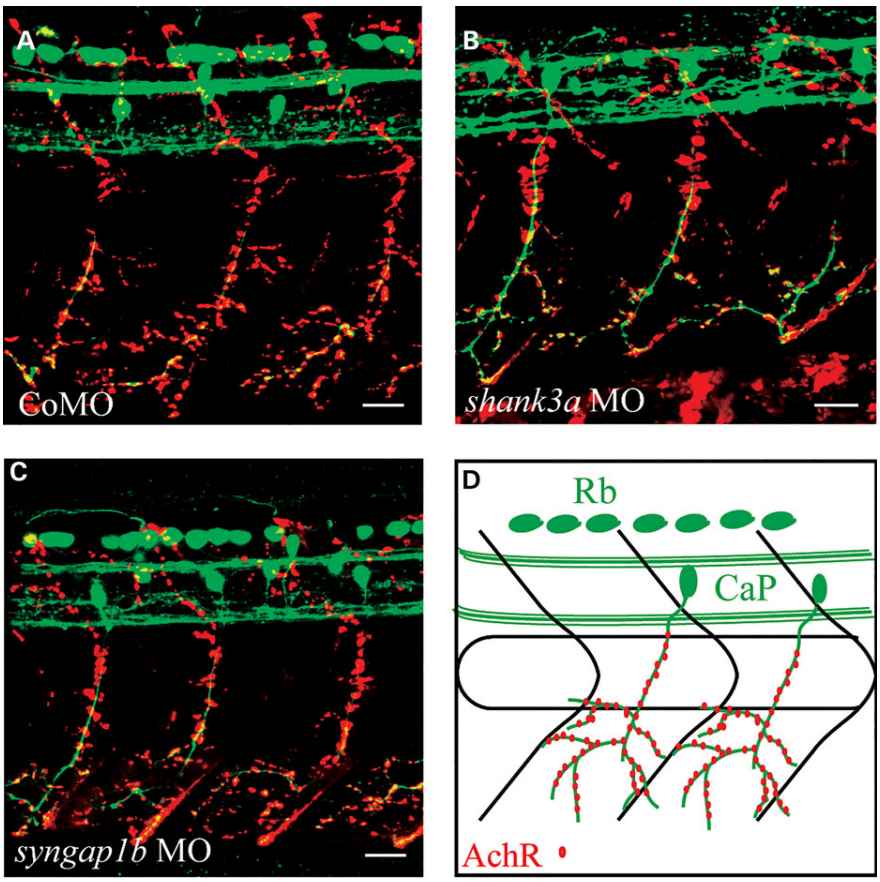

Figure 7. Motor neuron innervation of muscle is stage-appropriate in 48 hpf *syngap1b* and *shank3a* morphants. Lateral views of morphant spinal cords in stable transgenic SAIGFF213A:GFP embryos injected with Tetramethylrhodamine α-Bungarotoxin to label acetylcholine receptors (AchR). In the SAIGFF213A:GFP line, GFP is expressed in Caudal Primary (CaP) motor neurons and Rohon-Beard (Rb) sensory neurons. *syngap1b* ($n = 4$), *shank3a* ($n = 4$) and control ($n = 4$) morphants all exhibit stage-appropriate CaP motor neurons (green) and AchR clusters in muscle (red). Rb neurons are absent in *shank3a* morphants but present in both control and *syngap1b* morphants. Scale bars = 25 μm. The diagram in the lower right serves as a key.

may contribute to later phenotypes by disrupting embryonic critical periods essential for mature neural circuit function (72).

SHANK3 and *SYNGAP1* are expressed at embryonic stages in the central nervous system

As we report here for zebrafish, *SYNGAP1* and *SHANK3* orthologs are also expressed at embryonic stages in the nervous systems of human, mouse and *Xenopus* (73–77). In humans at 8 weeks post-conception, *SYNGAP1* expression is most pronounced in the developing hippocampal formation and amygdaloid complex, while both *SYNGAP1* and *SHANK3* show pronounced expression in the nascent cerebellum (upper rhombic lip) (76). In mouse embryos, *Syngap1* is expressed broadly throughout the body (E8.5) with a progressive restriction to the brain (E10.5) and then to specific brain regions (E16.5), such as the hippocampus, hypothalamus, dorsal thalamus and basal ganglia (73). Mouse *Shank3* expression has been reported in cardiac progenitor cells (E7.5–8.5) and later in whole brain cortex (E15; 74,75). Additionally, *Xenopus laevis* frog embryos express *shank3* during embryogenesis in the cardiovascular system, isthmus, brain, neural tube, retina and hypochord (77). Taken together, both *SYNGAP1* and *SHANK3* are expressed broadly in vertebrate embryos with a progressive enrichment to brain regions during development. Despite these expression profiles, the developmental roles of *Syngap1* and *Shank3* prior to synaptogenesis remain unknown.

Syngap1b and *shank3a* play critical roles in brain morphogenesis

Consistent with embryonic *SYNGAP1* and *SHANK3* expression in vertebrates, knockdown of *syngap1b*, *shank3a* or the combination disrupts brain morphogenesis suggesting novel embryonic roles for these genes. Our findings are in line with a recent and growing body of literature indicating that ASD pathobiology starts in the early embryo. For example, zebrafish knockdown and mutant models of z*DISC1* and *chd8* have revealed novel roles for these genes in regulating brain morphology as early as gastrulation (48,49). In addition, *DISC1* and ANK3 mutant mouse models have functionally linked these genes to neuronal migration

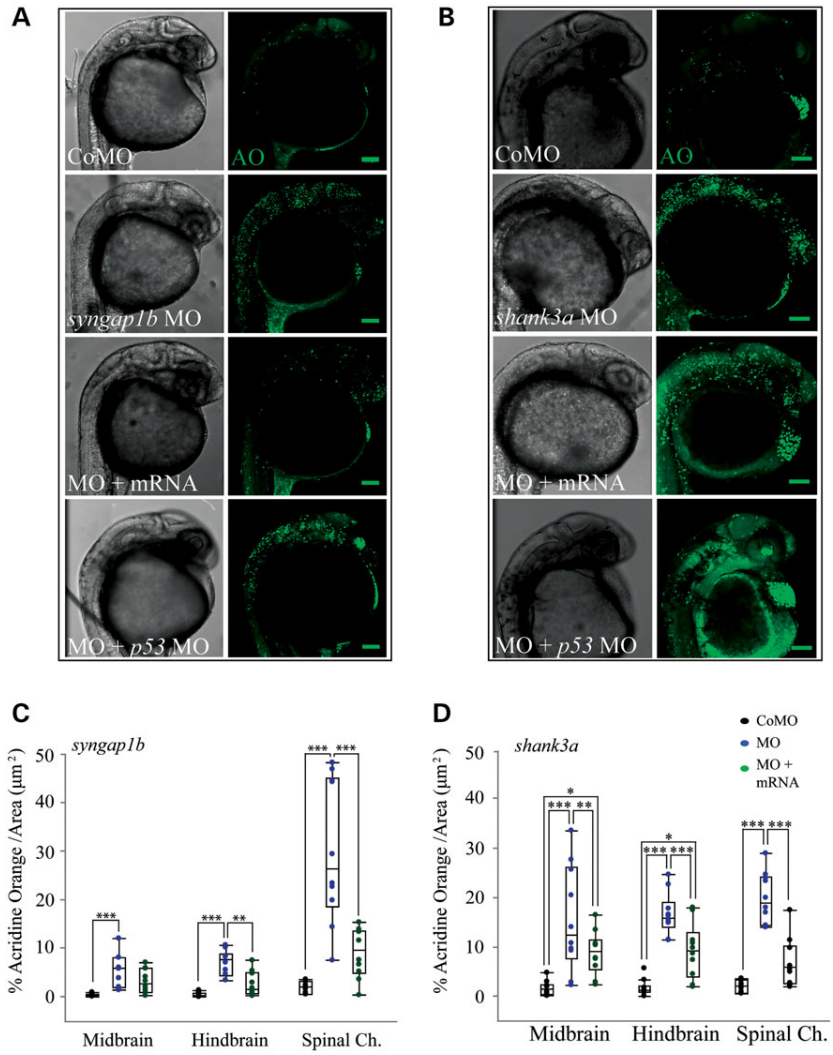

Figure 8. Cell death is increased in 28–30 hpf *syngap1b*, *shank3a* and *syngap1b/shank3a* morphants. (**A**) *shank3a* MO and (**B**) *syngap1b* MO were stained with acridine orange (AO) to visualize cell death. Morphants were also co-injected either with the corresponding human mRNA or *p53* MO to assess the nature of the cell death pathway and whether cell death was gene-specific. Scale bars = 100 µm. (**C** and **D**) Staining was quantified using the percent area fraction method (Fiji) in midbrain, hindbrain and spinal cord regions. Death is partially rescued in hindbrain and spinal cord regions by co-injection of either human (C) *SYNGAP1* mRNA ($n = 10$) or (D) human *SHANK3* mRNA ($n = 10$), respectively. Data were analyzed using a one-way ANOVA with a *post-hoc* means comparison and Bonferroni correction. Box plot lines represent the first quartile (bottom), median (middle) and third quartile (top). Asterisks indicate significance values for means comparison, $^{*}P < 0.01$, $^{**}P < 0.001$, $^{***}P < 0.0001$, (Supplementary Material, Tables S8–15).

during embryonic brain morphogenesis (78–80). Several studies on human ASD post-mortem tissues have suggested that neural patterning processes in the embryo may contribute generally to ASD pathophysiology (81–83). The disorganized cytoarchitecture and cortical layering typical of post-mortem ASD brains may be explained by aberrant neurogenesis and cellular migration in the embryo (82,84). Therefore, our findings are consistent with an emerging viewpoint that ASD pathobiology starts at embryonic stages when diverse signaling pathways regulate proliferation, migration and cell death of neural progenitors to shape the brain.

Likely a consequence of altered brain morphogenesis, another common phenotype in individuals with ASD is developmental delay. Indeed, developmental delays are a consistent diagnosis in patients with *SHANK3* and *SYNGAP1* mutations; however, the underlying causes of these developmental delays are largely unknown (23,24,28,31,63). Our results indicate that commonalities observed in developmental delays in zebrafish *syngap1b* and *shank3a* morphants arise though distinct mechanisms. Despite the fact that both *syngap1b* and *shank3a* models show increased cell death, the underlying mechanisms for cell death differ in *syngap1b* and *shank3a* morphants, with only *shank3a* morphant cell

death occurring through a p53-dependent pathway. Despite the ability to rescue *syngap1b* and *shank3a* morphant cell death with mRNAs encoding human orthologs, we are tentative about the extent of gene-specific cell death because cell death is also a commonly reported phenotype associated with morpholino toxicity. With this in mind, our results suggest that distinct molecular pathways underlie cell death in *syngap1b* and *shank3a* morphants yielding phenotypically similar developmental delays.

Behavioral phenotypes suggest disruptions in hindbrain regulation of swim circuits

Swimming behaviors are a sensitive indicator of early nervous system function in zebrafish due to a highly stereotyped and rapidly expanding repertoire of locomotor behaviors produced by well-characterized neuronal circuits (85,86). Early behaviors are produced by some of the first neurons to be born during neurogenesis. These include descending mid- and hindbrain interneurons that drive rhythmic firing in motor neurons to produce one of the first coordinated locomotory behaviors, the escape response (86,87) *Syngap1a, syngap1b, shank3a* and double *syngap1b/shank3a* morphant escape responses are characterized by unusually long-lasting and unproductive swimming which could result from reductions in the number of descending brain neurons that would normally function to activate and inhibit spinal cord circuits. This idea is supported by work in both zebrafish, where swimming behavior is triggered via hindbrain descending Glutamatergic V2a neurons, and *Xenopus laevis*, where neuronal activity in mid/hindbrain GABAergic neurons is associated with terminating bouts of swimming (88–90). Our data suggest that a stage-appropriate neuromuscular system paired with significantly delayed mid- and hindbrain regions could account for *syngap1* and *shank3* morphant behavioral deficits.

In addition to weaker swims, a proportion of *syngap1b, shank3a* and double *syngap1b/shank3a* morphants exhibited seizure-like behaviors consistent with some level of hyper-excitability or lack of proper inhibition. A disruption in establishing or maintaining the balance between neurons expressing excitatory and inhibitory neurotransmitters (E/I balance) has been put forward as a major convergent phenotype in individuals with ASD (8,72,91). Morphological analyses of postmortem brains from individuals with ASD find disordered GABAergic and glutamatergic processes in cortical mini-columns and depressed production of inhibitory GABA (92,93). E/I balance has also been explored in animal ASD models: Gogolla *et al.* (72) conducted a meta-analysis of ASD mouse models and found that a reduction in GABAergic neurons was a common phenotype with functional implications for early critical periods. The importance of E/I balance is underscored by the prevalence (25–30%) of epileptic symptoms in individuals with ASD, including those carrying *SYNGAP1* and *SHANK3* mutations (22–24). Epilepsy has been thought of as a disruption in E/I balance generating periods of asynchronous and abnormal behavior (91). Our results suggest that hyper-excitable behaviors are linked to brain-region-specific developmental delays. This hypothesis bears testing in the context of known circuits in stable mutant models.

Functional interactions and network susceptibility may explain *syngap1b* and *shank3a* phenotypes

Individuals with ASD tend to carry a higher mutational burden for both SNPs and CNVs (94). Although mutations linked to ASD occur in hundreds of distinct genes, common genetic and protein networks indicate high functional connectivity among genes and proteins causal for ASD. This connectivity is observed between Syngap1 and Shank3 that have been suggested to interact directly, while being functionally connected within the post-synaptic density of glutamatergic neurons (42). In addition, these functionally connected gene clusters, such as those associated with synapses, tend to have overlapping temporal and spatial gene expression (95). These patterns of expression indicate crucial networks, that when disrupted, bias an individual towards ASD. Therefore, it is not surprising that single gene knockdowns, or a combination of *syngap1b* and *shank3a* dual knockdowns produce similar phenotypes in light of their shared functions, protein interactions and temporal and spatial expression patterns.

Conclusion

Here we report for the first time that *syngap1* and *shank3* serve important functional roles at early stages of vertebrate brain morphogenesis that precede synaptogenesis. These models demonstrate that knocking down *syngap1b* and *shank3a* causes CNS-specific cell death and developmental delay in mid- and hindbrain regions that likely contributes to hyper-excitable behavior. By providing this window into early developmental, our findings in zebrafish support the emerging viewpoint that ASD gene mutations likely impact neonatal stages contributing to ASD pathology. In the future, it will be critical to establish stable zebrafish mutants to investigate the shared causes and long-term functional consequences of early developmental dysfunction.

Materials and Methods

Fish maintenance and embryo rearing

Transgenic lines Tg vglut2:dsRed (96) and Tg SaigFF213A (81) were used for all morpholino knockdown experiments. After briefly rinsing zygotes in deionized water, embryos and larvae were raised in glass petri plates filled with 28°C 'system water' (water from aquaria housing adult zebrafish) and staged by hours post-fertilization. Both adults and embryos were maintained on a 14:10 circadian light:dark cycle. Fish in our facility are cared for in accordance with National Institute of Health (NIH) animal care guidelines and the University of Miami's Institutional Animal Care and Use Committee (IACUC) have approved all animal protocols.

Evolutionary comparison of Syngap1 and shank proteins

Sequences of proteins belonging to the DABIP2 (Rasgaps including Syngap1) and Shank families were identified in genomes by using the NCBI blast program and confirmed by best reciprocal blast. Presence or absence data were collated and mapped onto a phylogenetic tree of animals (97). For the analysis of Shank3, sequences were aligned using Clustal Omega (98) and imported into Adobe Illustrator (Adobe Systems Inc., San Jose, CA, USA) where regions of high local similarity were identified.

Whole mount *in situ* hybridization

Larvae were dechorionated and placed in a mixture of fish facility system water and 0.003% phenothiourea at 24 hpf. RNA syntheses of sense and anti-sense probes were carried out using the DIG RNA labeling kit (SP6; Roche, Mannheim, Germany). See Supplementary Material, Table S1 for *in situ* hybridization primers used to amplify and synthesize RNA probes. The *in situ* protocol

was adapted from a previous study, with a hybridization buffer containing 70% formamide and incubations carried out at 55°C (99). Whole mount images were captured using an Olympus D71 micro-imager mounted on a compound Olympus microscope at ×40 and ×100 magnification.

RT–qPCR developmental time course

Total RNA was extracted from zebrafish embryos at 2, 5, 8, 12, 15, 24, 36, 48, 72, 96 and 120 hpf using TRIzol reagent (Life Technologies, Carlsbad, CA, USA). Three samples consisting of 25-pooled embryos at each time point were used for RNA extraction. Extracted RNA was treated with DNase (Life Technologies, Carlsbad, CA, USA) according to the manufacturer's protocol. All RNAs and templates were quantified using a NanoDrop ND-1000 spectrophotometer (Thermo Scientific, Pittsburgh PA, USA), with 260/280 ratios of between 1.9 and 2.0. Whole RNA samples were run on 1% agarose gels to determine RNA integrity. RT–qPCR was performed using the qScript One-Step SYBR Green qRT-PCR kit (Quanta Biosciences, Gaithersburg, MD, USA) to test the expression level of *syngap1a, syngap1b*, *shank3a*, *shank3b* and *eef1a1/1* during development. *eef1a1/1* was chosen as a housekeeping gene in a previous study (100) due to its consistent expression profile following 5 hpf. Primers (Integrated DNA Technologies, Coralville, IA, USA) for each gene used in this study were designed using primer3 and BLAT (https://genome.ucsc.edu/cgi-bin/hgBlat) against the zebrafish genome to confirm gene specificity (101). Each RT–qPCR reaction contained: 1X One-Step SYBR Green Master Mix, 200 nM forward and reverse gene-specific primer, 100 ng RNA template, 1X qScript One-Step RT and nuclease-free water to a final volume of 50 µl. The cycling conditions were: 48°C for 10 min; 95°C for 5 min; 40 cycles of 95°C for 10 s, 60°C for 20 s and 72°C for 45 s; 72–95°C for 20 min (melt analysis); 95°C for 15 s. RT–qPCR reactions were run using an Eppendorf Mastercycler ep realplex (Eppendorf, Hamburg, Germany). Absolute quantification of each sample was based on linear regression of standard curve samples (See Supplementary Material, Methods and Tables S2–S5 for RT–qPCR validation and analysis.)

Antisense morpholino oligonucleotide injections

Splice-inhibiting morpholino oligonucleotides (MOs; Gene Tools, LLC. Philomath, OR, USA; Supplementary Material, Table S6) were designed against the common exon–intron boundaries based upon *syngap1a*, *syngap1b, shank3a* and *shank3b* variants annotated in the Ensembl database. We found that the genome annotation of *shank3a* was inaccurate with the single gene reported as two discontinuous 3′ and 5′ segments. We designed a forward (5′-TGGAAACTTTGACCTGGCAG-3′) and a reverse primer (5′-GGGAGTGTGAGGAC AACGAG-3′) that spanned the gap and sequenced this middle portion of the *shank3a* gene. MO design was based on this assembled sequence and the correction was reported to Ensembl (GenBank accession no. LM994718). Lyophilized MOs were resuspended in nuclease free H_2O as 1 mM stock solution, aliquotted and stored at 4°C. To ensure full resuspension of stored MOs, stock solutions were heated to 65°C prior to making dilutions for injections. For injections, MOs were diluted with 1% fast green and injected into one-cell zygotes. To ensure that only successfully injected embryos were further analyzed, a few hours after injection, embryos were sorted for even distribution of the green color throughout yolk and embryo. For each morpholino, we generated dose–response curves by injecting a series of dilutions (2 nl bolus at 1, 0.5, 0.25 mM), scoring resulting phenotypes and comparing these to embryos injected with molarity-matched standard control morpholino (CoMO, Gene Tools, LLC). Dilutions with the highest behavioral penetrance that lacked severe morphological defects were used for more detailed analyses. To explore the possibility of synergy between gene duplicates (ohnologs), MOs for *syngap1a* and *syngap1b* were co-injected at doses that failed to cause with phenotypes when singly injected. The MOs from *syngap1b* and *shank3a*, *syngap1a* and *shank3a* and *syngap1b* and *shank3b* were also co-injected at sub-phenotypic doses to test for synergistic effects between zebrafish SYNGAP1 and SHANK3 orthologs at the level of behavior and morphology.

RT–PCR and sequencing to validate MO knockdown

RNA was harvested from a time series of 24, 32, 48 and 72 hpf embryos and larvae using TRIzol followed by DNASE treatment according to standard protocols (Life Technologies, Carlsbad, CA, USA). For cDNA synthesis, 1 µg of RNA was reverse transcribed using the SuperScript III™ First-Strand Synthesis System (Life Technologies). cDNA was then used as template for PCR to test for mis-splicing events induced by the MOs. Primer pairs for sequencing spanned each exon/intron boundary targeted by morpholinos (See Supplemental Material, Table S3 for a list of these primers.) However, the wild-type PCR product for *shank3a* did not show a shift in band size or number of bands, therefore we elected to use an intron reverse primer to show intron retention. Each PCR reaction contained: 1X GoTAQ hot start green master mix (Promega, Madison, WI), 500 nM forward and reverse primer, 100 ng of cDNA template and nuclease-free H_2O to a final volume of 10 µl. The cycling conditions were: 95°C for 2 min; 35 cycles of 95°C for 30 s, 55°C for 30 s, 72°C for 1 min; 72°C for 5 min and 4°C for storage. PCR products were run on a 1% agarose gel and checked for banding patterns and relative band intensities. Bands were gel-purified, and re-amplified for sequencing to determine how splicing was impacted by MO injections. To document morphant morphological defects, pictures were captured on an AxioCam MRm (Zeiss, Inc., Jena, Germany).

Behavioral and morphological analysis

To analyze morpholino-induced behavioral phenotypes, high-speed videos were captured using a Fastcam 1024PCI (Photron USA Inc., San Diego, CA, USA). This camera was either mounted on a dissecting scope, or for FLOTE analysis, mounted with a Fujinon lens in a customized behavioral chamber. Parameters were as follows: shutter speed of 1/1000 using an LED array for backlit illumination (Advance Illumination; Rochester VT; Backlight LED Illuminator), 512 × 512 resolution, a frame rate of 250 f/s to assess swimming qualitatively and 1000 f/s to assess swimming kinematics. Three touch-evoked behaviors, elicited using tungsten or fishing line probes, were recorded per individual. After capturing videos, Flote (56) was used to quantitate changes in axis curvature over time and swimming velocity. Shadows from the tungsten probe disrupt the Flote tracking software, and were lessened using fishing line probes.

For morphological analysis, images were captured on an Olympus D71 advanced micro-imager mounted on a Wild dissecting microscope. For cell death rescue experiments, the human *SYNGAP1* mRNA construct was cloned into a pCS2+ backbone, while the human *SHANK3* α-isoform was codon optimized using GeneART (Life Technologies) to address cloning difficulties associated with high GC content. Human *SYNGAP1* and *SHANK3* were linearized with *Sac*II and *Not*I, respectively, and capped mRNA was transcribed using the SP6 mMessage mMachine kit

(Life Technologies). Acridine Orange (Sigma, St Louis, MO, USA) was used to stain for cell death following a previously published protocol (60). After staining, embryos were anesthetized using 0.02% MS222 and mounted on a glass bottom dish in 3% methylcellulose. Images of stained embryos were collected as z-stacks on a Leica SP5 confocal microscope (Leica Microsystems, Wetzlar, Germany).

Excitatory/inhibitory immunohistochemical staining

To measure excitatory and inhibitory neurons, vglut2:DsRed embryos were counter stained with a primary antibody targeting γ-aminobutyric acid (GABA, a polyclonal GABA anti-rabbit, Sigma Aldrich, Poole, England). Morphants were collected and sorted at 48 hpf for vglut2:DsRed fluorescence and characteristic swimming behaviors. Prior to fixation, larvae were anesthetized on ice for 30 min. The water was then replaced with 4% paraformaldehyde (16% stock, Pierce Protein Biology Products, Rockford, IL, USA) in ×1 phosphate buffer solution (PBS) and samples were incubated on a rocker for 2 h at room temperature. After three washes of ×1 PBS, samples were placed in a ×1 PBS, 30% sucrose solution and rocked at 4°C for 2 h. Larvae were then embedded in tissue-freezing medium (Triangle Biomedical Sciences, Inc., Durham, NC, USA) and orientated to achieve horizontal section of the forebrain and transverse sections of the mid- and hindbrain. Frozen blocks of tissue were sectioned on a Leica CM1850 cryostat (Leica Microsystems, Wetzlar, Germany). Slides were incubated at room temperature for 10 min and then transferred to a Sequenza™ Slide Rack in Coverplates™ (Thermo Shandon Limited, Astmoor, Runcorn Cheshire WA7 1PR) and washed with a 0.4% TritonX-100 PBS solution (PBSTx). After washing, the sections were incubated in blocking solution (5% donkey serum in PBSTx) for 1 h followed by an overnight incubation in primary antibody PBSTx solution. A primary antibody targeting GABA was used at concentrations of 1:500 and 1:1000 for 48 and 96 hpf, respectively. Sections were then washed six times with ×1 PBS, followed by a 2 h incubation in a fluorescent secondary antibody (Alexa Fluor, goat anti-rabbit IgG, Molecular Probes, Eugene, OR, USA). Following secondary incubation, the sections were again washed six times with ×1 PBS. Sections were then mounted using 1-thiodiethanol (Sigma, St Louis, MO, USA) and viewed on a Leica SP5 confocal microscope (Leica Microsystems, Wetzlar, Germany). Single frames and z-stacks were captured for the 48 and 96 hpf sections, respectively.

Quantification of dye and immunohistochemical staining

Analyses of acridine orange staining and vglut2:dsred/GABA expression were performed using Fiji (102). For acridine orange staining of brain regions, sagittal z-stacks were measured using the percent area fraction function with an IsoData automatic threshold. The percent of acridine orange staining was then compared via ANOVA, with a *post-hoc* Student's *t*-test means comparison using Bonferroni correction for multiple comparisons in the statistical package JMP (SAS Institute Inc.). Fiji was also used to measure the area of immunohistochemical staining in transverse sections from forebrain (anterior-mid-thalamus and anterior optic tectum), posterior forebrain/midbrain (hypothalamus to tegmentum) and hindbrain (medulla oblongata). Differences in morphant GABA expression were quantified by counting GABA/DAPI positive cell bodies in brain hemi-segments. In contrast to GABA, vglut expression was quantified using the Fiji area fraction function because we could not distinguish individual cell bodies in the dorsal-most brain regions. The overall cortical area of specific brain regions was recorded to assess differences in overall brain size. Area measurements were calculated in microns squared. Statistical analyses were performed using Student's *t*-test. Brain regions were annotated following the scheme of Mueller *et al.* (103).

Supplementary Material

Supplementary Material is available at *HMG* online.

Acknowledgements

We would like to acknowledge the following people for their contribution to this study. Thanks to the University of Miami zebrafish facility staff, especially the facility manager Ricardo Cepeda, for keeping the zebrafish in excellent health. Undergraduate volunteers Andre Naranjo, Eduardo Keene and Rachel Salinger aided in the collection of behavioral videos and PCR. Thanks to Pantelis Tsouflas and Andrew Darr for providing *p53* morpholino, to Dr Jeffrey Prince for allowing us to use his Olympus D71 microimager for *in-situ* and morphology images, and to the imaging core laboratory in the Department of Biology at the University of Miami for assistance in confocal imaging and analysis. J.D.B. thanks the Marine Biological Laboratory (Woods Hole, MA, USA) for supporting early work on (i) developing reagents for studying shank3 in zebrafish and (ii) dissecting phenotypes associated with *shank3* knockdown.

Conflict of Interest statement. None declared.

Funding

This work was supported by the National Institutes of Health (MH103857 to J.E.D.) from the NIH National Institutes of Mental Health, to the Seaver Foundation (grant to J.D.B., fellowship to G.C.) and generous support from the John P. Hussman Foundation.

References

1. Kim, Y.S., Leventhal, B.L., Koh, Y.J., Fombonne, E., Laska, E., Lim, E.C., Cheon, K.A., Kim, S.J., Kim, Y.K., Lee, H. *et al.* (2011) Prevalence of autism spectrum disorders in a total population sample. *Am. J. Psychiatry*, **168**, 904–912.
2. American Psychiatric Association. (2013) *Diagnostic and Statistical Manual of Mental Disorders*, 5th edn. American Psychiatric Publishing, Arlington, VA.
3. Sanders, S.J., Ercan-Sencicek, A.G., Hus, V., Luo, R., Murtha, M.T., Moreno-De-Luca, D., Chu, S.H., Moreau, M.P., Gupta, A.R., Thomson, S.A. *et al.* (2011) Multiple recurrent de novo CNVs, including duplications of the 7q11.23 Williams syndrome region, are strongly associated with autism. *Neuron*, **70**, 863–885.
4. Pinto, D., Pagnamenta, A.T., Klei, L., Anney, R., Merico, D., Regan, R., Conroy, J., Magalhaes, T.R., Correia, C., Abrahams, B.S. *et al.* (2010) Functional impact of global rare copy number variation in autism spectrum disorders. *Nature*, **466**, 368–372.
5. Weiss, L.A., Arking, D.E., Daly, M.J. and Chakravarti, A. (2009) A genome-wide linkage and association scan reveals novel loci for autism. *Nature*, **461**, 802–808.
6. Griswold, A.J., Ma, D., Cukier, H.N., Nations, L.D., Schmidt, M. A., Chung, R.H., Jaworski, J.M., Salyakina, D., Konidari, I., Whitehead, P.L. *et al.* (2012) Evaluation of copy number variations reveals novel candidate genes in autism

spectrum disorder-associated pathways. *Hum. Mol. Genet.*, **21**, 3513–3523.
7. Yu, T.W., Chahrour, M.H., Coulter, M.E., Jiralerspong, S., Okamura-Ikeda, K., Ataman, B., Schmitz-Abe, K., Harmin, D.A., Adli, M., Malik, A.N. *et al.* (2013) Using whole-exome sequencing to identify inherited causes of autism. *Neuron*, **77**, 259–273.
8. Betancur, C. (2011) Etiological heterogeneity in autism spectrum disorders: more than 100 genetic and genomic disorders and still counting. *Brain Res.*, **1380**, 42–77.
9. Krumm, N., O'Roak, B.J., Shendure, J. and Eichler, E.E. (2014) A de novo convergence of autism genetics and molecular neuroscience. *Trends Neurosci*, **37**, 95–105.
10. Rosti, R.O., Sadek, A.A., Vaux, K.K. and Gleeson, J.G. (2014) The genetic landscape of autism spectrum disorders. *Dev. Med. and Child Neurol.*, **56**, 12–18.
11. Beunders, G., Voorhoeve, E., Golzio, C., Pardo, L.M., Rosenfeld, J.A., Talkowski, M.E., Simonic, I., Lionel, A.C., Vergult, S., Pyatt, R.E. *et al.* (2013) Exonic deletions in AUTS2 cause a syndromic form of intellectual disability and suggest a critical role for the C terminus. *Am. J. of Hum. Gen.*, **92**, 210–220.
12. Herbert, M.R. (2011) SHANK3, the synapse, and autism. *N. Engl. J. Med.*, **365**, 173–175.
13. Verpelli, C. and Sala, C. (2012) Molecular and synaptic defects in intellectual disability syndromes. *Curr. Opin. Neurobiol.*, **22**, 530–536.
14. Ting, J.T., Peca, J. and Feng, G. (2012) Functional consequences of mutations in postsynaptic scaffolding proteins and relevance to psychiatric disorders. *Annu. Rev. Neurosci.*, **35**, 49–71.
15. Cukier, H.N., Dueker, N.D., Slifer, S.H., Lee, J.M., Whitehead, P.L., Lalanne, E., Leyva, N., Konidari, I., Gentry, R.C., Hulme, W.F. *et al.* (2014) Exome sequencing of extended families with autism reveals genes shared across neurodevelopmental and neuropsychiatric disorders. *Mol. Autism*, **5**, 1.
16. Grant, S.G. (2012) Synaptopathies: diseases of the synaptome. *Curr. Opin. Neurobiol.*, **22**, 522–529.
17. Leblond, C.S., Heinrich, J., Delorme, R., Proepper, C., Betancur, C., Huguet, G., Konyukh, M., Chaste, P., Ey, E., Rastam, M. *et al.* (2012) Genetic and functional analyses of SHANK2 mutations suggest a multiple hit model of autism spectrum disorders. *PLoS Genet.*, **8**, e1002521.
18. Gaugler, T., Klei, L., Sanders, S.J., Bodea, C.A., Goldberg, A.P., Lee, A.B., Mahajan, M., Manaa, D., Pawitan, Y., Reichert, J. *et al.* (2014) Most genetic risk for autism resides with common variation. *Nat. Genet.*, **46**, 881–885.
19. Grabrucker, A.M. (2012) Environmental factors in autism. *Front. Psychiatry*, **3**, 118.
20. Grabrucker, S., Jannetti, L., Eckert, M., Gaub, S., Chhabra, R., Pfaender, S., Mangus, K., Reddy, P.P., Rankovic, V., Schmeisser, M.J. *et al.* (2014) Zinc deficiency dysregulates the synaptic ProSAP/Shank scaffold and might contribute to autism spectrum disorders. *Brain*, **137**, 137–152.
21. Jacob, J., Ribes, V., Moore, S., Constable, S.C., Sasai, N., Gerety, S.S., Martin, D.J., Sergeant, C.P., Wilkinson, D.G. and Briscoe, J. (2014) Valproic acid silencing of ascl1b/Ascl1 results in the failure of serotonergic differentiation in a zebrafish model of fetal valproate syndrome. *Dis. Mod. Mech.*, **7**, 107–117.
22. Klitten, L.L., Moller, R.S., Nikanorova, M., Silahtaroglu, A., Hjalgrim, H. and Tommerup, N. (2011) A balanced translocation disrupts SYNGAP1 in a patient with intellectual disability, speech impairment, and epilepsy with myoclonic absences (EMA). *Epilepsia*, **52**, e190–e193.
23. Berryer, M.H., Hamdan, F.F., Klitten, L.L., Moller, R.S., Carmant, L., Schwartzentruber, J., Patry, L., Dobrzeniecka, S., Rochefort, D., Neugnot-Cerioli, M. *et al.* (2013) Mutations in SYNGAP1 cause intellectual disability, autism, and a specific form of epilepsy by inducing haploinsufficiency. *Hum. Mutat.*, **34**, 385–394.
24. Phelan, K. and McDermid, H.E. (2012) The 22q13.3 deletion syndrome (Phelan-McDermid Syndrome). *Mol. Syndromol.*, **2**, 186–201.
25. Hamdan, F.F., Gauthier, J., Araki, Y., Lin, D.T., Yoshizawa, Y., Higashi, K., Park, A.R., Spiegelman, D., Dobrzeniecka, S., Piton, A. *et al.* (2011) Excess of de novo deleterious mutations in genes associated with glutamatergic systems in nonsyndromic intellectual disability. *Am. J. Hum. Genet.*, **88**, 306–316.
26. Zollino, M., Gurrieri, F., Orteschi, D., Marangi, G., Leuzzi, V. and Neri, G. (2011) Integrated analysis of clinical signs and literature data for the diagnosis and therapy of a previously undescribed 6p21.3 deletion syndrome. *Eur. J. Hum. Genet.*, **19**, 239–242.
27. Krepischi, A.C., Rosenberg, C., Costa, S.S., Crolla, J.A., Huang, S. and Vianna-Morgante, A.M. (2010) A novel de novo microdeletion spanning the SYNGAP1 gene on the short arm of chromosome 6 associated with mental retardation. *Am. J. Med. Genet. A*, **152A**, 2376–2378.
28. Hamdan, F.F., Gauthier, J., Spiegelman, D., Noreau, A., Yang, Y., Pellerin, S., Dobrzeniecka, S., Cote, M., Perreau-Linck, E., Carmant, L. *et al.* (2009) Mutations in SYNGAP1 in autosomal nonsyndromic mental retardation. *N. Engl. J. Med.*, **360**, 599–605.
29. Sarasua, S.M., Dwivedi, A., Boccuto, L., Chen, C.F., Sharp, J.L., Rollins, J.D., Collins, J.S., Rogers, R.C., Phelan, K. and Dupont, B.R. (2013) 22q13.2q13.32 genomic regions associated with severity of speech delay, developmental delay, and physical features in Phelan-McDermid syndrome. *Genet. Med.*, **16**, 318–328.
30. Soorya, L., Kolevzon, A., Zweifach, J., Lim, T., Dobry, Y., Schwartz, L., Frank, Y., Wang, A.T., Cai, G., Parkhomenko, E. *et al.* (2013) Prospective investigation of autism and genotype-phenotype correlations in 22q13 deletion syndrome and SHANK3 deficiency. *Mol. Autism.*, **4**, 18.
31. Betancur, C. and Buxbaum, J.D. (2013) SHANK3 haploinsufficiency: a "common" but underdiagnosed highly penetrant monogenic cause of autism spectrum disorders. *Mol. Autism.*, **4**, 17.
32. Boccuto, L., Lauri, M., Sarasua, S.M., Skinner, C.D., Buccella, D., Dwivedi, A., Orteschi, D., Collins, J.S., Zollino, M., Visconti, P. *et al.* (2013) Prevalence of SHANK3 variants in patients with different subtypes of autism spectrum disorders. *Eur. J. Hum. Genet.*, **21**, 310–316.
33. Durand, C.M., Betancur, C., Boeckers, T.M., Bockmann, J., Chaste, P., Fauchereau, F., Nygren, G., Rastam, M., Gillberg, I.C., Anckarsater, H. *et al.* (2007) Mutations in the gene encoding the synaptic scaffolding protein SHANK3 are associated with autism spectrum disorders. *Nat. Genet.*, **39**, 25–27.
34. Kelleher, R.J. III, Geigenmuller, U., Hovhannisyan, H., Trautman, E., Pinard, R., Rathmell, B., Carpenter, R. and Margulies, D. (2012) High-throughput sequencing of mGluR signaling pathway genes reveals enrichment of rare variants in autism. *PLoS One*, **7**, e35003.
35. Schaaf, C.P. and Zoghbi, H.Y. (2011) Solving the autism puzzle a few pieces at a time. *Neuron*, **70**, 806–808.
36. Peca, J., Feliciano, C., Ting, J.T., Wang, W., Wells, M.F., Venkatraman, T.N., Lascola, C.D., Fu, Z. and Feng, G. (2011) Shank3

mutant mice display autistic-like behaviours and striatal dysfunction. *Nature*, **472**, 437–442.
37. Clement, J.P., Aceti, M., Creson, T.K., Ozkan, E.D., Shi, Y., Reish, N.J., Almonte, A.G., Miller, B.H., Wiltgen, B.J., Miller, C.A. *et al.* (2012) Pathogenic SYNGAP1 mutations impair cognitive development by disrupting maturation of dendritic spine synapses. *Cell*, **151**, 709–723.
38. Wang, X., McCoy, P.A., Rodriguiz, R.M., Pan, Y., Je, H.S., Roberts, A.C., Kim, C.J., Berrios, J., Colvin, J.S., Bousquet-Moore, D. *et al.* (2011) Synaptic dysfunction and abnormal behaviors in mice lacking major isoforms of Shank3. *Hum. Mol. Genet.*, **20**, 3093–3108.
39. Bozdagi, O., Sakurai, T., Papapetrou, D., Wang, X., Dickstein, D.L., Takahashi, N., Kajiwara, Y., Yang, M., Katz, A.M., Scattoni, M.L. *et al.* (2010) Haploinsufficiency of the autism-associated Shank3 gene leads to deficits in synaptic function, social interaction, and social communication. *Mol. Autism.*, **1**, 15.
40. Yang, M., Bozdagi, O., Scattoni, M.L., Wohr, M., Roullet, F.I., Katz, A.M., Abrams, D.N., Kalikhman, D., Simon, H., Woldeyohannes, L. *et al.* (2012) Reduced excitatory neurotransmission and mild autism-relevant phenotypes in adolescent Shank3 null mutant mice. *J. Neurosci.*, **32**, 6525–6541.
41. Muhia, M., Yee, B.K., Feldon, J., Markopoulos, F. and Knuesel, I. (2010) Disruption of hippocampus-regulated behavioural and cognitive processes by heterozygous constitutive deletion of SynGAP. *Eur. J. Neurosci.*, **31**, 529–543.
42. Sakai, Y., Shaw, C.A., Dawson, B.C., Dugas, D.V., Al-Mohtaseb, Z., Hill, D.E. and Zoghbi, H.Y. (2011) Protein interactome reveals converging molecular pathways among autism disorders. *Sci. Transl. Med.*, **3**, 86ra49.
43. Rumbaugh, G., Adams, J.P., Kim, J.H. and Huganir, R.L. (2006) SynGAP regulates synaptic strength and mitogen-activated protein kinases in cultured neurons. *Proc. Natl Acad. Sci. USA*, **103**, 4344–4351.
44. Arons, M.H., Thynne, C.J., Grabrucker, A.M., Li, D., Schoen, M., Cheyne, J.E., Boeckers, T.M., Montgomery, J.M. and Garner, C.C. (2012) Autism-associated mutations in ProSAP2/Shank3 impair synaptic transmission and neurexin-neuroligin-mediated transsynaptic signaling. *J. Neurosci.*, **32**, 14966–14978.
45. Tropepe, V. and Sive, H.L. (2003) Can zebrafish be used as a model to study the neurodevelopmental causes of autism? *Genes Brain Behav.*, **2**, 268–281.
46. Elsen, G.E., Choi, L.Y., Prince, V.E. and Ho, R.K. (2009) The autism susceptibility gene met regulates zebrafish cerebellar development and facial motor neuron migration. *Dev. Biol.*, **335**, 78–92.
47. Eisen, J.S. and Smith, J.C. (2008) Controlling morpholino experiments: don't stop making antisense. *Development*, **135**, 1735–1743.
48. De Rienzo, G., Bishop, J.A., Mao, Y., Pan, L., Ma, T.P., Moens, C. B., Tsai, L.H. and Sive, H. (2011) Disc1 regulates both beta-catenin-mediated and noncanonical Wnt signaling during vertebrate embryogenesis. *FASEB J.*, **25**, 4184–4197.
49. Bernier, R., Golzio, C., Xiong, B., Stessman, H.A., Coe, B.P., Penn, O., Witherspoon, K., Gerdts, J., Baker, C., Vulto-van Silfhout, A.T. *et al.* (2014) Disruptive CHD8 mutations define a subtype of autism early in development. *Cell*, **158**, 263–276.
50. Saint-Amant, L. and Drapeau, P. (1998) Time course of the development of motor behaviors in the zebrafish embryo. *J. Neurobiol.*, **37**, 622–632.
51. Alie, A. and Manuel, M. (2010) The backbone of the postsynaptic density originated in a unicellular ancestor of choanoflagellates and metazoans. *BMC Evol. Biol.*, **10**, 34.
52. Tu, J.C., Xiao, B., Naisbitt, S., Yuan, J.P., Petralia, R.S., Brakeman, P., Doan, A., Aakalu, V.K., Lanahan, A.A., Sheng, M. *et al.* (1999) Coupling of mGluR/Homer and PSD-95 complexes by the Shank family of postsynaptic density proteins. *Neuron*, **23**, 583–592.
53. Naisbitt, S., Kim, E., Tu, J.C., Xiao, B., Sala, C., Valtschanoff, J., Weinberg, R.J., Worley, P.F. and Sheng, M. (1999) Shank, a novel family of postsynaptic density proteins that binds to the NMDA receptor/PSD-95/GKAP complex and cortactin. *Neuron*, **23**, 569–582.
54. Myers, P.Z., Eisen, J.S. and Westerfield, M. (1986) Development and axonal outgrowth of identified motoneurons in the zebrafish. *J. Neurosci.*, **6**, 2278–2289.
55. Tang, R., Dodd, A., Lai, D., McNabb, W.C. and Love, D.R. (2007) Validation of zebrafish (Danio rerio) reference genes for quantitative real-time RT-PCR normalization. *Acta Biochim. Biophys. Sin.*, **39**, 384–390.
56. Burgess, H.A. and Granato, M. (2007) Sensorimotor gating in larval zebrafish. *J. Neurosci.*, **27**, 4984–4994.
57. Gauthier, J., Champagne, N., Lafreniere, R.G., Xiong, L., Spiegelman, D., Brustein, E., Lapointe, M., Peng, H., Cote, M., Noreau, A. *et al.* (2010) De novo mutations in the gene encoding the synaptic scaffolding protein SHANK3 in patients ascertained for schizophrenia. *Proc. Natl Acad. Sci. USA*, **107**, 7863–7868.
58. Muto, A., Ohkura, M., Kotani, T., Higashijima, S., Nakai, J. and Kawakami, K. (2011) Genetic visualization with an improved GCaMP calcium indicator reveals spatiotemporal activation of the spinal motor neurons in zebrafish. *Proc. Natl Acad. Sci. USA*, **108**, 5425–5430.
59. Panzer, J.A., Gibbs, S.M., Dosch, R., Wagner, D., Mullins, M.C., Granato, M. and Balice-Gordon, R.J. (2005) Neuromuscular synaptogenesis in wild-type and mutant zebrafish. *Dev. Biol.*, **285**, 340–357.
60. Furutani-Seiki, M., Jiang, Y.J., Brand, M., Heisenberg, C.P., Houart, C., Beuchle, D., van Eeden, F.J., Granato, M., Haffter, P., Hammerschmidt, M. *et al.* (1996) Neural degeneration mutants in the zebrafish, Danio rerio. *Development*, **123**, 229–239.
61. Robu, M.E., Larson, J.D., Nasevicius, A., Beiraghi, S., Brenner, C., Farber, S.A. and Ekker, S.C. (2007) p53 activation by knockdown technologies. *PLoS Genet.*, **3**, e78.
62. Yeo, W. and Gautier, J. (2005) XNGNR1-dependent neurogenesis mediates early neural cell death. *Mech. Dev.*, **122**, 635–644.
63. Shcheglovitov, A., Shcheglovitova, O., Yazawa, M., Portmann, T., Shu, R., Sebastiano, V., Krawisz, A., Froehlich, W., Bernstein, J.A., Hallmayer, J.F. *et al.* (2013) SHANK3 and IGF1 restore synaptic deficits in neurons from 22q13 deletion syndrome patients. *Nature*, **503**, 267–271.
64. Durand, C.M., Perroy, J., Loll, F., Perrais, D., Fagni, L., Bourgeron, T., Montcouquiol, M. and Sans, N. (2012) SHANK3 mutations identified in autism lead to modification of dendritic spine morphology via an actin-dependent mechanism. *Mol. Psychiatry*, **17**, 71–84.
65. Grabrucker, A.M., Knight, M.J., Proepper, C., Bockmann, J., Joubert, M., Rowan, M., Nienhaus, G.U., Garner, C.C., Bowie, J.U., Kreutz, M.R. *et al.* (2011) Concerted action of zinc and ProSAP/Shank in synaptogenesis and synapse maturation. *EMBO J.*, **30**, 569–581.

66. Roussignol, G., Ango, F., Romorini, S., Tu, J.C., Sala, C., Worley, P.F., Bockaert, J. and Fagni, L. (2005) Shank expression is sufficient to induce functional dendritic spine synapses in aspiny neurons. *J. Neurosci.*, **25**, 3560–3570.
67. Verpelli, C., Dvoretskova, E., Vicidomini, C., Rossi, F., Chiappalone, M., Schoen, M., Di Stefano, B., Mantegazza, R., Broccoli, V., Bockers, T.M. *et al.* (2011) Importance of Shank3 protein in regulating metabotropic glutamate receptor 5 (mGluR5) expression and signaling at synapses. *J. Biol. Chem.*, **286**, 34839–34850.
68. Muhia, M., Willadt, S., Yee, B.K., Feldon, J., Paterna, J.C., Schwendener, S., Vogt, K., Kennedy, M.B. and Knuesel, I. (2012) Molecular and behavioral changes associated with adult hippocampus-specific SynGAP1 knockout. *Learn. Mem.*, **19**, 268–281.
69. Oksenberg, N., Stevison, L., Wall, J.D. and Ahituv, N. (2013) Function and regulation of AUTS2, a gene implicated in autism and human evolution. *PLoS Genet.*, **9**, e1003221.
70. Tucker, B., Richards, R. and Lardelli, M. (2004) Expression of three zebrafish orthologs of human FMR1-related genes and their phylogenetic relationships. *Dev. Genes Evol.*, **214**, 567–574.
71. Tucker, B., Richards, R.I. and Lardelli, M. (2006) Contribution of mGluR and Fmr1 functional pathways to neurite morphogenesis, craniofacial development and fragile X syndrome. *Hum. Mol. Genet.*, **15**, 3446–3458.
72. Gogolla, N., Leblanc, J.J., Quast, K.B., Sudhof, T.C., Fagiolini, M. and Hensch, T.K. (2009) Common circuit defect of excitatory-inhibitory balance in mouse models of autism. *J. Neurodev. Disord.*, **1**, 172–181.
73. Porter, K., Komiyama, N.H., Vitalis, T., Kind, P.C. and Grant, S. G. (2005) Differential expression of two NMDA receptor interacting proteins, PSD-95 and SynGAP during mouse development. *Eur. J. Neurosci.*, **21**, 351–362.
74. Uchino, S., Wada, H., Honda, S., Nakamura, Y., Ondo, Y., Uchiyama, T., Tsutsumi, M., Suzuki, E., Hirasawa, T. and Kohsaka, S. (2006) Direct interaction of post-synaptic density-95/Dlg/ZO-1 domain-containing synaptic molecule Shank3 with GluR1 alpha-amino-3-hydroxy-5-methyl-4-isoxazole propionic acid receptor. *J. Neurochem.*, **97**, 1203–1214.
75. Masino, A.M., Gallardo, T.D., Wilcox, C.A., Olson, E.N., Williams, R.S. and Garry, D.J. (2004) Transcriptional regulation of cardiac progenitor cell populations. *Circ. Res.*, **95**, 389–397.
76. Miller, J.A., Ding, S.L., Sunkin, S.M., Smith, K.A., Ng, L., Szafer, A., Ebbert, A., Riley, Z.L., Royall, J.J., Aiona, K. *et al.* (2014) Transcriptional landscape of the prenatal human brain. *Nature*, **508**, 199–206.
77. Gessert, S., Schmeisser, M.J., Tao, S., Boeckers, T.M. and Kuhl, M. (2011) The spatio-temporal expression of ProSAP/shank family members and their interaction partner LAP-SER1 during Xenopus laevis development. *Dev. Dyn.*, **240**, 1528–1536.
78. Mao, Y., Ge, X., Frank, C.L., Madison, J.M., Koehler, A.N., Doud, M.K., Tassa, C., Berry, E.M., Soda, T., Singh, K.K. *et al.* (2009) Disrupted in schizophrenia 1 regulates neuronal progenitor proliferation via modulation of GSK3beta/beta-catenin signaling. *Cell*, **136**, 1017–1031.
79. Ming, G.L. and Song, H. (2009) DISC1 partners with GSK3beta in neurogenesis. *Cell*, **136**, 990–992.
80. Singh, K.K., De Rienzo, G., Drane, L., Mao, Y., Flood, Z., Madison, J., Ferreira, M., Bergen, S., King, C., Sklar, P. *et al.* (2011) Common DISC1 polymorphisms disrupt Wnt/GSK3beta signaling and brain development. *Neuron*, **72**, 545–558.
81. Voineagu, I., Wang, X., Johnston, P., Lowe, J.K., Tian, Y., Horvath, S., Mill, J., Cantor, R.M., Blencowe, B.J. and Geschwind, D.H. (2011) Transcriptomic analysis of autistic brain reveals convergent molecular pathology. *Nature*, **474**, 380–384.
82. Stoner, R., Chow, M.L., Boyle, M.P., Sunkin, S.M., Mouton, P. R., Roy, S., Wynshaw-Boris, A., Colamarino, S.A., Lein, E.S. and Courchesne, E. (2014) Patches of disorganization in the neocortex of children with autism. *N. Engl. J. Med.*, **370**, 1209–1219.
83. Fatemi, S.H., Aldinger, K.A., Ashwood, P., Bauman, M.L., Blaha, C.D., Blatt, G.J., Chauhan, A., Chauhan, V., Dager, S. R., Dickson, P.E. *et al.* (2012) Consensus paper: pathological role of the cerebellum in autism. *Cerebellum*, **11**, 777–807.
84. Wegiel, J., Kuchna, I., Nowicki, K., Imaki, H., Wegiel, J., Marchi, E., Ma, S.Y., Chauhan, A., Chauhan, V., Bobrowicz, T.W. *et al.* (2010) The neuropathology of autism: defects of neurogenesis and neuronal migration, and dysplastic changes. *Acta Neuropathol.*, **119**, 755–770.
85. Brustein, E., Saint-Amant, L., Buss, R.R., Chong, M., McDearmid, J.R. and Drapeau, P. (2003) Steps during the development of the zebrafish locomotor network. *J. Physiol. Paris*, **97**, 77–86.
86. McLean, D.L. and Fetcho, J.R. (2011) Movement, technology and discovery in the zebrafish. *Curr. Opin. Neurobiol.*, **21**, 110–115.
87. Chapouton, P. and Godinho, L. (2010) Neurogenesis. *Methods Cell Biol.*, **100**, 73–126.
88. Perrins, R., Walford, A. and Roberts, A. (2002) Sensory activation and role of inhibitory reticulospinal neurons that stop swimming in hatchling frog tadpoles. *J. Neurosci.*, **22**, 4229–4240.
89. Kimura, Y., Satou, C., Fujioka, S., Shoji, W., Umeda, K., Ishizuka, T., Yawo, H. and Higashijima, S.I. (2013) Hindbrain V2a Neurons in the Excitation of Spinal Locomotor Circuits during Zebrafish Swimming. *Curr. Biol.*, **10**, 843–849.
90. Ljunggren, E.E., Haupt, S., Ausborn, J., Ampatzis, K. and El Manira, A. (2014) Optogenetic activation of excitatory premotor interneurons is sufficient to generate coordinated locomotor activity in larval zebrafish. *J. Neurosci.*, **34**, 134–139.
91. Gatto, C.L. and Broadie, K. (2010) Genetic controls balancing excitatory and inhibitory synaptogenesis in neurodevelopmental disorder models. *Front. Synaptic Neurosci.*, **2**, 4.
92. Casanova, M.F., Buxhoeveden, D.P., Switala, A.E. and Roy, E. (2002) Minicolumnar pathology in autism. *Neurology*, **58**, 428–432.
93. Fatemi, S.H., Halt, A.R., Stary, J.M., Kanodia, R., Schulz, S.C. and Realmuto, G.R. (2002) Glutamic acid decarboxylase 65 and 67 kDa proteins are reduced in autistic parietal and cerebellar cortices. *Biol. Psychiatry*, **52**, 805–810.
94. Pinto, D., Delaby, E., Merico, D., Barbosa, M., Merikangas, A., Klei, L., Thiruvahindrapuram, B., Xu, X., Ziman, R., Wang, Z. *et al.* (2014) Convergence of genes and cellular pathways dysregulated in autism spectrum disorders. *Am. J. Hum. Genet.*, **94**, 677–694.
95. Parikshak, N.N., Luo, R., Zhang, A., Won, H., Lowe, J.K., Chandran, V., Horvath, S. and Geschwind, D.H. (2013) Integrative functional genomic analyses implicate specific molecular pathways and circuits in autism. *Cell*, **155**, 1008–1021.
96. Satou, C., Kimura, Y. and Higashijima, S. (2012) Generation of multiple classes of V0 neurons in zebrafish spinal cord: progenitor heterogeneity and temporal control of neuronal diversity. *J. Neurosci.*, **32**, 1771–1783.
97. Ryan, J.F., Pang, K., Schnitzler, C.E., Nguyen, A.D., Moreland, R.T., Simmons, D.K., Koch, B.J., Francis, W.R., Havlak, P.,

Smith, S.A. *et al.* (2013) The genome of the ctenophore Mnemiopsis leidyi and its implications for cell type evolution. *Science*, **342**, 1242592.
98. McWilliam, H., Li, W., Uludag, M., Squizzato, S., Park, Y.M., Buso, N., Cowley, A.P. and Lopez, R. (2013) Analysis Tool Web Services from the EMBL-EBI. *Nucleic. Acids. Res.*, **41**, 597–600.
99. Thisse, C., Thisse, B., Schilling, T.F. and Postlethwait, J.H. (1993) Structure of the zebrafish snail1 gene and its expression in wild-type, spadetail and no tail mutant embryos. *Development*, **119**, 1203–1215.
100. Ganser, L.R., Yan, Q., James, V.M., Kozol, R., Topf, M., Harvey, R.J. and Dallman, J.E. (2013) Distinct phenotypes in zebrafish models of human startle disease. *Neurobiol. Dis.*, **60**, 139–151.
101. Rozen, S. and Skaletsky, H. (2000) Primer3 on the WWW for general users and for biologist programmers. *Methods Mol. Biol.*, **132**, 365–386.
102. Schindelin, J., Arganda-Carreras, I., Frise, E., Kaynig, V., Longair, M., Pietzsch, T., Preibisch, S., Rueden, C., Saalfeld, S., Schmid, B. *et al.* (2012) Fiji: an open-source platform for biological-image analysis. *Nat. Methods*, **9**, 676–682.
103. Mueller, T., Vernier, P. and Wullimann, M.F. (2006) A phylotypic stage in vertebrate brain development: GABA cell patterns in zebrafish compared with mouse. *J. Comp. Neurol.*, **494**, 620–634.

frontiers | Frontiers in Molecular Neuroscience

TYPE Original Research
PUBLISHED 10 July 2024
DOI 10.3389/fnmol.2024.1401746

OPEN ACCESS

EDITED BY
Han Wang,
Soochow University, China

REVIEWED BY
Judit García-González,
Icahn School of Medicine at Mount Sinai, United States
Suhyun Kim,
Korea University, Republic of Korea

*CORRESPONDENCE
Julia E. Dallman
✉ j.dallman@miami.edu

RECEIVED 15 March 2024
ACCEPTED 04 June 2024
PUBLISHED 10 July 2024

CITATION
Sumathipala SH, Khan S, Kozol RA, Araki Y, Syed S, Huganir RL and Dallman JE (2024) Context-dependent hyperactivity in *syngap1a* and *syngap1b* zebrafish models of SYNGAP1-related disorder.
Front. Mol. Neurosci. 17:1401746.
doi: 10.3389/fnmol.2024.1401746

Context-dependent hyperactivity in *syngap1a* and *syngap1b* zebrafish models of SYNGAP1-related disorder

Sureni H. Sumathipala[1,2], Suha Khan[1], Robert A. Kozol[1,3], Yoichi Araki[4], Sheyum Syed[5], Richard L. Huganir[4] and Julia E. Dallman[1]*

[1]Department of Biology, University of Miami, Coral Gables, FL, United States, [2]Department of Biological Sciences, North Carolina State University, Raleigh, NC, United States, [3]Department of Biological Sciences, St. John's University, Queens, NY, United States, [4]Department of Neuroscience and Kavli Neuroscience Discovery Institute, Johns Hopkins University School of Medicine, Baltimore, MD, United States, [5]Department of Physics, University of Miami, Coral Gables, FL, United States

Background and aims: SYNGAP1-related disorder (SYNGAP1-RD) is a prevalent genetic form of Autism Spectrum Disorder and Intellectual Disability (ASD/ID) and is caused by *de novo* or inherited mutations in one copy of the *SYNGAP1* gene. In addition to ASD/ID, SYNGAP1 disorder is associated with comorbid symptoms including treatment-resistant-epilepsy, sleep disturbances, and gastrointestinal distress. Mechanistic links between these diverse symptoms and *SYNGAP1* variants remain obscure, therefore, our goal was to generate a zebrafish model in which this range of symptoms can be studied.

Methods: We used CRISPR/Cas9 to introduce frameshift mutations in the *syngap1a* and *syngap1b* zebrafish duplicates (*syngap1ab*) and validated these stable models for Syngap1 loss-of-function. Because *SYNGAP1* is extensively spliced, we mapped splice variants to the two zebrafish *syngap1a* and *b* genes and identified mammalian-like isoforms. We then quantified locomotory behaviors in zebrafish *syngap1ab* larvae under three conditions that normally evoke different arousal states in wild-type larvae: aversive, high-arousal acoustic, medium-arousal dark, and low-arousal light stimuli.

Results: We show that CRISPR/Cas9 indels in zebrafish *syngap1a* and *syngap1b* produced loss-of-function alleles at RNA and protein levels. Our analyses of zebrafish Syngap1 isoforms showed that, as in mammals, zebrafish Syngap1 N- and C-termini are extensively spliced. We identified a zebrafish *syngap1* α1-like variant that maps exclusively to the *syngap1b* gene. Quantifying locomotor behaviors showed that *syngap1ab* mutant larvae are hyperactive compared to wild-type but to differing degrees depending on the stimulus. Hyperactivity was most pronounced in low arousal settings, and hyperactivity was proportional to the number of mutant *syngap1* alleles.

Limitations: *Syngap1* loss-of-function mutations produce relatively subtle phenotypes in zebrafish compared to mammals. For example, while mouse *Syngap1* homozygotes die at birth, zebrafish *syngap1ab−/−* survive to adulthood and are fertile, thus some aspects of symptoms in people with *SYNGAP1*-Related Disorder are not likely to be reflected in zebrafish.

Conclusion: Our data support mutations in zebrafish *syngap1ab* as causal for hyperactivity associated with elevated arousal that is especially pronounced in low-arousal environments.

KEYWORDS

zebrafish, sensory-processing, autism, syngap1, haploinsufficiency mutant profiling

Background

SYNGAP1-related disorder (SYNGAP1-RD), also known as SYNGAP1 syndrome, is caused by genetic variants in the *SYNGAP1* gene and is one of the most prevalent genetic forms of intellectual disability (ID) (Hamdan et al., 2010, 2011; Berryer et al., 2013; Satterstrom et al., 2020; Fu et al., 2022). Since the first patient report in 2009, there are now about ~1,400 known SYNGAP1 patients worldwide, though with advocacy and awareness, these numbers continue to rise (curesyngap1.org; May 2024). While ID and epilepsy are the most penetrant symptoms, some people with SYNGAP1 RD also present with Autism Spectrum Disorder (ASD; ~50%), gastrointestinal distress (~68%), developmental delay, hypersensitivity to sound and light, high pain thresholds (~72%), and challenging behaviors that include increased risk-taking, aggression, and self-injury (~73%) (Pinto et al., 2010; Carvill et al., 2013; Kilinc et al., 2018; Weldon et al., 2018; Jimenez-Gomez et al., 2019; Vlaskamp et al., 2019; Naveed et al., 2023; Thomas et al., 2024). The majority of SYNGAP1-RD-causing variants are *de novo*, occurring in the child but not in their parents (Hamdan et al., 2010, 2011; Berryer et al., 2013); SYNGAP1-RD is caused by haploinsufficiency, therefore, being heterozygous for a *SYNGAP1* variant can be sufficient to cause symptoms, with the median age of seizure onset being two years (Vlaskamp et al., 2019).

To better understand genotype/phenotype relationships in SYNGAP1-RD, we generated loss-of-function mutations in zebrafish *syngap1a* and *syngap1b* duplicates using CRISPR/cas9 (Varshney et al., 2016). We focused on translationally-relevant phenotypes in six-day-old larvae that correspond to early childhood in people. With accessible early development, optically transparent embryos, high fecundity, and established methods for genetic manipulation, zebrafish complement extant rodent models to understand the role of disease genes in development and behavior (Ijaz and Hoffman, 2016; Kozol et al., 2016; Thyme et al., 2019; Campbell et al., 2023; Weinschutz Mendes et al., 2023). While mammals have a single *SYNGAP1*, zebrafish *syngap1* is duplicated due to a whole genome duplication event 50–80 million years ago and retention of both *syngap1a* and *syngap1b* ohnologs (Glasauer and Neuhauss, 2014; Kozol et al., 2016). Two recent papers generated zebrafish *syngap1b* models that differ from the model we report here because they only target the "b" duplicate of the zebrafish *syngap1* ohnologs (Colon-Rodriguez et al., 2020; Griffin et al., 2021).

Mammalian *SYNGAP1* mRNAs are extensively spliced at N- and C-termini and the C-terminal isoforms α1, α2, β, and γ have been functionally characterized (Guo et al., 2009; McMahon et al., 2012; Araki et al., 2020; Kilinc et al., 2022). The α1 isoform is highly enriched at the post-synaptic density of glutamatergic synapses through a four amino-acid PDZ-interacting domain by which it interacts with the synaptic scaffolding protein PSD-95 (Chen et al., 1998; Kim et al., 1998; Komiyama et al., 2002). Here we annotate zebrafish mRNAs for how they might correspond to these mammalian isoforms and map zebrafish isoforms to *syngap1a* and *syngap1b* genes.

Individuals with SYNGAP1-RD show sensory hyperactivity, sometimes even seizures, in response to sensory stimuli such as eating, light, sound, touch, and/or pain (Vlaskamp et al., 2019). These symptoms are a major concern of the SYNGAP1 parents and caregivers because they can put these individual's lives at risk (Vlaskamp and Scheffer, 2020; Lyons-Warren et al., 2022). Consistent with the human symptoms, rodent models also show sensory-induced hyperactivity as well as seizures that can be induced by loud sounds (Guo et al., 2009; Ozkan et al., 2014; Michaelson et al., 2018; Creson et al., 2019; Sullivan et al., 2020). To assess sensory-induced behaviors in *syngap1ab* zebrafish mutants, we used two standard sensorimotor assays: vibration to evoke the acoustic startle response (ASR) and transitions between light and dark to evoke the visual-motor response (VMR) (Emran et al., 2008; Gao et al., 2014; Dunn et al., 2016). Because changes to sensory habituation could contribute to sensory processing issues in SYNGAP1 patients (Tavassoli et al., 2014; Robertson and Baron-Cohen, 2017; Oldehinkel et al., 2019), we also conducted a short-term habituation assay to see how the *syngap1ab* zebrafish mutant larvae behave towards supra-threshold stimuli that are presented in rapid succession.

Like mammalian models, our zebrafish *syngap1ab* mutant models exhibit hyperactivity in both ASR and VMR assays. Hyperactivity was least pronounced in response to aversive acoustic stimuli and most pronounced during low-arousal light conditions. By analyzing the frequency distributions of movement distance and rest duration, we show that *syngap1ab* model hyperactivity in the light is due to higher-frequency, larger movements that resemble goal-directed behaviors associated with heightened states of arousal.

Methods

Fish maintenance and husbandry

All the zebrafish larvae and adults used in this study were reared at the University of Miami Zebrafish facility as per IACUC protocol #18–129. Water temperatures were maintained at 28°C and both adult and larval zebrafish were exposed to a circadian cycle of 14 h light/10 h dark. Water housing adult zebrafish was continuously monitored for pH and conductivity to maintain conditions within an optimal range (pH 7–8.1; conductivity 350–800 mOsm). Upon collection, embryos were rinsed briefly in reverse osmosis water and reared in 10 cm petri dishes containing 'system water' (taken from water housing adults). Dishes were cleaned daily to remove unfertilized eggs and prevent fungal growth that could limit oxygen and stunt early embryonic growth. Larvae used for behavioral assays were raised ~50 larvae per petri dish to minimize competition and developmental delays.

CRISPR/Cas9 generation of *syngap1ab* mutant zebrafish

Syngap1ab mutants were generated using CRISPR/Cas9 genome editing technology (Varshney et al., 2016). One cell stage WT embryos were injected with small guide RNA (sgRNA; Integrated

DNA Technologies-IDT Coralville IA) designed using CHOPCHOP online software (Montague et al., 2014) to target exon 4 of *syngap1a* gene (400 pg) and exon 5 of *syngap1b* gene (400 pg), along with Cas9 protein (PNA Bio Thousand Oaks CA; 100 pg). Embryos were either injected with *syngap1a* or *syngap1b* sgRNA using a foot-pedal-controlled Milli-Pulse Pressure Injector (MPPI-3 from Applied Scientific Instrumentation ASI Eugene OR). Resulting mosaic F0 larvae were reared to adulthood and crossed to wild-type animals to generate an F1 generation for Sanger sequencing to identify *syngap1a* and *syngap1b* mutant alleles with indels resulting from CRISPR editing (see below). Upon identification of the mutant *syngap1a* and *syngap1b* alleles, adults were in-crossed to obtain *syngap1ab* double mutants. Adult *syngap1a*b mutant fish, used to spawn larvae for experiments, span F2-F5 generations. To obtain *syngap1ab*+/− larvae, adult male *syngap1ab*−/− were outcrossed to WT (AB/TL, https://zfin.org/action/genotype/view/ZDB-GENO-031202-1) females. To obtain *syngap1ab*−/− larvae, *syngap1ab*−/− adults were in-crossed. For simplicity, zebrafish that are heterozygous in both *syngap1a* and *syngap1b* genes are denoted as *syngap1ab*+/−, and those homozygous in both *syngap1a* and *syngap1b* genes are denoted as *syngap1ab*−/−. All the wild-type (WT) larvae used for this study were AB/TL unless otherwise stated and are denoted as *syngap1ab*+/+.

Syngap1ab alleles used in this study

The molecular identity of CRISPR alleles was determined by obtaining a small caudal fin sample from each anesthetized (200 mg/L of Tricaine (MS-222)) F1 adult fish. Genomic DNA was extracted by digesting each fin sample in 50 µL of 50 mM NaOH at 95°C for 1 h, the HotSHOT method (Samarut et al., 2016). To determine larval genotypes, each larva was anesthetized by either placing them on ice for 30 min or by using 200 mg/L Tricaine (MS-222). Upon complete anesthetization, larval genomic DNA (gDNA) samples were isolated using the HotSHOT method, as detailed above but using only 20 µL of 50 mM NaOH.

Gene-specific primers (Table 1) for both genes were designed using Primer3 software. Primer3 input sequences for each gene was selected based on their Cas9 target regions. For PCR, each reaction mixture contained 5 µL of 10x GOTaq Polymerase (Promega Madison WI), 0.5 µL from each 10 µM forward primer and reverse primer, 3 µL of nuclease-free water, and 1 µL of gDNA (from either larvae or adult-fin-clip digestions). Resulting PCR products were sent out for sequencing (Eurofins Genomics, LLC Louisville KY) and the results were read and analyzed using the ApE—A plasmid Editor v2.0.61 (Davis and Jorgensen, 2022) and SnapGene viewer software to determine the *syngap1a* and *syngap1b* mutant alleles (Supplementary Figure S1).

Syngap1a and *syngap1b* isoform identification

To better characterize zebrafish *syngap1ab* splice variants, mRNA sequences (both published and predicted), were obtained from the NCBI protein database. To test for evidence of isoform expression, these sequences were searched against Expressed Sequence Tags (EST) and Transcriptome Shotgun Assembly (TSA) databases. Expressed isoforms were then BLASTed against the UCSC zebrafish genome browser to identify unique and common exons (Figure 1).

qPCR

To check for nonsense-mediated mRNA decay in *syngap1ab* mutants, qPCR was used to quantify relative *syngap1ab* expression levels in *syngap1ab* mutant larvae compared to WT larvae, both groups at 7 days post-fertilization (dpf). To extract RNA, larvae were anesthetized by placing them on ice for 30 min before using TRIzol (Life Technologies, Carlsbad, CA) following manufacturer's protocol. For each genotype (WT, *syngap1ab*+/−, and *syngap1ab*−/−), we conducted at least eight experimental replicates with 20 larvae pooled together per replicate. 1 µg of RNA was used as input for RT-PCR. To enhance syngap1 cDNA in each sample, *syngap1a* and *syngap1b* gene-specific primers were used with Eukaryotic translation elongation factor 1 like 1 *eef1a1l1* (ZFIN) as the internal control. cDNA was made using SuperScript III (Invitrogen™/ ThermoFisher Scientific) and incubating at 50°C for 1 h followed by 15 min at 70°C. qPCR was carried out using GoTaq qPCR Probe Kit (Promega) in a QuantStudio3 RT-PCR system (Applied Biosystems™, Waltham MA) following manufacturer's protocol. Cycling conditions were as follows: Activation step of 95°C for 10 min, followed by PCR with 40 cycles of 95°C for 15 s and 60°C for 1 min, followed by a melt curve of 95°C for 15 s and 60°C for 1 min. Relative levels of gene expression were calculated using the ΔΔCt method. For this method cycle threshold Ct values for *syngap1a* and *syngap1b* genes were first normalized to Ct values of the internal control *eef1a1l1* by calculating ΔCt: $Ct_{syngap1a}$-$Ct_{eef1a1l1}$ and $Ct_{syngap1b}$-$Ct_{eef1a1l1}$. Fold-changes in *syngap1* gene expression were then compared in WT, *syngap1ab*+/−, and *syngap1ab*−/− larvae by calculating $2^{-\Delta\Delta Ct}$ with ΔΔCt:$\Delta Ct_{syngap1ab\ mutant}$-$\Delta Ct_{WT}$. Fold changes in *syngap1ab* mutants were calculated by dividing

TABLE 1 *Syngap1* primers used for genotyping and qPCR.

Gene	Forward primer (5′–3′)	Reverse primer (5′–3′)
PCR primers used for genotyping		
syngap1a	GTGTTTTAGAGCACGCTCGTG	TCGAAATGGCTGTGTAGGGG
syngap1b	GTAGAAGACTGAAGGGGTCC	ACTTACCGCTCCTGGTCG
qPCR primers (From Kozol et al., 2016)		
syngap1a	CCTGAAGCTCATCGCACAC	GGGTCCACCTCACAGTTCTC
syngap1b	GACGACAGATCTCCATGCAC	GAGGAGTGGCGAGAGATGAA
eef1a1	CTGGAGGCCAGCTCAAACAT	ATCAAGAAGAGTAGTACCGCTAGC

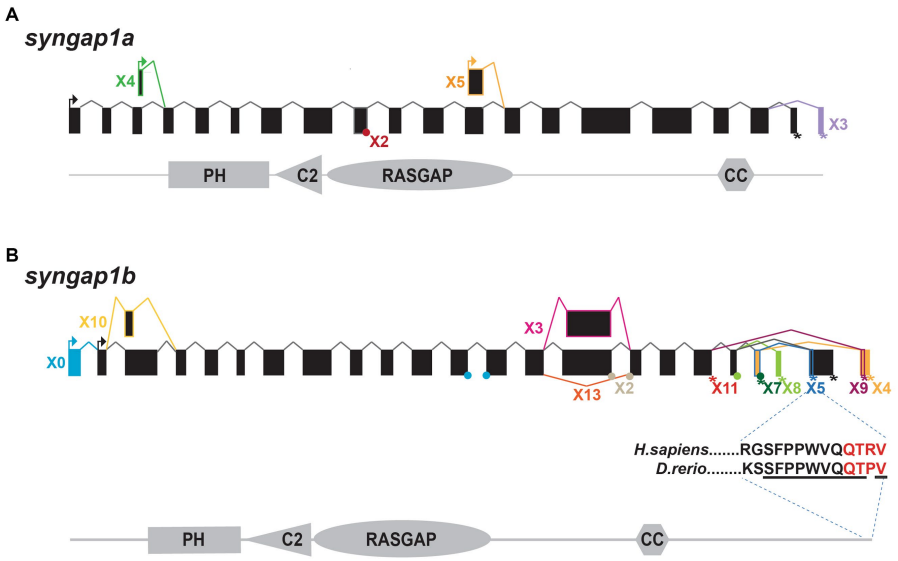

FIGURE 1
Zebrafish *syngap1a* and *syngap1b* isoforms. NCBI database searches revealed **(A)** five *syngap1a* (X1–X5) and **(B)** eleven *syngap1b* isoforms (X0, X2–5, X7–11, and X13) with evidence of expression. Transcriptional start sites are shown with arrows and stop codons are shown using an asterisk (*). Alternative splice sites are shown either using a dot (if the exon is missing <10 bp) or a box (if the difference is >10 bp). Isoform X*, box and connecting line colors denote exons and stop codons that are unique to the different isoforms. Black boxes and lines represent common exons/transcription start sites. The insert below the syngap1b X5 shows ten of eleven C-term amino acids (underlined) are identical to the human α1 isoform, with the PDZ-interacting domain shown in red.

WT values. Group comparisons were made using 2-way ANOVA (gene and genotype) followed by Tukey's multiple comparison test.

Western blot analysis

Brain regions (mouse) or whole brains (zebrafish) were excised from C57BL6 mice or adult zebrafish. Tissues were lysed in 10 volumes (for zebrafish, each brain was considered ~15 mg) of lysis buffer (50 mM Tris pH 8.0, 100 mM NaCl, 1 mM EDTA, 1 mM EGTA, 1% TritonX-100, 0.2% SDS, 0.5% Sodium deoxycholate, with complete Protease inhibitor EDTA-free mix (Roche/MilliporeSIGMA Burlington MA)) using a Dounce homogenizer to obtain homogenized tissue samples. Each sample was then diluted by 1:10 using lysis buffer and ~20 μL from each sample was loaded into each gel lane. Based on these experimental settings, each sample, i.e., for both zebrafish and mouse tissue samples, contained about 29 μg of proteins per 20 μL. Samples were first probed with SYNGAP1 antibodies (Abcam ab3344 or NOVUS nbp2-27541) and were followed by probing with secondary antibodies (anti-rabbit IgG IRDye680; LICOR 926-68071 or anti-goat IgG IRDye680; LICOR 926-68074). Resulting signals were measured and imaged using the fluorescence-based Odyssey CLx Imaging System (LICORbio Lincoln NE).

Analysis of *syngap1a* and *syngap1b*'s relative importance for survival

To test for the potential effects of *syngap1a* and *syngap1b* mutant alleles on larval survival, three batches of *syngap1ab*+/− in-crosses were genotyped at six dpf. Data were analyzed using Prism GraphPad software (v9.1) to determine whether observed allele representation differed significantly from predicted using a Chi-square test.

Short-term habituation assay

To test whether the larvae show habituation in response to acoustic stimuli, a short-term habituation assay was used as described in Wolman et al. (2015). After 30 min of light adaptation, 6 dpf WT and *syngap1ab*+/− larvae were presented with 5 phases of acoustic stimulation using a DanioVision™ observation chamber (Noldus Leesburg VA). Phase 1 consisted of 10 tap stimuli (intensity level 3) delivered at a 20 s inter stimulus interval (ISI). Phase 2 consisted of 10 tap stimuli (intensity level 5) delivered at also at a 20 s ISI. Phase 3, the habituation test, consisted of 30 tap stimuli (intensity level 5) delivered at 1 s ISI. Phase 4 was a 3 min rest period. Lastly phase 5 consisted of 10 tap stimuli (intensity level 5), delivered at a 20 s ISI. Total distance moved by each larva per second was analyzed to measure short-term habituation. Data were analyzed using Prism GraphPad software (v9.1) to compare WT and *syngap1ab*+/− groups using a 2-way ANOVA (Phase and Genotype) followed by a Tukey's multiple comparison test.

Visual motor response (VMR) assay

Syngap1ab mutants and WT 6 dpf larvae larvae were placed in a 96-well plate containing system water. Prior to starting the experiment, larvae were dark adapted for 1 h and at 28°C in the Noldus

DanioVision™ behavioral observation chamber. Ethovision® XT 11 software (Noldus) was used to program the delivery of stimuli and to analyze the results. Images were captured at 40 Hz. For the visual-motor response (VMR) assay, larvae were exposed to 5 min of 12% (high-light settings) lights-on stimulus followed by 5 min of lights-off stimulus. Larval movements were recorded for four consecutive light on/off cycles and their activity/movements were recorded for a total duration of 40 min. Larvae were then genotyped using the genotyping assays previously described and analyzed for the total distance moved/time. The resulting data were further analyzed using GraphPad Prism 9.1 software to compare WT, *syngap1ab*+/−, and *syngap1ab*−/− groups using Kruskal-Wallis ANOVA followed by Dunn's multiple comparison tests.

Displacement and dwell-time analyses

To test whether the observed hyperactivity is due to increased initiation of movements or increased distance moved, the displacement and dwell-time data from raw, exported data produced by Ethovision® XT 11 software were analyzed using MATLAB scripts[1] to examine behavioral probability distributions. Resulting data were plotted using Prism GraphPad (V9.1) and WT and *syngap1ab* groups compared using a two-sample Kolmogorov–Smirnov test.

Results

Zebrafish *syngap1b* but not *syngap1a* encodes an isoform that is similar to the mammalian PDZ-interacting Syngap1α1

While mammals including humans have a single *SYNGAP1* gene that encodes a 1,343 amino acid, ~149 kDa protein (Komiyama et al., 2002), there are two *syngap1* ohnologs present in the zebrafish genome. The zebrafish *syngap1a* gene is found on chromosome 16 and encodes a 1,290 amino acid, ~146 kDa protein whereas the *syngap1b* gene is found on chromosome 19 and encodes a 1,507 amino acid, ~160 kDa protein. Like rodents and humans, both zebrafish *Syngap1a* and *Syngap1b* have four, highly conserved protein–protein interacting domains: pleckstrin homology (PH), C2, RasGAP, and coiled-coiled (CC).

We characterized zebrafish Syngap1 isoforms based on NCBI databases and comparisons to mammalian isoforms. In mammalian Syngap1, there are four well-characterized, alternatively-spliced Syngap1 isoforms, α1, α2, β, and γ, that vary at their C-termini (McMahon et al., 2012). To assess whether zebrafish *syngap1a* and *syngap1b* genes might encode similar isoforms, we curated all published and predicted *syngap1ab* isoforms. Similar to the mammalian isoforms, for both zebrafish *syngap1a* and *syngap1b* genes, exons encoding the four protein interaction domains occur in all isoforms with many alternative exons at both N- and C-termini. Based on expressed sequence databases, we were able to identify five *syngap1a* and eleven *syngap1b* isoforms (Figure 1). Of the human C-term isoforms, α1 is the most studied and is localized to the post-synapse by a four amino acid (QTRV) PDZ-interacting domain. Interestingly, we were able to find a zebrafish *syngap1b* C-term isoform X5 with a putative mammalian-like PDZ-interacting domain that had ten of eleven of the terminal amino acids identical to those of the human *SYNGAP1* α1 isoform (Figure 1B). We were unable to find mammalian-like isoforms (α2, β, and γ) due to the highly variable C-terminal ends in the zebrafish isoforms.

CRISPR/Cas9-generated alleles produce loss-of-function SYNGAP1 models

To better understand how pathogenic mutations in *syngap1* result in altered behaviors, we used CRISPR/Cas9 to generate zebrafish loss-of-function mutations. In humans, pathogenic variants span the *SYNGAP1* gene (Hamdan et al., 2011; Berryer et al., 2013; Vlaskamp et al., 2019; Gamache et al., 2020). To mutate a region of the gene that would affect the majority of isoforms, we targeted the earliest shared exons, exon 4 and exon 5 in *syngap1a* and *syngap1b* respectively, to generate loss-of-function alleles. CRISPR/Cas9 induces indels causing reading frame shifts and introducing premature stop codons. Upon sequence analyses of F1 adult crispants, we selected two mutant alleles for *syngap1a* (*syngap1a* + 7 nucleotide insertion and *syngap1a* − 22 nucleotide deletion) and one allele for *syngap1b* with a − 14 nucleotide deletion, all of which would be predicted to result in a severely truncated proteins that were less than 200aa (Figure 2B). To best recapitulate human SYNGAP1 variant haploinsufficiency, we used double-heterozygous larvae for *syngap1a* + 7 and *syngap1b* − 14, and to further assess complete loss-of-function, we used double-homozygous larvae (here onwards denoted as *syngap1ab*+/− and *syngap1ab*−/− respectively).

We tested for loss-of-function of *syngap1* at the level of protein and mRNA. Western blot analysis carried out using adult zebrafish brain lysates showed reduced Syngap1 protein levels in *syngap1ab*−/− brain tissues (Figure 2C). qPCR analysis of RNA harvested from 7-day-old larvae showed reduced RNA transcripts in both *syngap1ab*+/− (adjusted *p* values for *syngap1a* = 0.001, and *syngap1b* = 0.0495) and *syngap1ab*−/− (adjusted *p* values for *syngap1a* = 0.0699 and *syngap1b* = 0.0312) mutant larvae compared to WT larvae supporting non-sense mediated decay (Figure 2D). Taken together, these results show that our CRISPR/cas9 generated *Syngap1ab* zebrafish mutants show reduced mRNA and protein expression, supporting the use of these alleles as haploinsufficient models.

Evidence for functional complementarity between *syngap1a* and *syngap1b* genes

To study potential interactions between Syngap1a and Syngap1b proteins, we analyzed larval survival from each of the nine genotypes resulting from *syngap1ab*+/− in-crosses. When *syngap1b* mutant alleles outnumbered *syngap1a* mutant alleles, larval survival was much lower than expected (Supplementary Figures S2A,B; $p < 0.0001$). By contrast, zebrafish in which there were more *syngap1a* than *syngap1b* mutant alleles were over-represented and zebrafish in which there were an equal number of *syngap1a* and *syngap1b* mutant alleles were as expected. These observations suggest that each ohnolog contributes

1 https://github.com/sheyums/Sureni_Sumathipala_syngap1.git

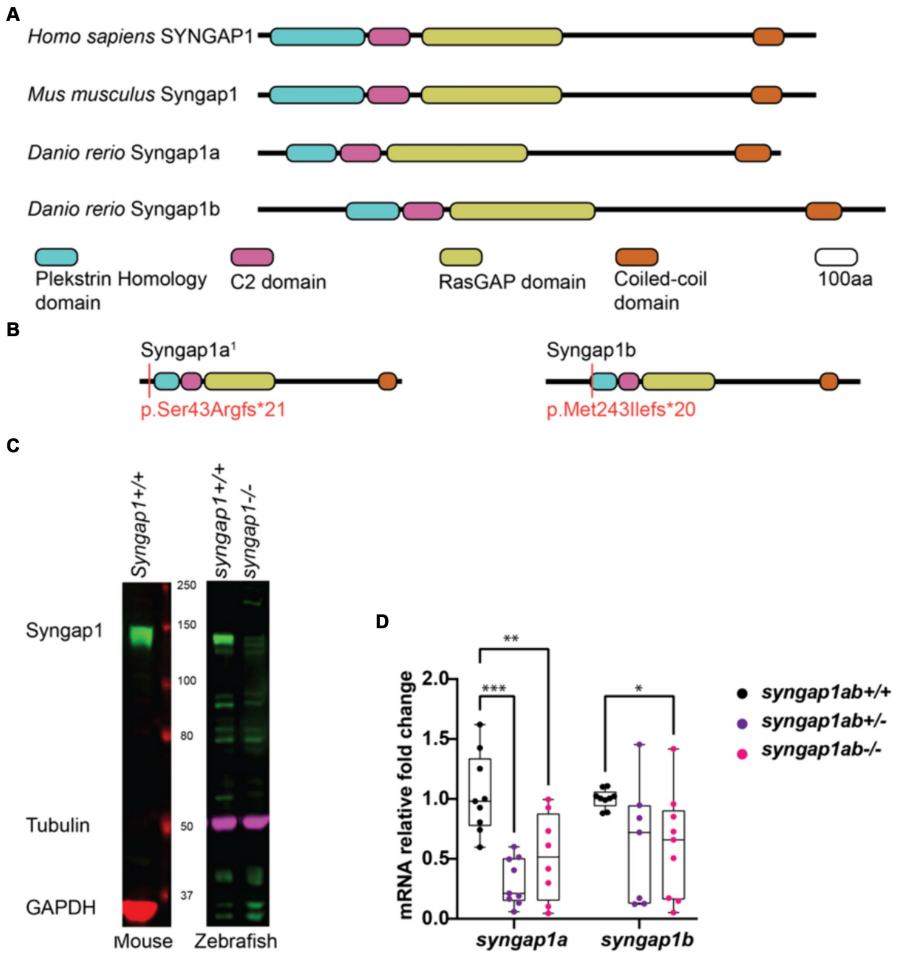

FIGURE 2
Zebrafish loss-of-function model for human SYNGAP1-RD. **(A)** Mammalian SYNGAP1 protein (*H. sapiens* and *M. musculus*) has four main protein interacting domains; pleckstrin homology (PH) domain, C2 domain, RasGAP domain, and coiled-coiled (CC) domain. Zebrafish (*D. rerio*) Syngap1 orthologs; Syngap1a and Syngap1b show domain conservation with that of mammals. **(B)** Syngap1ab protein diagrams show sites of CRISPR induced mutations. Resulting CRISPR mutants used for phenotypic analyses: *syngap1a*[1] allele p.Ser43Argfs*21 and *syngap1b* allele p.Met149Ilefs*9. *syngap1a*[1] had an amino acid change from a serine to an arginine at position 43 introducing a premature stop codon, 21 amino acids downstream. *Syngap1b* mutant allele had a change of methionine to an isoleucine at position 49 introducing a premature stop codon 9 amino acids downstream. **(C)** Western blots illustrate the expression of SYNGAP1 in whole brain lysates from adult mice and zebrafish. In wild-type zebrafish, the Syngap1 protein was detected at a similar molecular weight (~150 kDa) to that of the mouse SYNGAP1, using a rat anti-Syngap1 antibody. GAPDH and tubulin were used as the loading controls for mouse and zebrafish, respectively. **(D)** Mutant *syngap1ab* larvae showed reduced *syngap1a* and *syngap1b* mRNA expression levels at 7dpf. Group comparisons were made using 2-way ANOVA followed by Tukey's multiple comparison test. *p* value asterisks represent: $*p < 0.05$, $**p < 0.01$; $***p < 0.001$; $****p < 0.0001$.

distinct functional roles so that the *syngap1a* ohnolog, likely due to its inability to encode the Syngap1 α1 isoform, cannot make up for loss of *syngap1b* ohnolog.

Syngap1ab+/− larvae show greater dynamic range, elevated response probability, and normal habituation in response to acoustic stimuli

Given that SYNGAP1 is known to be important for sensory processing, we wanted to test the dynamic range of *syngap1ab*+/− zebrafish responses to vibration stimuli of medium and high intensity as well as their ability to habituate to repeated, high-intensity, high-frequency stimuli. To assess these factors, we used an assay described in Wolman et al. (2015) in which 6 days-post-fertilization (dpf) larvae were exposed to different intensity vibrations with different inter-stimulus intervals (ISIs) during phases 1–5 of the assay (Figure 3A). We allowed larvae to acclimate to the Noldus chamber for 30 min before exposing them to vibrational stimuli. During phases 1 and 2, 10 taps of medium-intensity (level 3) and high-intensity (level 5) respectively were delivered with 20 s ISI. During phase 3, habituation was tested by delivering 30 high-intensity taps with 1 s ISI. This was followed by a 3 min rest period in phase 4.

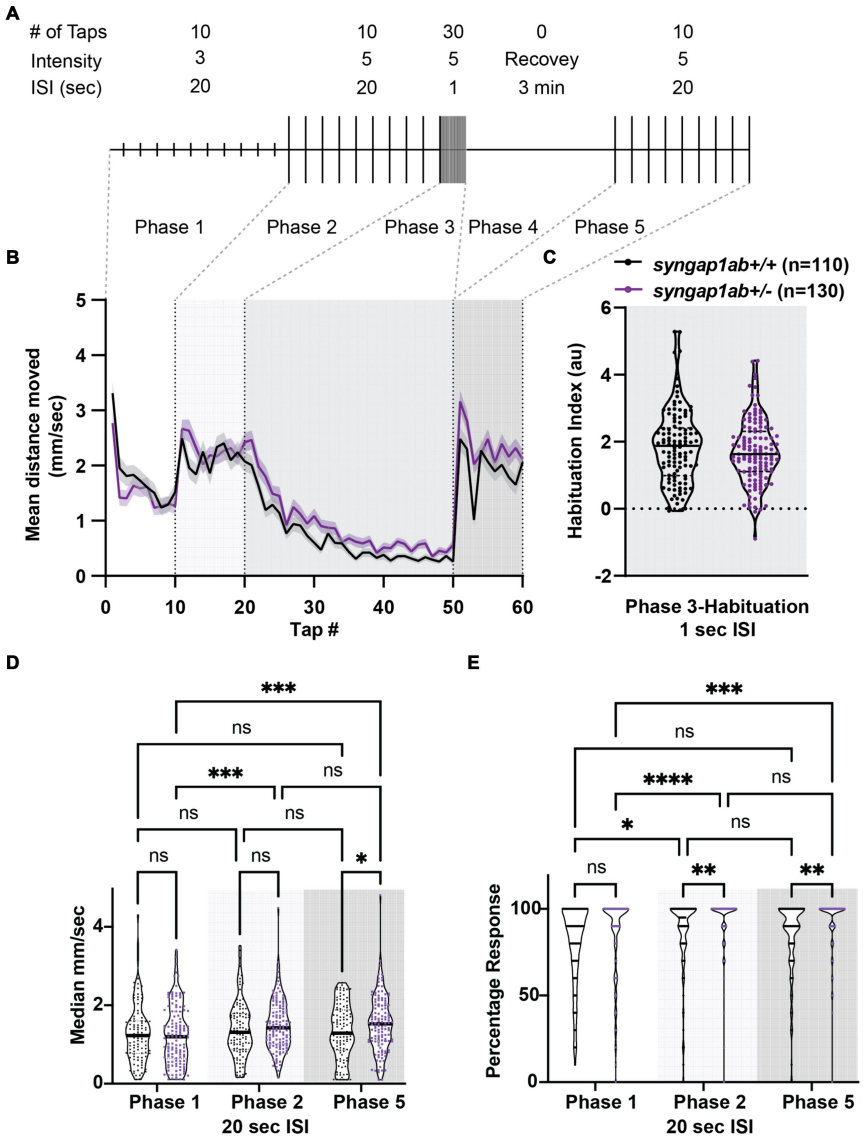

FIGURE 3
*Syngap1a*b larvae show short-term habituation to vibrational stimuli and more movement in response to stronger stimuli. **(A)** A schematic representation of the habituation assay (modified from Wolman et al., 2015) is shown. **(B)** Mean ± standard error movement velocity of WT and *syngap1a*b+/– larvae 1 s post-vibration. **(C)** Habituation indices were calculated per larva by subtracting the mean velocity post-habituation (taps 41–50) from the mean velocity pre-habituation (taps 11–20). **(D)** The median velocity mm/s moved per phase is shown for WT and *syngap1ab+/–* larvae. **(E)** Percentage response per phase is shown for WT and *syngap1ab+/–* larvae. A mixed effects model of genotype and phase was conducted and when $p < 0.05$ was followed by a Tukey's multiple comparison test. *$p < 0.05$; **$p < 0.01$; ***$p < 0.001$; ****$p < 0.0001$.

Finally, phase 5 was a repeat of phase 2 with 10 high-intensity taps delivered with 20 s ISI. Overall, *syngap1ab+/–* larvae (n = 130 from 3 independent crosses) responded very similarly to WT larvae (n = 110 from three independent crosses) (Figure 3B), with a normal degree of habituation to high frequency stimuli (Figure 3C).

Despite these similarities, there were subtle differences. *syngap1ab+/–* larvae showed consistently elevated responses to high-intensity stimuli during phases 2 and 5. To determine whether this was due to larger movements and/or an increased probability of response, we calculated median movement velocity per larva (Figure 3D) and their response probability (Figure 3E) during Phases 1, 2, and 5. For median movement velocity (calculated across taps in a given phase), a mixed effects model of phase and genotype indicated a significant effect of phase ($p = 0.0018$). The subsequent Tukey's multiple comparison test showed that *syngap1+/–* larvae moved further in response to high-intensity vibrations in phases 2 and 5 than to

medium-intensity vibrations in phase 1 ($p = 0.0006$ and 0.0007 respectively) while WT larvae moved similar distances during phases 1, 2, and 5. For probability of response, a mixed effects model indicated effects of both phase ($p < 0.0001$) and genotype ($p = 0.0009$). The subsequent Tukey's multiple comparison test showed that *syngap1*+/− larvae had a higher response probability to stronger vibrational stimuli ($p < 0.0001$ Phase 1 vs. 2; $p = 0.0002$ Phase 1 vs. 5) and that this higher response probability to high-intensity stimuli was greater in *syngap1*+/− than WT larvae ($p = 0.0049$ Phase 2; $p = 0.0014$ Phase 5).

Therefore, in response to stronger stimuli, *syngap1*+/− are more likely to move and move faster, indicating a larger dynamic range of response in *syngap1*+/− larvae. This higher probability of response to the same stimulus is also consistent with higher levels of arousal in *syngap1*+/− larvae.

Syngap1ab mutant hyperactivity is most pronounced in low-arousal settings

We next assessed visual-motor responses (VMR) (Burgess and Granato, 2007; Emran et al., 2008) in the *syngap1ab* models. For this assay, larval movements were recorded during four cycles of lights-on to lights-off transitions. Larval activity was measured as the total distance moved every 30 s. Larvae show robust increases in locomotor activity when presented with a sudden transition from light to darkness (Supplementary Figure S3; Figure 4A). Compared to WT larvae, both *syngap1ab*+/− and *syngap1ab*−/− larvae showed increased activity ($p < 0.0001$) during both lights-on and lights-off cycles (Figure 4B). During lights-off periods *syngap1ab*+/− showed the greatest movement but this trend was somewhat variable across different batches of larvae (Supplementary Figure S3B); during lights-on, hyperactivity was consistent across batches of larvae and was dependent on the number of mutant *syngap1* alleles with *syngap1ab*−/− showing the greatest movement (Figure 4; Supplementary Figure S3).

For the preceding assays, WT, *syngap1ab*+/−, and *syngap1ab*−/− larvae resulted from independent crosses. To rule out the influence of distinct parental genetic backgrounds on the observed behavior, we also examined VMR in larvae resulting from an in-cross between *syngap1ab*+/− adults (Supplementary Figures S2C,D). Consistent with the previous results, during both lights-on (Supplementary Figure S2C) and lights-off cycles (Supplementary Figure S2D), *syngap1ab*−/− had the highest activity levels among all the resulting genotypes.

Syngap1ab hyperactivity in the light resembles WT behavior in the dark

The hyperactivity we observed in the *syngap1ab* mutant models could be due to either increased movement frequency, increased distance traveled per movement, or both. To distinguish among these possibilities, we analyzed the larval movement at a higher temporal resolution. Data were sampled every 25 ms, a much higher temporal resolution than the distance per 30 s shown in the preceding figures. Zebrafish movement bouts last ~250 ms and so 40 Hz resolution is sufficient to capture the majority of bouts with multiple timepoints. We focused on two parameters: the time interval between two consecutive movement bouts, denoted as "dwell time," and the distance traveled per bout, denoted as "displacement." These high-resolution activity data were organized and analyzed using custom-written MATLAB scripts to assess the probability of different behaviors, described by displacement and dwell time, during light and dark conditions.

Given highly stochastic individual larval movements, to assess overall patterns of both high and low frequency events across the distribution, we captured a large number of data points from over 100 individuals per genotype and then divided the total bouts by the number of individuals to generate and "idealized larva" for each genotype (Figures 4B,C). When bouts were pooled across individuals of a genotype, there were > 10^5 bouts per genotype and light condition (Lights-On: WT n = 119,135, *syngap1ab*+/− n = 196,594, and *syngap1ab*−/− n = 158,443; Lights-Off: WT n = 652,368, *syngap1ab*+/− n = 777,525, and *syngap1ab*−/− n = 507,720) coming from 173 WT, 167 *syngap1ab*+/−, and 119 *syngap1ab*−/− individual larvae. This analysis shows that the differences between genotypes are much more pronounced in the light/low arousal settings, than in the dark/higher arousal setting.

We next looked at probability distributions of dwell times (the time between movements) and distance traveled per movement (Figure 5). WT larvae in the dark had shorter dwell times and larger movements than WT in the light (Figures 5Ai,ii). These differences in WT light and dark behaviors are highlighted by plots below that show the relative probabilities in Dark versus Light for both dwell time and displacements (Figures 5Aiii,iv). Next, we compared *syngap1ab*+/− and WT in the light (Figure 5B) and in the dark (Figure 5C). In the dark, *syngap1ab*+/− and *syngap1ab*−/− had dwell time and displacement distributions that were very similar to WT larvae (Figures 5Ci–iv). By contrast, in the light, *syngap1ab*−/− and *syngap1ab*+/− mutants displayed both more frequent, and larger displacements compared to WT larvae (Figures 5Bi,ii). These differences between *syngap1*+/− and WT larvae in the light are highlighted by plots below that show the relative probabilities of *syngap1*+/− (purple) and *syngap1*−/− (pink) versus WT (Figures 5Biii,iv). These analyses showed that *syngap1*-WT (in light) resembles dark–light WT comparisons, indicating that *syngap1* mutants behavior in the light resembles that of WT behavior in the dark. Taken together, behavioral experiments show context-dependent hyperactivity that is most subtle during aversive, acoustic stimuli, is intermediate in the dark, and is most pronounced in normally low arousal well-lit environments.

Discussion

In this study, we generated a zebrafish model of *SYNGAP1-RD* and characterized zebrafish *syngap1ab* splice-variants as they relate to mammalian *Syngap1* and zebrafish *syngap1a* and *syngap1b* duplicates. This provided background for the stable zebrafish mutant model of SYNGAP1-RD we generated using CRISPR/cas9 genome editing of both *syngap1a* and *synagp1b* duplicates; mutations were validated as loss-of-function alleles at both mRNA and protein levels. We provide evidence that *syngap1a* and *syngap1b* play complementary functional roles in zebrafish with higher larval mortality when *syngap1b* mutant alleles outnumber those from *syngap1a*. Focusing on balanced *syngap1a* and *syngap1b* mutant genotypes for more detailed analyses,

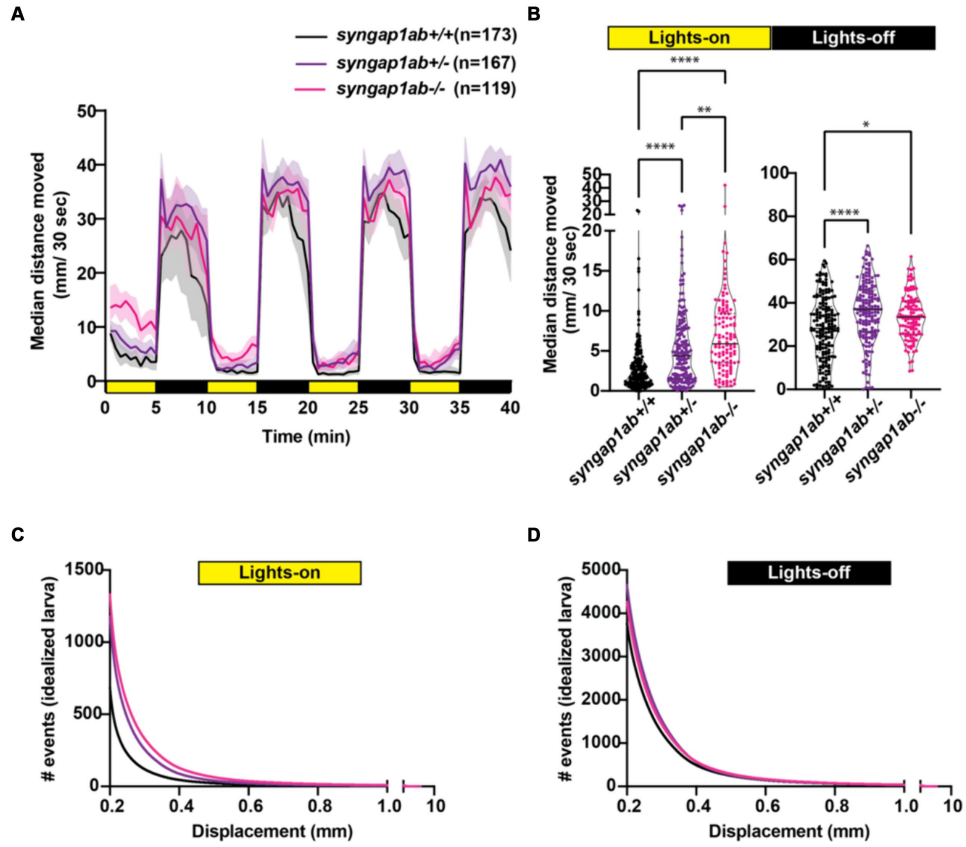

FIGURE 4
Syngap1 model hyperactivity is most pronounced during light cycles due to a higher frequency of larger movements. **(A)** Median ± 95% confidence interval distance moved by each 6 dpf larva per 30 s, when exposed to 5 min of lights-on and 5 min of lights-off alternating cycles across five different independent trials (Supplementary Figure S3). **(B)** During lights-on cycles, *syngap1ab* mutants showed increased activity levels in a genotype dependent manner where *syngap1ab−/−* were more active than *syngap1ab+/−* which were more active than the WT larvae. During lights-off cycles, *syngap1ab* mutant larvae showed significantly increased activity compared to WT larvae but there were no significant differences in the activity levels between *syngap1ab−/−* and *syngap1ab+/−* larvae. Statistical analyses between genotypes were carried out using Kruskal-Wallis test followed by Dunn's multiple comparison test. *p* value asterisks represent: **p* < 0.05; ***p* < 0.01; ****p* < 0.001; *****p* < 0.0001. Displacement distribution of "idealized larva" during lights-on **(C)** and lights-off **(D)** conditions. Graphs were generated by pooling all displacement events during lights-on WT n = 119,135, *syngap1ab+/−* n = 196,594, and *syngap1ab−/−* n = 158,443 and during lights-off WT n = 652,368, *syngap1ab+/−* n = 777,525, and *syngap1ab−/−* n = 507,720 and then dividing these by the number of larvae: 173 WT, 167 *syngap1ab+/−*, and 119 *syngap1ab−/−*.

we showed that, as in mammalian models and humans, the zebrafish *syngap1ab* models show context-dependent hyperactivity that is especially pronounced in low arousal settings.

Similar to mammalian Syngap1 isoforms (Gou et al., 2020; Yang et al., 2023), both Syngap1 zebrafish orthologs show extensive splicing at both N- and C-termini as well as splice-variants in the middle of the gene that only change a few amino acids. We provide evidence that *syngap1b* but not the *syngap1a* encodes an α1-like isoform, the most extensively studied of the mammalian Syngap1 isoforms (Chen et al., 1998; Kim et al., 1998; Walkup et al., 2016; Araki et al., 2020). In mammals, the α1 isoform has been shown to be enriched at the post-synaptic density of glutamatergic synapses by interacting with PSD-95 (Chen et al., 1998; Kim et al., 1998; Komiyama et al., 2002). In mice, loss of the α1 isoform alone is sufficient to produce cognitive deficits and seizures (Kilinc et al., 2022). The α1 isoform is also critical for long-term-potentiation-based forms of learning, toggling the strength of the synapse in an activity-dependent manner by competing with AMPA glutamate receptors for PSD95 binding sites (Araki et al., 2024). The unique expression of the Syngap1 α1 isoform by the *syngap1b* gene may help to explain higher mortality in zebrafish larvae with more *syngap1b* than *syngap1a* mutant alleles. We were not able to determine which of the zebrafish splice-variants corresponded to the other well-characterized mammalian Syngap1 α2, β, and γ isoforms (Kilinc et al., 2018; Araki et al., 2020; Gou et al., 2020), due to sequence divergence in the zebrafish consistent with differences that have been previously described in the zebrafish synapse proteome (Bayes et al., 2017).

Other zebrafish models of SYNGAP1-RD mutated only the *syngap1b* gene (Colon-Rodriguez et al., 2020; Griffin et al., 2021). Our differential survival results would predict that the phenotypes reported in *syngap1b* models may relate to a functional imbalance between *syngap1a* and *syngap1b*. Our more in-depth subsequent analyses,

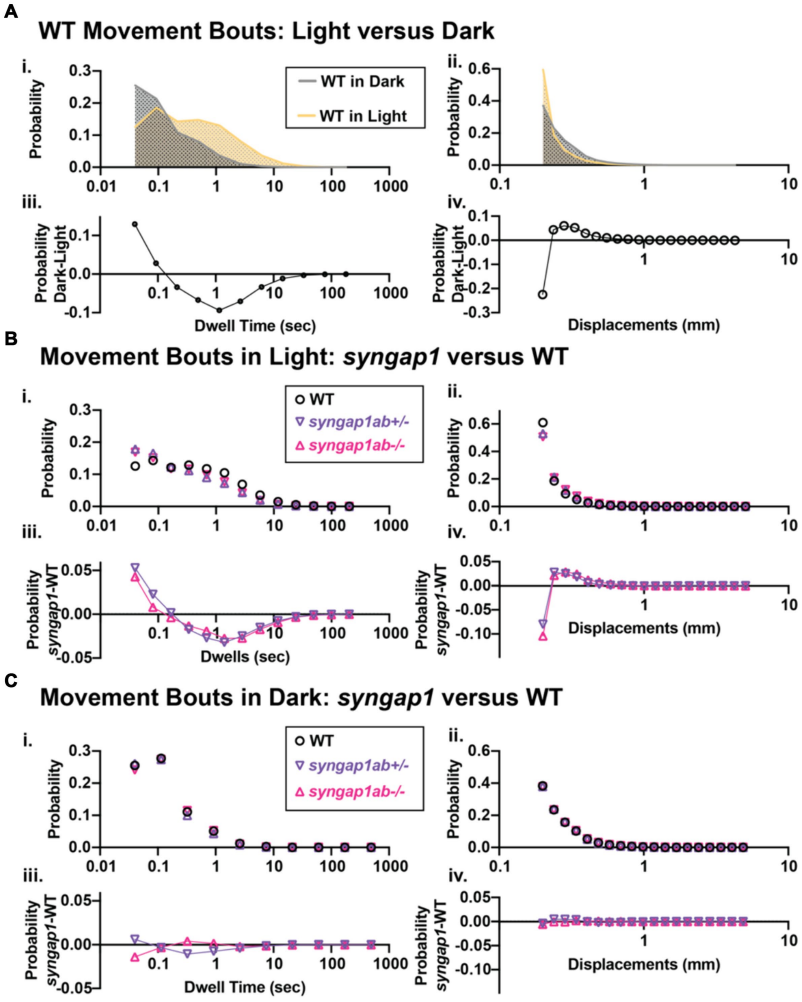

FIGURE 5
Syngap1ab mutants showed heightened arousal during lights-on cycles with more frequent and larger displacements. **(Ai,ii)** Probability distributions of dwell times **(Ai)** and displacements **(Aii)** are plotted for all 173 WT(*syngap1ab+/+*) larvae during lights-on (yellow) and lights-off (dark; checkered) cycles. Below **(Aiii,iv)** compare movements in dark and light by plotting probability in dark minus the probability in light. WT larvae moved farther more frequently in dark than in light. **(B,C)** Probability distributions of dwell time **(Bi, Ci)** and displacements **(Bii, Cii)** are plotted for all 173 WT, 167 *syngap1ab+/–* and 119 *syngap1ab+/–* mutant larvae. Below probability distribution plots **(Biii,iv, Ciii,iv)** compare movements in *syngap1ab+/–* (purple) and *syngap1ab–/–* (pink) to WT (black) by plotting probability in *syngap1ab* mutants minus the probability in WT. In dark, *syngpa1ab+/–* larvae moved more frequently than either WT or *syngap1ab–/–* larvae while all genotypes had similar displacement distributions. By contrast, in light, both *syngpa1ab+/–* and *syngap1ab–/–* larvae moved more frequently and farther than WT following a similar pattern that WT larvae showed during dark periods. *p* values were calculated using two-sample Kolmogorov–Smirnov test and for lights-on displacement: p(WT vs. *syngap1ab+/–*) = 0, p(WT vs. *syngap1ab–/–*) = 0, and p(*syngap1ab+/–* vs. *syngap1ab–/–*) = $p < 10^{-70}$ and during lights-off displacement; p(WT vs. *syngap1ab+/–*) = 10^{-26}, p(WT vs. *syngap1ab–/–*) = 1.5×10^{-11}, and p(*syngap1ab+/–* vs. *syngap1ab–/–*) = $p < 10^{-45}$, lights-on dwell time (WT vs. *syngap1ab+/–*) = 0, p(WT vs. *syngap1ab–/–*) = 0, and p(*syngap1ab+/–* vs. *syngap1ab–/–*) = $p < 10^{-31}$ and lights-off dwell time; p(WT vs. *syngap1ab+/–*) = 10^{-200}, p(WT vs. *syngap1ab–/–*) = 10^{-50}, and p(*syngap1ab+/–* vs. *syngap1ab–/–*) = $p < 10^{-200}$.

therefore, focused on larvae with balanced heterozygous mutations in both *syngap1a* and *syngap1b* in an effort to recapitulate mammalian haploinsufficiency.

In humans, altered sensory processing encompasses sensory hyperactivity/ hypoactivity and sensory seeking, and is a core symptom of an ASD diagnosis (Marco et al., 2011; Kirby et al., 2017; Robertson and Baron-Cohen, 2017; Damiano-Goodwin et al., 2018). In SYNGAP1-RD specifically, sensory-seeking behaviors include an affinity for contact with flowing water and/or perpetual motion (Wright et al., 2022). Syngap1 haploinsufficiency in both mice and humans alters sensory responses in a way that is context dependent, impacting simple sensory responses, entrainment, and habituation (Carreno-Munoz et al., 2022) and causing increased risk-taking behaviors (Kilinc et al., 2018; Weldon et al., 2018). Further studies on sleep in people with SYNGAP1-RD (Smith-Hicks et al., 2021) and mouse models, show

disrupted sleep and seizures that are more common at night and often come in clusters that predict transitions between REM and non REM sleep (Sullivan et al., 2020). Taken together, this collection of symptoms is consistent with a heightened state of arousal and difficulties with behavioral state transitions in people with SYNGAP1-RD.

Similar to mammalian SYNGAP1-RD models, our *syngap1ab* zebrafish mutant models exhibit context-dependent hyperactivity. In high arousal contexts generated by strong, aversive acoustic stimuli, WT and *syngap1*+/− larvae produced similar highly-stereotyped, high-velocity escape responses, related to startle responses in mammals by their short latency from the stimulus and their dependence on reticulospinal neurons (Liu and Fetcho, 1999; Eaton et al., 2001; Korn and Faber, 2005). In contrast to WT, *syngap1ab*+/− larvae had a larger dynamic range of responses compared to WT. Larger displacements in response to aversive, acoustic stimuli have been described in zebrafish glucocorticoid receptor mutants that have chronically elevated glucocorticoids due to a lack of feedback inhibition (Griffiths et al., 2012). Unlike glucocorticoid receptor mutants however, our *syngap1ab*+/− model also moves faster and more frequently in the light. Therefore, *syngap1ab*+/− hyperactivity likely involves other arousal pathways.

In both mammals and zebrafish, arousal pathways including dopamine, QRFP, serotonin, and hypocretin/orexin among others have been linked to increased locomotion (Chiu and Prober, 2013; Lovett-Barron et al., 2017; Corradi and Filosa, 2021; Tan et al., 2022). Moreover, gain-of-function experiments in zebrafish have shown that overexpressing either hypocretin/orexin or CART (cocaine and amphetamine regulated transcript) is sufficient to increase the probability that zebrafish larvae will respond to acoustic stimuli (Prober et al., 2006; Woods et al., 2014); and overexpression of any one of hypocretin/orexin, calcitonin gene related peptide (cgrp), or cholecystokinin (cck) is sufficient to increase daytime movement frequencies (Woods et al., 2014). Thus, overactivation of select arousal pathways is consistent with *syngap1ab*+/− hyperactivity.

We found that *syngap1*+/− hyperactivity was greatest in the light, a setting characterized by low arousal, long dwell times and short movements in WT larvae. Both *syngap1ab*+/− and *syngap1ab*−/− larvae exhibited short dwell times and large movements, similar to WT movements when they are suddenly transitioned to the dark (Burgess and Granato, 2007; Emran et al., 2008; Kozol et al., 2021). Increased WT movements with sudden darkness have been shown to reflect a goal-directed, light-seeking behaviors also known as dark phototaxis (Horstick et al., 2017). Goal-directed increases in activity can also result from internal states, such as hunger, studied in 7-day-old zebrafish larvae that no longer have a yolk supply (Filosa et al., 2016; Wee et al., 2019). In this study, hyperactive *syngap1ab* mutants were 6-day-olds and therefore their hyperactivity was not likely to be driven by hunger. Hunger-induced hyperactivity is associated with reduced cortisol, increased activity in the serotonergic raphe neurons and increased risk-taking as larvae approach objects that could be either food items or predators (Filosa et al., 2016). Like hunger, flowing water can also evoke more frequent movements that are dependent upon serotonergic dorsal raphe serotonergic pathways (Yokogawa et al., 2012). It is possible that the hyperactivity that we observe in the *syngap1ab*+/− larvae in low arousal settings is a form of sensory-seeking behavior.

Limitations

Zebrafish are less affected by Syngap1 loss-of-function than mammals. This difference suggests that phenotypes in zebrafish *syngap1ab* mutants might be less pronounced than symptoms in people with SYNGAP1-RD. Milder phenotypes in zebrafish than in mammals have been observed in several mutant models that affect synapses (Ono et al., 2001, 2002; Mongeon et al., 2008; Wang et al., 2008). One of the reasons for this is that at the time they are undergoing bursts of synaptogenesis, around birth in mice and around 3 dpf in zebrafish, they are vastly different sizes. Due to their relatively small size, zebrafish larvae do not need to breathe to supply their tissues with oxygen. For example, it is possible to generate a healthy, paralyzed, transparent zebrafish larva for *in vivo* imaging of physiological processes such as angiogenesis (Davis et al., 2021) because simple oxygen diffusion is sufficient to support oxidative processes. By contrast, in mice, the same mutations would prove lethal at birth when the pups have to breathe to provide oxygen to their tissues. These differences may help to explain why mutations in similar genes can be viable in the zebrafish model but more severe and/or lethal in the mammalian models.

Conclusion

Studies in people with diverse genetic forms of neurodevelopmental conditions and in animal models show that, despite some shared aspects of etiology, including changes to neuro- and gliogenesis and altered excitatory/inhibitory balance (Hoffman et al., 2016; Willsey et al., 2021), detailed changes in neuroanatomy, behavioral profiles, and associated symptoms exhibit substantial differences by genotype supporting the existence of subtypes (Ellegood et al., 2015; Thyme et al., 2019; Zerbi et al., 2021; Zoodsma et al., 2022; Weinschutz Mendes et al., 2023). In the case of *SYNGAP1*, both human and animal model studies point to arousal pathways as playing an important role in context-dependent hyperactivity. These condition-specific phenotypes can serve as the basis for the development of precision therapies in animal models like zebrafish that are suited to high-throughput, high-content screening (Hoffman et al., 2016).

Data availability statement

The datasets presented in this study can be found in online repositories. The names of the repository/repositories and accession number(s) can be found in the article/Supplementary material.

Ethics statement

The animal study was approved by University of Miami IACUC protocol #18-129. The study was conducted in accordance with the local legislation and institutional requirements.

Author contributions

SHS: Conceptualization, Data curation, Formal analysis, Investigation, Methodology, Resources, Supervision, Validation,

Visualization, Writing – original draft, Writing – review & editing. SK: Data curation, Investigation, Project administration, Writing – original draft, Writing – review & editing. RK: Conceptualization, Methodology, Resources, Writing – original draft, Writing – review & editing. YA: Formal analysis, Methodology, Writing – original draft, Writing – review & editing. SS: Data curation, Formal analysis, Software, Visualization, Writing – original draft, Writing – review & editing, Funding acquisition. RH: Funding acquisition, Resources, Writing – original draft, Writing – review & editing. JD: Conceptualization, Data curation, Formal analysis, Funding acquisition, Investigation, Methodology, Project administration, Supervision, Validation, Visualization, Writing – original draft, Writing – review & editing.

Funding

The author(s) declare financial support was received for the research, authorship, and/or publication of this article. This work was supported by Bridge Funds from the College of Arts and Sciences at the University of Miami and NIH grants MH103857 and HD093021, and SFARI #719401 to JD, NIH grants MH112151 and NS03671 to RH, and NSF IOS#2131037 to SS.

Acknowledgments

We would like to thank the SYNGAP1 Foundation, the SYNGAP1 Research Fund, and individuals with SRID and their families for their support and advocacy. We thank Millie Rogers, Adhikansh Jain, and Dr. James Baker for their valuable feedback that improved the manuscript. We would like to acknowledge the excellent care of the zebrafish provided by the University of Miami Zebrafish Facility manager Ricardo Cepeda.

Conflict of interest

The authors declare that the research was conducted in the absence of any commercial or financial relationships that could be construed as a potential conflict of interest.

Publisher's note

Supplementary material

The Supplementary material for this article can be found online at: https://www.frontiersin.org/articles/10.3389/fnmol.2024.1401746/full#supplementary-material

References

Araki, Y., Hong, I., Gamache, T. R., Ju, S., Collado-Torres, L., Shin, J. H., et al. (2020). SynGAP isoforms differentially regulate synaptic plasticity and dendritic development. *eLife* 9:9. doi: 10.7554/eLife.56273

Araki, Y., Rajkovich, K. E., Gerber, E. E., Gamache, T. R., Johnson, R. C., Tran, T. H. N., et al. (2024). SynGAP regulates synaptic plasticity and cognition independently of its catalytic activity. *Science* 383:eadk1291. doi: 10.1126/science.adk1291

Bayes, A., Collins, M. O., Reig-Viader, R., Gou, G., Goulding, D., Izquierdo, A., et al. (2017). Evolution of complexity in the zebrafish synapse proteome. *Nat. Commun.* 8:14613. doi: 10.1038/ncomms14613

Berryer, M. H., Hamdan, F. F., Klitten, L. L., Moller, R. S., Carmant, L., Schwartzentruber, J., et al. (2013). Mutations in SYNGAP1 cause intellectual disability, autism, and a specific form of epilepsy by inducing haploinsufficiency. *Hum. Mutat.* 34, 385–394. doi: 10.1002/humu.22248

Burgess, H. A., and Granato, M. (2007). Modulation of locomotor activity in larval zebrafish during light adaptation. *J. Exp. Biol.* 210, 2526–2539. doi: 10.1242/jeb.003939

Campbell, P. D., Lee, I., Thyme, S., and Granato, M. (2023). Mitochondrial proteins encoded by the 22q11.2 neurodevelopmental locus regulate neural stem and progenitor cell proliferation. *Mol. Psychiatry* 28, 3769–3781. doi: 10.1038/s41380-023-02272-z

Carreno-Munoz, M. I., Chattopadhyaya, B., Agbogba, K., Cote, V., Wang, S., Levesque, M., et al. (2022). Sensory processing dysregulations as reliable translational biomarkers in SYNGAP1 haploinsufficiency. *Brain* 145, 754–769. doi: 10.1093/brain/awab329

Carvill, G. L., Heavin, S. B., Yendle, S. C., McMahon, J. M., O'Roak, B. J., Cook, J., et al. (2013). Targeted resequencing in epileptic encephalopathies identifies de novo mutations in CHD2 and SYNGAP1. *Nat. Genet.* 45, 825–830. doi: 10.1038/ng.2646

Chen, H. J., Rojas-Soto, M., Oguni, A., and Kennedy, M. B. (1998). A synaptic Ras-GTPase activating protein (p135 SynGAP) inhibited by CaM kinase II. *Neuron* 20, 895–904. doi: 10.1016/S0896-6273(00)80471-7

Chiu, C. N., and Prober, D. A. (2013). Regulation of zebrafish sleep and arousal states: current and prospective approaches. *Front. Neural Circuits* 7:58. doi: 10.3389/fncir.2013.00058

Colon-Rodriguez, A., Uribe-Salazar, J. M., Weyenberg, K. B., Sriram, A., Quezada, A., Kaya, G., et al. (2020). Assessment of autism zebrafish mutant models using a high-throughput larval phenotyping platform. *Front. Cell Dev. Biol.* 8:586296. doi: 10.3389/fcell.2020.586296

Corradi, L., and Filosa, A. (2021). Neuromodulation and behavioral flexibility in larval zebrafish: from neurotransmitters to circuits. *Front. Mol. Neurosci.* 14:718951. doi: 10.3389/fnmol.2021.718951

Creson, T. K., Rojas, C., Hwaun, E., Vaissiere, T., Kilinc, M., Jimenez-Gomez, A., et al. (2019). Re-expression of SynGAP protein in adulthood improves translatable measures of brain function and behavior. *eLife* 8:8. doi: 10.7554/eLife.46752

Damiano-Goodwin, C. R., Woynaroski, T. G., Simon, D. M., Ibanez, L. V., Murias, M., Kirby, A., et al. (2018). Developmental sequelae and neurophysiologic substrates of sensory seeking in infant siblings of children with autism spectrum disorder. *Dev. Cogn. Neurosci.* 29, 41–53. doi: 10.1016/j.dcn.2017.08.005

Davis, A. E., Castranova, D., and Weinstein, B. M. (2021). Rapid generation of pigment free, immobile zebrafish embryos and larvae in any genetic background using CRISPR-Cas9 dgRNPs. *Zebrafish* 18, 235–242. doi: 10.1089/zeb.2021.0011

Davis, M. W., and Jorgensen, E. M. (2022). ApE, a plasmid editor: a freely available DNA manipulation and visualization program. *Front. Bioinform.* 2:818619. doi: 10.3389/fbinf.2022.818619

Dunn, T. W., Gebhardt, C., Naumann, E. A., Riegler, C., Ahrens, M. B., Engert, F., et al. (2016). Neural circuits underlying visually evoked escapes in larval zebrafish. *Neuron* 89, 613–628. doi: 10.1016/j.neuron.2015.12.021

Eaton, R. C., Lee, R. K., and Foreman, M. B. (2001). The Mauthner cell and other identified neurons of the brainstem escape network of fish. *Prog. Neurobiol.* 63, 467–485. doi: 10.1016/S0301-0082(00)00047-2

Ellegood, J., Anagnostou, E., Babineau, B. A., Crawley, J. N., Lin, L., Genestine, M., et al. (2015). Clustering autism: using neuroanatomical differences in 26 mouse models to gain insight into the heterogeneity. *Mol. Psychiatry* 20, 118–125. doi: 10.1038/mp.2014.98

Emran, F., Rihel, J., and Dowling, J. E. (2008). A behavioral assay to measure responsiveness of zebrafish to changes in light intensities. *J. Vis. Exp.* 20:923. doi: 10.3791/923

Filosa, A., Barker, A. J., Dal Maschio, M., and Baier, H. (2016). Feeding state modulates behavioral choice and processing of prey stimuli in the zebrafish tectum. *Neuron* 90, 596–608. doi: 10.1016/j.neuron.2016.03.014

Fu, J. M., Satterstrom, F. K., Peng, M., Brand, H., Collins, R. L., Dong, S., et al. (2022). Rare coding variation provides insight into the genetic architecture and phenotypic context of autism. *Nat. Genet.* 54, 1320–1331. doi: 10.1038/s41588-022-01104-0

Gamache, T. R., Araki, Y., and Huganir, R. L. (2020). Twenty years of SynGAP research: from synapses to cognition. *J. Neurosci.* 40, 1596–1605. doi: 10.1523/JNEUROSCI.0420-19.2020

Gao, Y., Chan, R. H., Chow, T. W., Zhang, L., Bonilla, S., Pang, C. P., et al. (2014). A high-throughput zebrafish screening method for visual mutants by light-induced locomotor response. *IEEE/ACM Trans. Comput. Biol. Bioinform.* 11, 693–701. doi: 10.1109/TCBB.2014.2306829

Glasauer, S. M., and Neuhauss, S. C. (2014). Whole-genome duplication in teleost fishes and its evolutionary consequences. *Mol. Gen. Genomics.* 289, 1045–1060. doi: 10.1007/s00438-014-0889-2

Gou, G., Roca-Fernandez, A., Kilinc, M., Serrano, E., Reig-Viader, R., Araki, Y., et al. (2020). SynGAP splice variants display heterogeneous spatio-temporal expression and subcellular distribution in the developing mammalian brain. *J. Neurochem.* 154, 618–634. doi: 10.1111/jnc.14988

Griffin, A., Carpenter, C., Liu, J., Paterno, R., Grone, B., Hamling, K., et al. (2021). Phenotypic analysis of catastrophic childhood epilepsy genes. *Commun. Biol.* 4:680. doi: 10.1038/s42003-021-02221-y

Griffiths, B. B., Schoonheim, P. J., Ziv, L., Voelker, L., Baier, H., and Gahtan, E. (2012). A zebrafish model of glucocorticoid resistance shows serotonergic modulation of the stress response. *Front. Behav. Neurosci.* 6:68. doi: 10.3389/fnbeh.2012.00068

Guo, X., Hamilton, P. J., Reish, N. J., Sweatt, J. D., Miller, C. A., and Rumbaugh, G. (2009). Reduced expression of the NMDA receptor-interacting protein SynGAP causes behavioral abnormalities that model symptoms of schizophrenia. *Neuropsychopharmacology* 34, 1659–1672. doi: 10.1038/npp.2008.223

Hamdan, F. F., Gauthier, J., Araki, Y., Lin, D. T., Yoshizawa, Y., Higashi, K., et al. (2011). Excess of de novo deleterious mutations in genes associated with glutamatergic systems in nonsyndromic intellectual disability. *Am. J. Hum. Genet.* 88, 306–316. doi: 10.1016/j.ajhg.2011.02.001

Hamdan, F. F., Gauthier, J., Rouleau, G. A., and Michaud, J. L. (2010). De novo mutations in SYNGAP1 associated with non-syndromic mental retardation. *Med. Sci. (Paris)* 26, 133–135. doi: 10.1051/medsci/2010262133

Hoffman, E. J., Turner, K. J., Fernandez, J. M., Cifuentes, D., Ghosh, M., Ijaz, S., et al. (2016). Estrogens suppress a behavioral phenotype in zebrafish mutants of the autism risk gene, CNTNAP2. *Neuron* 89, 725–733. doi: 10.1016/j.neuron.2015.12.039

Horstick, E. J., Bayleyen, Y., Sinclair, J. L., and Burgess, H. A. (2017). Search strategy is regulated by somatostatin signaling and deep brain photoreceptors in zebrafish. *BMC Biol.* 15:4. doi: 10.1186/s12915-016-0346-2

Ijaz, S., and Hoffman, E. J. (2016). Zebrafish: a translational model system for studying neuropsychiatric disorders. *J. Am. Acad. Child Adolesc. Psychiatry* 55, 746–748. doi: 10.1016/j.jaac.2016.06.008

Jimenez-Gomez, A., Niu, S., Andujar-Perez, F., McQuade, E. A., Balasa, A., Huss, D., et al. (2019). Phenotypic characterization of individuals with SYNGAP1 pathogenic variants reveals a potential correlation between posterior dominant rhythm and developmental progression. *J. Neurodev. Disord.* 11:18. doi: 10.1186/s11689-019-9276-y

Kilinc, M., Arora, V., Creson, T. K., Rojas, C., Le, A. A., Lauterborn, J., et al. (2022). Endogenous Syngap1 alpha splice forms promote cognitive function and seizure protection. *eLife* 11:11. doi: 10.7554/eLife.75707

Kilinc, M., Creson, T., Rojas, C., Aceti, M., Ellegood, J., Vaissiere, T., et al. (2018). Species-conserved SYNGAP1 phenotypes associated with neurodevelopmental disorders. *Mol. Cell. Neurosci.* 91, 140–150. doi: 10.1016/j.mcn.2018.03.008

Kim, J. H., Liao, D., Lau, L. F., and Huganir, R. L. (1998). SynGAP: a synaptic RasGAP that associates with the PSD-95/SAP90 protein family. *Neuron* 20, 683–691. doi: 10.1016/S0896-6273(00)81008-9

Kirby, A. V., Boyd, B. A., Williams, K. L., Faldowski, R. A., and Baranek, G. T. (2017). Sensory and repetitive behaviors among children with autism spectrum disorder at home. *Autism* 21, 142–154. doi: 10.1177/1362361316632710

Komiyama, N. H., Watabe, A. M., Carlisle, H. J., Porter, K., Charlesworth, P., Monti, J., et al. (2002). SynGAP regulates ERK/MAPK signaling, synaptic plasticity, and learning in the complex with postsynaptic density 95 and NMDA receptor. *J. Neurosci.* 22, 9721–9732. doi: 10.1523/JNEUROSCI.22-22-09721.2002

Korn, H., and Faber, D. S. (2005). The Mauthner cell half a century later: a neurobiological model for decision-making? *Neuron* 47, 13–28. doi: 10.1016/j.neuron.2005.05.019

Kozol, R. A., Abrams, A. J., James, D. M., Buglo, E., Yan, Q., and Dallman, J. E. (2016). Function over form: modeling groups of inherited neurological conditions in zebrafish. *Front. Mol. Neurosci.* 9:55. doi: 10.3389/fnmol.2016.00055

Kozol, R. A., James, D. M., Varela, I., Sumathipala, S. H., Zuchner, S., and Dallman, J. E. (2021). Restoring Shank3 in the rostral brainstem of shank3ab−/− zebrafish autism models rescues sensory deficits. *Commun. Biol.* 4:1411. doi: 10.1038/s42003-021-02920-6

Liu, K. S., and Fetcho, J. R. (1999). Laser ablations reveal functional relationships of segmental hindbrain neurons in zebrafish. *Neuron* 23, 325–335. doi: 10.1016/S0896-6273(00)80783-7

Lovett-Barron, M., Andalman, A. S., Allen, W. E., Vesuna, S., Kauvar, I., Burns, V. M., et al. (2017). Ancestral circuits for the coordinated modulation of brain state. *Cell* 171, 1411–1423.e17. doi: 10.1016/j.cell.2017.10.021

Lyons-Warren, A. M., McCormack, M. C., and Holder, J. L. Jr. (2022). Sensory processing phenotypes in Phelan-McDermid syndrome and SYNGAP1-related intellectual disability. *Brain Sci.* 12:137. doi: 10.3390/brainsci12020137

Marco, E. J., Hinkley, L. B., Hill, S. S., and Nagarajan, S. S. (2011). Sensory processing in autism: a review of neurophysiologic findings. *Pediatr. Res.* 69, 48R–54R. doi: 10.1203/PDR.0b013e3182130c54

McMahon, A. C., Barnett, M. W., O'Leary, T. S., Stoney, P. N., Collins, M. O., Papadia, S., et al. (2012). SynGAP isoforms exert opposing effects on synaptic strength. *Nat. Commun.* 3:900. doi: 10.1038/ncomms1900

Michaelson, S. D., Ozkan, E. D., Aceti, M., Maity, S., Llamosas, N., Weldon, M., et al. (2018). SYNGAP1 heterozygosity disrupts sensory processing by reducing touch-related activity within somatosensory cortex circuits. *Nat. Neurosci.* 21, 1–13. doi: 10.1038/s41593-018-0268-0

Mongeon, R., Gleason, M. R., Masino, M. A., Fetcho, J. R., Mandel, G., Brehm, P., et al. (2008). Synaptic homeostasis in a zebrafish glial glycine transporter mutant. *J. Neurophysiol.* 100, 1716–1723. doi: 10.1152/jn.90596.2008

Montague, T. G., Cruz, J. M., Gagnon, J. A., Church, G. M., and Valen, E. (2014). CHOPCHOP: a CRISPR/Cas9 and TALEN web tool for genome editing. *Nucleic Acids Res.* 42, W401–W407. doi: 10.1093/nar/gku410

Naveed, H., McCormack, M., and Holder, J. L. Jr. (2023). Social behavioral impairments in SYNGAP1-related intellectual disability. *Front. Pediatr.* 11:1188117. doi: 10.3389/fped.2023.1188117

Oldehinkel, M., Mennes, M., Marquand, A., Charman, T., Tillmann, J., Ecker, C., et al. (2019). Altered connectivity between cerebellum, visual, and sensory-motor networks in autism Spectrum disorder: results from the EU-AIMS longitudinal European autism project. *Biol. Psychiatry Cogn. Neurosci. Neuroimaging* 4, 260–270. doi: 10.1016/j.bpsc.2018.11.010

Ono, F., Higashijima, S., Shcherbatko, A., Fetcho, J. R., and Brehm, P. (2001). Paralytic zebrafish lacking acetylcholine receptors fail to localize rapsyn clusters to the synapse. *J. Neurosci.* 21, 5439–5448. doi: 10.1523/JNEUROSCI.21-15-05439.2001

Ono, F., Shcherbatko, A., Higashijima, S., Mandel, G., and Brehm, P. (2002). The zebrafish motility mutant twitch once reveals new roles for rapsyn in synaptic function. *J. Neurosci.* 22, 6491–6498. doi: 10.1523/JNEUROSCI.22-15-06491.2002

Ozkan, E. D., Creson, T. K., Kramar, E. A., Rojas, C., Seese, R. R., Babyan, A. H., et al. (2014). Reduced cognition in Syngap1 mutants is caused by isolated damage within developing forebrain excitatory neurons. *Neuron* 82, 1317–1333. doi: 10.1016/j.neuron.2014.05.015

Pinto, D., Pagnamenta, A. T., Klei, L., Anney, R., Merico, D., Regan, R., et al. (2010). Functional impact of global rare copy number variation in autism spectrum disorders. *Nature* 466, 368–372. doi: 10.1038/nature09146

Prober, D. A., Rihel, J., Onah, A. A., Sung, R. J., and Schier, A. F. (2006). Hypocretin/orexin overexpression induces an insomnia-like phenotype in zebrafish. *J. Neurosci.* 26, 13400–13410. doi: 10.1523/JNEUROSCI.4332-06.2006

Robertson, C. E., and Baron-Cohen, S. (2017). Sensory perception in autism. *Nat. Rev. Neurosci.* 18, 671–684. doi: 10.1038/nrn.2017.112

Samarut, E., Lissouba, A., and Drapeau, P. (2016). A simplified method for identifying early CRISPR-induced indels in zebrafish embryos using high resolution melting analysis. *BMC Genomics* 17:547. doi: 10.1186/s12864-016-2881-1

Satterstrom, F. K., Kosmicki, J. A., Wang, J., Breen, M. S., De Rubeis, S., An, J. Y., et al. (2020). Large-scale exome sequencing study implicates both developmental and functional changes in the neurobiology of autism. *Cell* 180, 568–584.e23. doi: 10.1016/j.cell.2019.12.036

Smith-Hicks, C., Wright, D., Kenny, A., Stowe, R. C., McCormack, M., Stanfield, A. C., et al. (2021). Low-dose Perampanel rescues cortical gamma dysregulation associated with Parvalbumin interneuron GluA2 upregulation in epileptic Syngap1(+/−) mice. *Biol. Psychiatry* 87, 829–842. doi: 10.1016/j.biopsych.2019.12.025

Sullivan, B. J., Ammanuel, S., Kipnis, P. A., Araki, Y., Huganir, R. L., and Kadam, S. D. (2020). Sleep abnormalities in the Synaptopathies-SYNGAP1-related intellectual disability and Phelan-McDermid syndrome. *Brain Sci.* 11:1229. doi: 10.3390/brainsci1091229

Tan, J. X. M., Ang, R. J. W., and Wee, C. L. (2022). Larval zebrafish as a model for mechanistic discovery in mental health. *Front. Mol. Neurosci.* 15:900213. doi: 10.3389/fnmol.2022.900213

Tavassoli, T., Miller, L. J., Schoen, S. A., Nielsen, D. M., and Baron-Cohen, S. (2014). Sensory over-responsivity in adults with autism spectrum conditions. *Autism* 18, 428–432. doi: 10.1177/1362361313477246

Thomas, B. R., Ludwig, N. N., Falligant, J. M., Kurtz, P. F., and Smith-Hicks, C. (2024). Severe behavior problems in SYNGAP1-related disorder: a summary of 11 consecutive patients in a tertiary care specialty clinic. *Epilepsy Behav.* 150:109584. doi: 10.1016/j.yebeh.2023.109584

Thyme, S. B., Pieper, L. M., Li, E. H., Pandey, S., Wang, Y., Morris, N. S., et al. (2019). Phenotypic landscape of schizophrenia-associated genes defines candidates and their shared functions. *Cell* 177, 478–491.e20. doi: 10.1016/j.cell.2019.01.048

Varshney, G. K., Carrington, B., Pei, W., Bishop, K., Chen, Z., Fan, C., et al. (2016). A high-throughput functional genomics workflow based on CRISPR/Cas9-mediated targeted mutagenesis in zebrafish. *Nat. Protoc.* 11, 2357–2375. doi: 10.1038/nprot.2016.141

Vlaskamp, D. R. M., and Scheffer, I. E. (2020). Author response: SYNGAP1 encephalopathy: a distinctive generalized developmental and epileptic encephalopathy. *Neurology* 94:370. doi: 10.1212/WNL.0000000000009010

Vlaskamp, D. R. M., Shaw, B. J., Burgess, R., Mei, D., Montomoli, M., Xie, H., et al. (2019). SYNGAP1 encephalopathy: a distinctive generalized developmental and epileptic encephalopathy. *Neurology* 92, e96–e107. doi: 10.1212/WNL.0000000000006729

Walkup, W. G., Mastro, T. L., Schenker, L. T., Vielmetter, J., Hu, R., Iancu, A., et al. (2016). A model for regulation by SynGAP-alpha1 of binding of synaptic proteins to PDZ-domain 'Slots' in the postsynaptic density. *eLife* 5:5. doi: 10.7554/eLife.22495

Wang, M., Wen, H., and Brehm, P. (2008). Function of neuromuscular synapses in the zebrafish choline-acetyltransferase mutant Bajan. *J. Neurophysiol.* 100, 1995–2004. doi: 10.1152/jn.90517.2008

Wee, C. L., Nikitchenko, M., Wang, W. C., Luks-Morgan, S. J., Song, E., Gagnon, J. A., et al. (2019). Zebrafish oxytocin neurons drive nocifensive behavior via brainstem premotor targets. *Nat. Neurosci.* 22, 1477–1492. doi: 10.1038/s41593-019-0452-x

Weinschutz Mendes, H., Neelakantan, U., Liu, Y., Fitzpatrick, S. E., Chen, T., Wu, W., et al. (2023). High-throughput functional analysis of autism genes in zebrafish identifies convergence in dopaminergic and neuroimmune pathways. *Cell Rep.* 42:112243. doi: 10.1016/j.celrep.2023.112243

Weldon, M., Kilinc, M., Lloyd Holder, J. Jr., and Rumbaugh, G. (2018). The first international conference on SYNGAP1-related brain disorders: a stakeholder meeting of families, researchers, clinicians, and regulators. *J. Neurodev. Disord.* 10:6. doi: 10.1186/s11689-018-9225-1

Willsey, H. R., Exner, C. R. T., Xu, Y., Everitt, A., Sun, N., Wang, B., et al. (2021). Parallel in vivo analysis of large-effect autism genes implicates cortical neurogenesis and estrogen in risk and resilience. *Neuron* 109:1409. doi: 10.1016/j.neuron.2021.03.030

Wolman, M. A., Jain, R. A., Marsden, K. C., Bell, H., Skinner, J., Hayer, K. E., et al. (2015). A genome-wide screen identifies PAPP-AA-mediated IGFR signaling as a novel regulator of habituation learning. Neuron. 2015 Mar 18;85(6):1200-11. doi: 10.1016/j.neuron.2015.02.025. Epub 2015 Mar 5. *Erratum in: Neuron*. 87, 906–907.

Woods, I. G., Schoppik, D., Shi, V. J., Zimmerman, S., Coleman, H. A., Greenwood, J., et al. (2014). Neuropeptidergic signaling partitions arousal behaviors in zebrafish. *J. Neurosci.* 34, 3142–3160. doi: 10.1523/JNEUROSCI.3529-13.2014

Wright, D., Kenny, A., Eley, S., McKechanie, A. G., and Stanfield, A. C. (2022). Clinical and behavioural features of SYNGAP1-related intellectual disability: a parent and caregiver description. *J. Neurodev. Disord.* 14:34. doi: 10.1186/s11689-022-09437-x

Yang, R., Feng, X., Arias-Cavieres, A., Mitchell, R. M., Polo, A., Hu, K., et al. (2023). Upregulation of SYNGAP1 expression in mice and human neurons by redirecting alternative splicing. *Neuron* 111, 1637–1650.e5. doi: 10.1016/j.neuron.2023.02.021

Yokogawa, T., Hannan, M. C., and Burgess, H. A. (2012). The dorsal raphe modulates sensory responsiveness during arousal in zebrafish. *J. Neurosci.* 32, 15205–15215. doi: 10.1523/JNEUROSCI.1019-12.2012

Zerbi, V., Pagani, M., Markicevic, M., Matteoli, M., Pozzi, D., Fagiolini, M., et al. (2021). Brain mapping across 16 autism mouse models reveals a spectrum of functional connectivity subtypes. *Mol. Psychiatry* 26, 7610–7620. doi: 10.1038/s41380-021-01245-4

Zoodsma, J. D., Keegan, E. J., Moody, G. R., Bhandiwad, A. A., Napoli, A. J., Burgess, H. A., et al. (2022). Disruption of grin2B, an ASD-associated gene, produces social deficits in zebrafish. *Mol. Autism.* 13:38. doi: 10.1186/s13229-022-00516-3